GEOLOGIC CONTROLS ON NITROGEN ISOTOPES IN MARINE BLACK SHALE: A CASE STUDY OF THE WOODFORD SHALE, ANADARKO BASIN, OKLAHOMA

By

KEITH THOMAS RIVERA

Bachelor of Science in Geology

California State University San Bernardino

San Bernardino, California

2011

Submitted to the Faculty of the
Graduate College of the
Oklahoma State University
in partial fulfillment of
the requirements for
the Degree of
MASTER OF SCIENCE
December, 2013

GEOLOGIC CONTROLS ON NITROGEN ISOTOPES IN MARINE BLACK SHALES: A CASE STUDY OF THE WOODFORD SHALE, ANADARKO BASIN, OKLAHOMA

Thesis Approved:

Dr. Tracy M. Quan

Thesis Adviser

Dr. Eliot Atekwana

Dr. Jack Pashin

ACKNOWLEDGEMENTS

I would like to express my deepest gratitude to the faculty of the Boone Pickens School of Geology; in particular to my thesis advisor, Dr. Tracy M. Quan, for the time and energy she spent guiding me through this project. I would also like to thank my committee members, Dr. Eliot Atekwana and Dr. Jack Pashin, for their time and suggestions. I am also extremely grateful for Dr. Jim Puckette for the advice, guidance and input he gave me throughout the project.

This project could not have moved forward without generous financial support from the GEO OCE-0916914 grant from the National Science Foundation (NSF), the 2012 Kate and Takken Scholarship of the Oklahoma Geological Society, and fellowships from Devon Energy Corporation and QEP Resources, Inc.

I am very grateful for my mom, dad and sister who have always had high expectations of me, which gave me the drive to push forward and never settle. Thank you for always supporting me throughout my life, even when things did not go exactly as planned.

I would also like to thank Chris Geyer for his assistance and knowledge in the geochemistry laboratory. A special thanks goes out to Vi and Jonathan for all of their help at the core library.

Name: KEITH RIVERA

Date of Degree: DECEMBER, 2013

Title of Study: GEOLOGIC CONTROLS ON NITROGEN ISOTOPES IN MARINE BLACK SHALE: A CASE STUDY OF THE WOODFORD SHALE, ANADARKO BASIN, OKLAHOMA

Major Field: GEOLOGY

Abstract:

Determining depositional environments of organic-rich black shale can enhance the identification of hydrocarbon producing intervals. Several methods have been utilized to identify depositional environments; however, for this study an isotopic approach was used. Bulk sedimentary $\delta^{15}N$ signals have been used to identify water column redox states of sediments, but affects of thermal maturity on $\delta^{15}N$ are unknown. Understanding the thermal maturity alterations on bulk sedimentary $\delta^{15}N$ is relevant to identifying target intervals for ultimate hydrocarbon recovery. In attempt to understand the depositional, diagenetic, and thermal maturation affects on the bulk sedimentary $\delta^{15}N$ signals, we sampled the Devonian-age Woodford Shale at different depths from the depocenter of the Anadarko Basin to an outcrop east of the Anadarko Shelf in the Ozark Plateau to test different thermal maturity levels. The R_o maturity levels of the Woodford Shale at the sample locations ranged from 0.56 % to 1.43 %, which cover oil generation to gas generation.

The results indicate that the $\delta^{15}N$ values of the Woodford Shale produce two different populations. One population has an average $\delta^{15}N$ value that is 3.4 ‰ heavier than the average $\delta^{15}N$ value of the other population. On an individual location and basin wide scale, deeper sediments are isotopically lighter than shallower sediments in terms of nitrogen, and these deeper sediments are more thermally mature. Data suggests high concentrations of redox sensitive trace metals, uranium (U) and molybdenum (Mo), are associated with the population of low bulk sedimentary $\delta^{15}N$ values, while low concentrations of U and Mo and the presence of burrows are associated with the population of high bulk sedimentary $\delta^{15}N$ values. The observed relationship between bulk sedimentary $\delta^{15}N$ and R_o is opposite than that expected to be seen by nitrogen isotopes affected by thermal maturity. On the other hand, the observed relationship between bulk sedimentary $\delta^{15}N$ and trace metal concentrations indicates that bulk sedimentary $\delta^{15}N$ values are strongly influenced by the redox state of the water column during deposition. This relationship was observed on both an individual scale and basin wide scale, which suggests redox water column conditions changed during Woodford deposition and were locally dependent.

TABLE OF CONTENTS

Chapter Page

LIST OF TABLES

Table Page

Table Page

LIST OF FIGURES

Figure Page

Figure Page

CHAPTER I

INTRODUCTION

Determining the depositional environments of organic-rich black shale can assist in the identification of hydrocarbon producing intervals. Nitrogen isotopes have been utilized to identify the depositional environments of sediment and sedimentary rock (Holmes et al., 1996; Altabet et al., 1998; Lehmann et al., 2002; Hulth et al., 2005; Knies et al., 2007; Strapoć et al., 2010; Godfrey and Glass, 2011); however how these isotopes are affected by diagenesis and thermal maturity is largely unknown. Certain questions arise while addressing this problem: (1) do $\delta^{15}N$ values change in proportion with the degree of thermal maturity, (2) does thermal maturity shift the initial $\delta^{15}N$ values disproportionately between sediments subjected to different thermal maturity levels to generate the final bulk sedimentary $\delta^{15}N$ values, or (3) does the initial $\delta^{15}N$ value of organic matter have greater influence on the final bulk sedimentary $\delta^{15}N$ values than the effects caused by thermal maturity? In order to evaluate whether thermal maturity affects bulk sedimentary $\delta^{15}N$ values of marine shale, the processes and reactions dictating the nitrogen cycle that produce initial $\delta^{15}N$ values of organic matter within the water column must be understood.

In marine ecosystems, nitrogen is converted between forms through a variety of biologically mediated reactions (Figure 1; Quan and Falkowski, 2009; Zonneveld et al., 2010) and is used by microorganisms to synthesize structural components or to gain energy to grow

(Gruber, 2008). The most abundant form of nitrogen in surface waters of marine environments is dissolved nitrogen (N_2), though it is not bioavailable to the majority of microorganisms (Gruber, 2008). However, a few microorganisms are able to utilize and fix N_2 with the aid of the nitrogenase enzyme, converting it into labile nitrogen for other organisms to use (Wada, 1980; Quan et al., 2008; Quan and Falkowski, 2009; Whittaker et al., 2011; Adigwe, 2012). The available nitrogen forms are converted between forms through the variety of reactions that make up the nitrogen cycle (Figure 1). The reactions responsible for the conversion between different nitrogen forms are strongly influenced by the redox states of the water column and have an associated isotopic fractionation factor, which produces either an isotopically heavier or lighter reactant relative to the substrate. Because nitrogen isotopes are redox sensitive, they can be used to characterize depositional environments (Holmes et al., 1996; Altabet et al., 1998; Lehmann et al., 2002; Hulth et al., 2005; Knies et al., 2007; Quan and Falkowski, 2008; Strapoć et al., 2010; Godfrey and Glass, 2011). However, accurate representations of water column processes using nitrogen isotopes rely on well-preserved sedimentary organic matter (Altabet and Francois, 1994).

Preservation of organic matter in the water column and sediment is a function of oxygen exposure, duration of particle sinking as a consequence of particle size and water depth, sedimentation rate, accumulation rate, and sealing efficiency (Mobius et al., 2011; Robinson et al., 2012). The more intensely organic matter is oxidized, the more degraded it becomes, which has been shown to alter the $\delta^{15}N$ values of exported nitrogen from its initial values (Mobius et al., 2011). Conversely, when oxygen levels are low and degradation of organic matter is limited, the initial $\delta^{15}N$ values of organic matter are not subject to diagenetic alteration (Mobius et al., 2011; Adigwe, 2012; Robinson et al., 2012). This results in final bulk sedimentary $\delta^{15}N$ values that reflect the initial $\delta^{15}N$ values if organic matter. Therefore, organic matter must be preserved in both the water column and in the sediments after deposition in order for the final bulk

sedimentary $\delta^{15}N$ values to reflect the redox state of the water column (Higgins et al., 2010; Higgins et al., 2012; Robinson et al., 2012). Despite the variability imposed on the initial $\delta^{15}N$ values of organic matter by degradation in the water column, Robinson et al. (2012) found that $\delta^{15}N$ values of exported nitrogen reflect the water column redox states and becomes recorded in the sediments as bulk sedimentary $\delta^{15}N$.

The initial $\delta^{15}N$ values of the exported nitrogen are a direct result of the reactions that make up the nitrogen cycle. Of those reactions, nitrogen fixation, nitrification, and denitrification are predominant through geologic time (Figure 1), which are responsible for the nitrogen input, conversion between redox states, and nitrogen output of the water column (Wada, 1980; Bowen, 1988; Checkley and Miller, 1989; Schlessinger, 1997; Karl and Michaels, 2001; Faure and Mensing, 2005; Gondwe et al., 2008). Nitrogen fixation is responsible for introducing a significant amount of bioavailable nitrogen into the water column by fixing atmospheric N_2 (Quan et al., 2008; Quan and Falkowski, 2009; Whittaker et al., 2011). Nitrogen fixation is characterized by a relatively small, negative initial $\delta^{15}N$ value (Sachs and Repeta, 1999; Quan and Falkowski, 2009). The effects of nitrogen fixation on the nitrate pool results in a relatively small fractionation factor (Wada, 1980; Checkley and Miller, 1989; Karl and Michaels, 2001; Quan et al., 2008), which is then incorporated into organic matter by organisms and accumulated in the sediments.

Denitrification, unlike nitrogen fixation, is responsible for the output of nitrogen from the water column, converting nitrate into nitrogen gas. Incomplete denitrification of organic matter in the water column generally has a large, positive fractionation factor on the nitrate pool (Wada, 1980; Mariotti et al., 1981; Voss et al., 2001; Robinson et al., 2006; Quan et al., 2008, Quan and Falkowski, 2009; Adigwe, 2012). Fractionation associated with denitrification preferentially selects the lighter ^{14}N-rich nitrate, leaving behind an isotopically heavy substrate, which is

reflected in the organic matter that is incorporated into sediment (Robinson et al., 2006; Quan et al., 2008; Quan and Falkowski, 2009).

Denitrification is not the only reaction responsible for the output of nitrogen from the water column; in fact the anammox process removes bioavailable nitrogen from the water column through the reaction between NH_4 and NO_2 to produce N_2 and H_2O (Canfield et al., 2005; Gruber, 2008). Similar to denitrification, anammox is inhibited by oxygen in the water column (Jetten et al., 2001), and at low oxygen concentrations NH_4 cannot be oxidized. The complexities associated with the relationship between anammox and oxygen require that anaerobic ammonium oxidizers and aerobic nitrifying bacteria to coexist under oxygen limiting conditions (Hulth et al., 2005; Gruber, 2008). Nitrifiers oxidize the ammonium to nitrite and deplete the water column of oxygen, while anammox bacteria convert nitrite and the remaining ammonium to N_2 (Hulth et al., 2005). In several cases, the depth interval of the anammox process is narrowly constrained to anoxic waters where nitrate and nitrite were present (Dalsgaard et al., 2003; Kuypers et al., 2003). Although it has been identified in marine ecosystems as the cause of fixed nitrogen loss in oxygen minimum zones (OMZ) (Dalsgaard et al., 2003; Kuypers et al., 2003; Hulth et al., 2005; Kuypers et al., 2005), the quantitative significance of this process is still unknown. As for the nitrogen isotopic signals of anammox, Rayleigh fractionation may explain the pattern of the initial $\delta^{15}N$ values, where the product is progressively isotopically heavier than the reactant (Xing and Clark, 2011). Though this study was performed in a wastewater treatment plant, anammox has been identified in marine systems (Dalsgaard et al., 2003; Kuypers et al., 2003; Hulth et al., 2005; Kuypers et al., 2005) and it is assumed that the isotopically heavy products will eventually be transferred to the sediments. Because anammox is still relatively unfamiliar and its effects on the nitrogen isotope signal on geologic timescales are unknown, we account for its influence under the denitrification heading. Since the initial $\delta^{15}N$ value of organic matter deposited in sediments is representative of the fractionation processes within the water column (Robinson et al., 2006;

Quan et al., 2008; Quan and Falkowski, 2009), measuring the bulk $\delta^{15}N$ in sediments can be used to infer which reaction is predominant, nitrogen fixation or denitrification.

It is now evident now water column redox states during sediment deposition indirectly affect the sedimentary nitrogen isotopic values (Quan et al., 2008; Quan and Falkowski, 2009), and can be explained by evaluating the varying effects on the initial $\delta^{15}N$ values of organic matter caused by different oxygen concentrations in the water column (Quan and Falkowski, 2009). Nitrifying bacteria are inherent aerobes, whereas denitrifiers are generally confined to suboxic zones in the water column and are considerably complex organisms (Zumf, 1997; Granger et al., 2008; Kritee et al., 2012). Though high levels of oxygen in the water column can hinder the denitrification process (Canfield et al., 2005; Robinson et al., 2006; Quan et al., 2008; Quan and Falkowski, 2009), denitrifiers have the ability to survive in the presence of low levels of oxygen (Canfield et al., 2005; Quan et al., 2008; Quan and Falkowski, 2009).

When concentrations of oxygen in the water column are negligible, nitrate formation is limited, which leads to the complete usage of water column nitrate via denitrification. This results in the denitrification reaction going to completion, and thus no measurable isotopic fractionation. Therefore, the initial $\delta^{15}N$ values of organic matter produce in anoxic environments reflect the nitrogen fixation process, which produces relatively small initial $\delta^{15}N$ values (Figure 2; Canfield et al., 2005; Quan et al., 2008; Quan and Falkowski, 2009). With the increase of oxygen in the water column to suboxic environments, oxidation of ammonium via nitrification takes place. This produces nitrate in the water column, which is made available for denitrifying bacteria. The increased degree of denitrification results in an increase in the initial $\delta^{15}N$ values of organic matter produced in suboxic environments, which is illustrated in Figure 2 (Quan et al., 2008; Quan and Falkowski, 2009). At a critical point, oxygen concentrations in the water column become too high and begin inhibiting the denitrification process. This critical point represents the

Figure 1. Basic schematic of the nitrogen cycle in marine settings with the associated redox states. The horizontal scale represents the redox states associated with each nitrogen form. Each reaction has an associated fractionation factor affecting the $\delta^{15}N$ values of the product. NH_4^+ and NO_3^- are both assimilated to produce N_{org}, which eventually is deposited in the sediments (Figure taken from Galloway, 2005 (after Karl, 2002)).

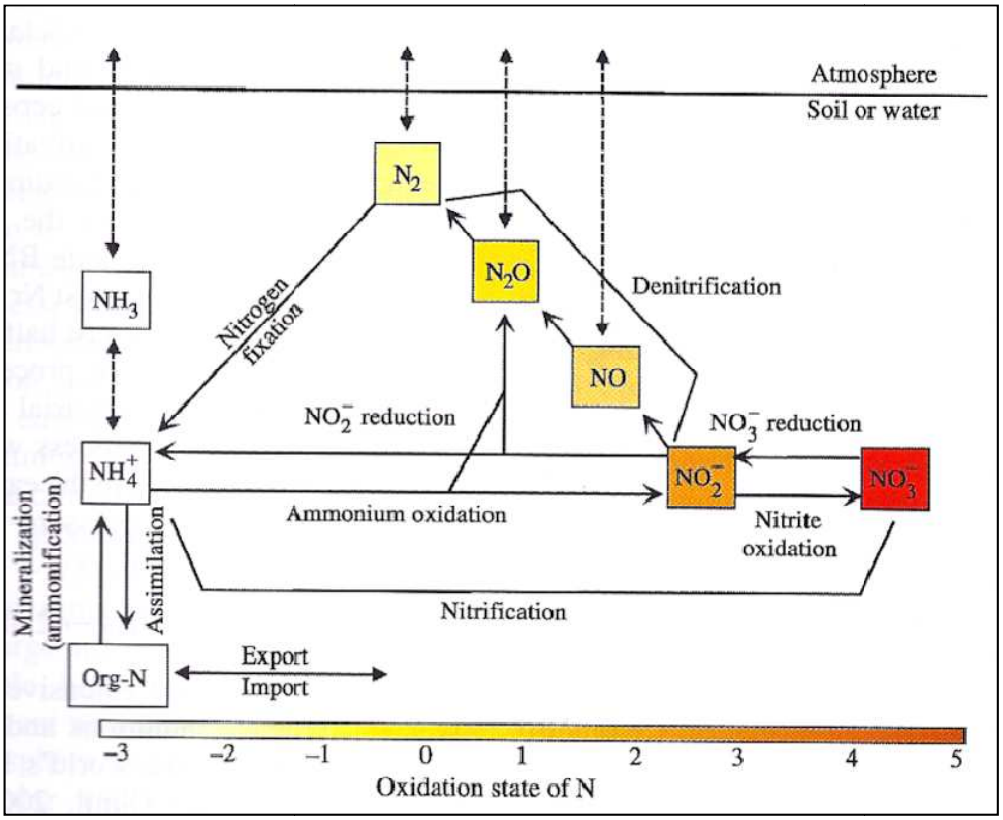

maximum rate of denitrification, and at this point denitrification and nitrate production are in kinetic equilibrium (Quan et al., 2008; Quan and Falkowski, 2009). A decrease in degree of denitrification results in relatively small initial $\delta^{15}N$ values of organic matter produced in oxic environments, as shown in Figure 2. The nitrogen isotopic signal of the residual nitrate becomes incorporated into the sediments via organic matter produced by microorganisms, which reflects the processes within the water column.

A conceptual model linking the bulk sedimentary $\delta^{15}N$ values to water column oxygenation (Figure 2) can be used to interpret the different environments in which sediments

were deposited. This model explains that denitrification occurs at a specific range of oxygen concentration levels, where enough oxygen in the water column must be present to produce nitrates, but not too high to hinder the denitrification process (Quan et al., 2008, Quan and Falkowski, 2009). These approximate O_2 concentrations are constrained to a narrow range from 15 to 40 μM (Quan et al., 2008), which is characteristic of suboxic environments (Robinson, 2006; Quan et al., 2008; Quan and Falkowski, 2009). In general, relatively small and depleted bulk sedimentary $\delta^{15}N$ values can be attributed to sediments deposited in either fully oxic or anoxic waters. On the other hand, intervals that contain bulk sedimentary $\delta^{15}N$ values that are relatively enriched can be attributed to sediments deposited in suboxic waters.

It is apparent now that the bulk sedimentary $\delta^{15}N$ values reflect the redox states of the water column at the time of deposition. Studies have investigated the degradation and preservation of organic matter and their affects the initial $\delta^{15}N$ values of organic matter (Altabet and Francois, 1994; Galbraith et al., 2004; Robinson et al., 2012). As mentioned earlier, preservation of organic matter is a function of oxygen exposure time, duration of particle sinking as a consequence of particle size and water depth, sedimentation rate, accumulation rate and sealing efficiency (Mobius et al., 2011; Robinson et al., 2012). Therefore, preservation is greatest in oxygen minimum zones (OMZ), areas of high sedimentation rate, and sediment with high sealing efficiency (Robinson et al., 2012). Where oxygen concentrations are high, organic matter degradation is suggested to result in bulk sedimentary $\delta^{15}N$ values that are enriched relative to the initial $\delta^{15}N$ values (Mobius et al, 2011). However, despite degradation of organic matter, the $\delta^{15}N$ values of sedimentary organic nitrogen reflect the initial $\delta^{15}N$ values of the sinking flux of the organic matter (Robinson et al., 2012). Experimental data from recent studies show that bulk sedimentary $\delta^{15}N$ values primarily reflect the $\delta^{15}N$ of exported nitrogen (Higgins et al., 2010; Higgins et al., 2012; Robinson et al., 2012), which in turn reflect the redox state of the water column. Though the mechanism(s) responsible for post-depositional alterations of the bulk

Figure 2. A schematic representation of the effects of oxygen (O_2) concentrations on the bulk sedimentary $\delta^{15}N$ values. As O_2 concentrations increase from zero, the bulk sedimentary $\delta^{15}N$ values increase to a maximum critical point. As O_2 concentrations continue to rise, bulk sedimentary $\delta^{15}N$ values decrease. Anoxic and oxic conditions result in relatively low depleted bulk sedimentary $\delta^{15}N$ values, while suboxic conditions result in relatively large enriched bulk sedimentary $\delta^{15}N$ values. Modified from Quan and Falkowski (2009).

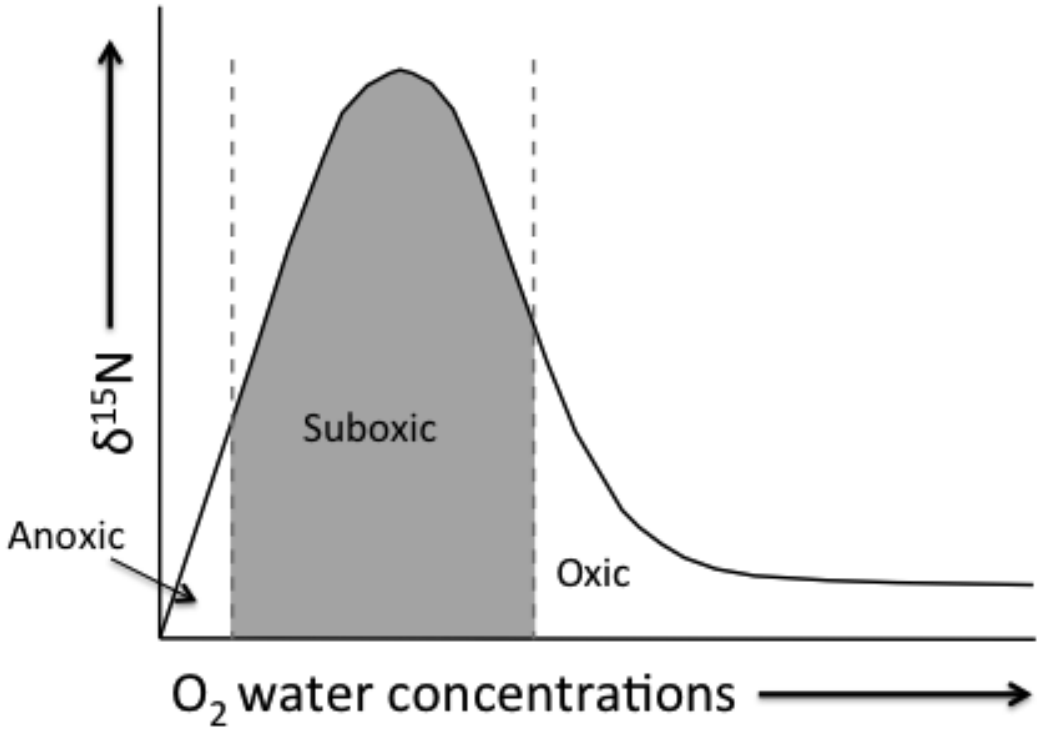

sedimentary $\delta^{15}N$ values are relatively unknown, this study aims to determine the effects thermal maturity have on the initial $\delta^{15}N$ values of deposited organic matter.

Major mechanisms for post-burial alteration of sedimentary organic matter are sedimentary diagenesis and thermal maturity, the latter of which defines the level of rock alteration that includes the generation of hydrocarbons. The evolution of organic nitrogen through thermal maturity initially exhibits a relative increase in weight percent (wt. %) nitrogen due to the preferential loss of carbon, oxygen and hydrogen in the early oil window (R_o ~0.55%) (Boudou et al., 1984a; Boudou et al., 2008). Similarly, a study measuring the nitrogen content of bitumen, aqueous solution and residual content with increasing thermal maturity indicates an

increase of nitrogen concentrations in the aqueous phase with the increase of thermal maturity (Barth et al., 1996). However, a study measuring nitrogen in kerogen and residual organic matter found nitrogen concentrations do not change until sediment enters the thermogenic gas window (R_o ~0.80%) (Barth et al., 1996; Vandenbroucke and Largeau, 2007; Boudou et al., 2008). Instead, nitrogen compounds changes with increasing maturity, and the amount of nitrogen reflects differences in the source organic matter (Vandenbroucke and Lagreau, 2007). The relationship between nitrogen concentrations and thermal maturity is not straightforward and depends on the phase of organic matter: i.e. kerogen, bitumen, or aqueous phase (Barth et al., 1996, Vandenbroucke and Lagreau, 2007).

The increase of nitrogen concentrations in the oil window observed by Boudou et al. (1984a) and Boudou et al. (2008) is accompanied with little to no fractionation, however bulk sedimentary $\delta^{15}N$ values seem to increase when maturity levels reach the gas window (Boudou et al., 1984a). Simple thermal degradation would result in a Rayleigh-type isotope fractionation (Boudou et al., 2008), leaving the sedimentary organic matter rich in ^{15}N (Zhu et al., 2000; Oldenburg et al., 2007). Bulk sedimentary $\delta^{15}N$ values of immature sediments are depleted relative to mature sedimentary organic matter, and further more bulk sedimentary $\delta^{15}N$ values of post-mature sedimentary organic matter are more enriched than both (Zhu et al., 2000). Therefore, assuming that the organic matter in this study was deposited under similar depositional environments, the initial $\delta^{15}N$ values should be similar. If these initial $\delta^{15}N$ values are affected by thermal maturity, then the measured bulk sedimentary $\delta^{15}N$ values should exhibit isotopic enrichment from immature to mature sediments and mature to post-mature sediments. However, if the bulk sedimentary $\delta^{15}N$ values do not follow this enrichment pattern, then possibly the redox state of the water column during sediment and organic matter deposition may influence the bulk sedimentary $\delta^{15}N$ values greater than thermal maturity.

This study tests the effects of thermal maturity and redox conditions on the bulk sedimentary $\delta^{15}N$ values of organic-rich shale to improve understanding of the response of nitrogen isotopes to fundamental geologic processes. Samples were gathered from 3 wells in the Anadarko Basin and one outcrop in the Ozark Plateau (Figure 3). The sample distribution covers tectonically shallow, intermediate, and deep geologic environments, which exhibit an array of maturity levels from the oil window to the upper part of the thermogenic gas window. The samples were analyzed using Isotope Ratio Mass Spectrometry (IRMS) for isotopic compositions, an Elemental Analyzer (EA) for total nitrogen and total carbon concentrations, and Inductively Coupled Plasma-Mass Spectrometry (ICP-MS) for concentration data of major, trace, and rare-earth elements. Thermal maturity (R_o) values were measured directly for the ROETUN and H2B cores; therefore those measurements will be used. However, for the CO1A core, thermal maturity was projected using isoreflectance maps from Cardott (2012). As for the JMOC samples, vitrinite reflectance was identified using conodont color alteration indices. The purpose of this study is to 1) use the isotopic and elemental compositions to provide insight to the depositional environments represented by the samples, 2) test for the effects of thermal maturity on the nitrogen isotopic composition of marine shale, and 3) further understand what influences the nitrogen isotopic signal of marine sediment. To test the effects of thermal maturity on the nitrogen isotopic compositions of the marine shale, a few assumptions were made: i) the sedimentary organic matter of the marine shale in this study contains similar initial $\delta^{15}N$ values, which was a result of similar redox water column conditions during sediment deposition, ii) the sedimentary organic matter of the marine shale in this study is of a similar source, and iii) hydrocarbon production rates of the marine shale in this study remained constant through time.

The validity of assumptions (i) and (ii) will be evaluated in this study using the data collected. However, the data collected is insufficient to determine the hydrocarbon production rate of the marine shale in this study, therefore assumption (iii) is presumed valid. If assumption

(i) is in fact invalid, then the bulk sedimentary $\delta^{15}N$ values should reflect the different water column redox states, where anoxic and oxic environments result in relatively lower initial $\delta^{15}N$ values than suboxic environments (Wada, 1980; Mariotti et al., 1981; Checkley and Miller, 1989; Sachs and Repeta, 1999; Karl and Michaels, 2001; Voss et al., 2001; Robinson et al., 2006; Canfield, 2005; Quan et al., 2008; Quan and Falkowski, 2009). However, whether assumption (i) is valid or invalid, the potential for thermal maturity effects on the $\delta^{15}N$ values can still be addressed by evaluating the relationships between the bulk sedimentary $\delta^{15}N$ values and their sample locations, depths within the basin and respective thermal maturity values. If assumption (ii) is in fact invalid, then organic $\delta^{13}C$ values at each sample location would exhibit different isotopic signals, as well as the initial $\delta^{15}N$ values of organic matter (Peters et al., 1978; Wada et al., 1987; Jasper and Gagosian, 1990; and Kuramoto and Minagawa, 2001). The plot showing the relationship of the organic $\delta^{13}C$ values between the sample locations can be used to evaluate the validity of assumption (ii).

CHAPTER II

STUDY AREA

2.1 Geologic History

This study focuses on Woodford Shale in the Anadarko Basin, and Chattanooga Shale (Woodford equivalent) in the Ozark Plateau to compare the effects of thermal maturity on the nitrogen isotopes. The four sample locations consists of three cores located within the Anadarko Basin, Reotzal UN-1 (ROETUN), the Hall 2-B (H2B), and the Cement Ordovician 1-A (CO1A) and one outcrop located in Jane, MO (JMOC) in the Ozark Plateau (Figure 3). The depositional history of what is now the Anadarko Basin began when Iapetan rifting occurred in a structure commonly referred to as the Southern Oklahoma Aulacogen (SOA) during Cambrian time (Cardott and Lambert, 1982; Gallardo and Blackwell, 1999; Watson, 2008). The rift was subsequently filled with igneous rocks (Cardott and Lambert, 1982; Johnson, 1989; Gallardo and Blackwell, 1999; Watson, 2008). Post-rift subsidence of the SOA occurred through Mississippian time (Cardott and Lambert, 1982; Johnson, 1989; Gallardo and Blackwell, 1999; Watson, 2008). Subsidence resulted in a large accumulation of sediment, predominantly carbonate with lesser shale and sandstone (Figure 4; Johnson, 1989; Watson, 2008). These sediments became the early Paleozoic Timbered Hills Group, Cambrian-Ordovician Arbuckle Group, Ordovician Simpson and Viola Groups, Ordovician Sylvan Shale, and Ordovician-Devonian Hunton Group (Johnson, 1989; Watson, 2008). Carbonate deposition occurred largely in relatively shallow water and kept pace with slow subsidence rates (Rechlin, 2003; Watson,

Figure 3. Base map of the study area showing Oklahoma and neighboring states showing sample locations. The location of the outcrop and the wells traverses across the Anadarko basin from the Ozark Plateau, representing different depths of the Woodford. The Jane, MO outcrop is located on the Ozark Plateau and the wells are located in the Anadarko Basin, indicated by the light blue shaded region. The following sample locations range from shallowest to deepest: Jane, MO outcrop, Roetzal UN-1, Hall 2-B, and Cement Ord-1A. Modified from Johnson (2008).

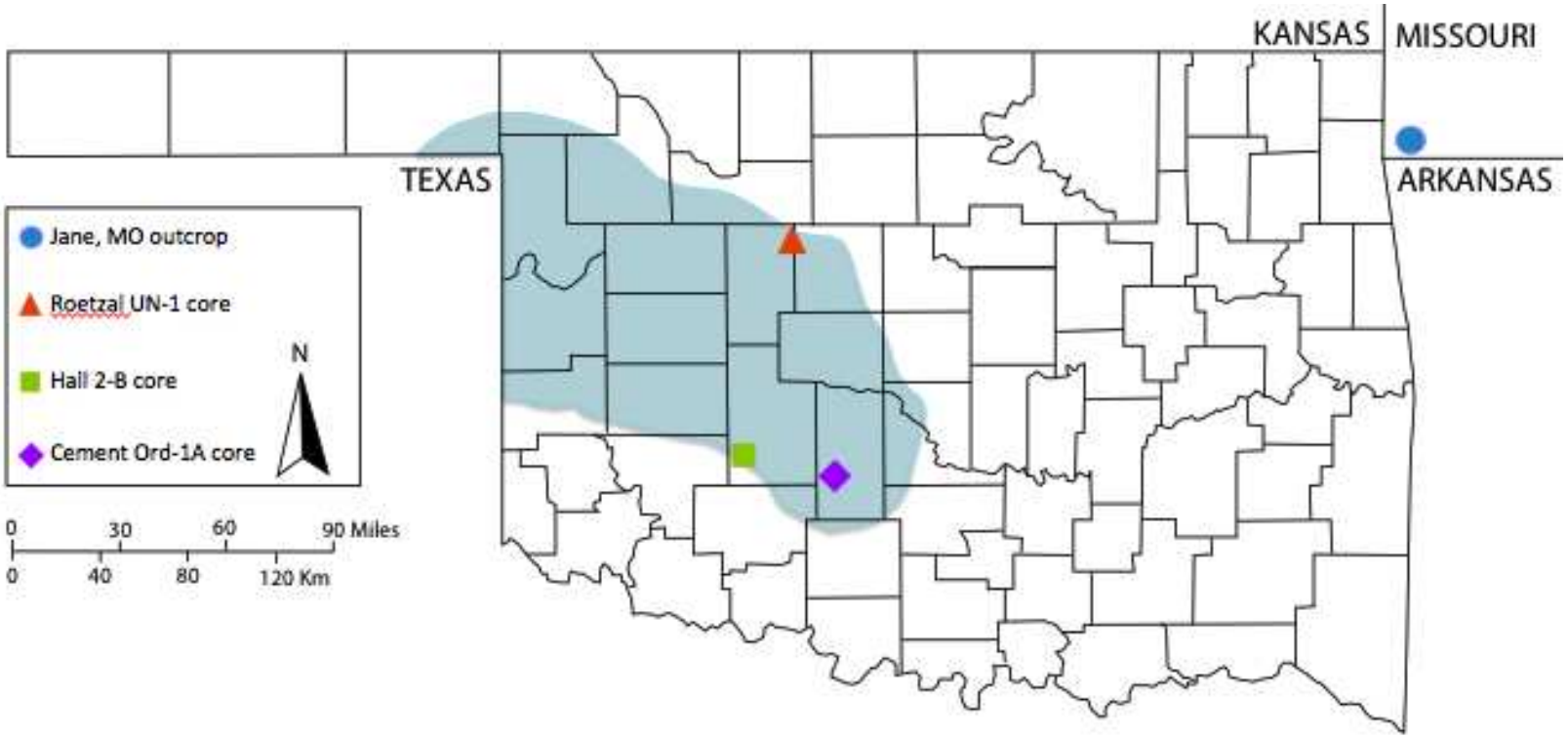

2008).

Eustatic sea-level fluctuations were evident throughout early Paleozoic time by cycles observed in the Arbuckle Group (Franseen et al., 2004) and unconformities in the Hunton Group (Kuykendall and Fritz, 2001). The unconformities were most likely a result of lowstands of relative sea level. A significant lowstand in Middle Devonian time produced a regional unconformity between the Hunton Group and the Woodford Shale (Cardott and Lambert, 1982; Kuykendall and Fritz, 2001). At points of greater erosion, the Hunton is completely eroded away and absent from the stratigraphy. Sea-level rise is recorded by the deposition of organic-rich sediment, such as the Woodford Shale.

Woodford Shale deposition extended into Early Mississippian time, when an epicontinental sea covered most of present day North America (Figure 4; Cardott and Lambert, 1982; Ettensohn, 2009; Johnson, 1989; Watson, 2008). The deepest portion of the sea arguably existed within the SOA (Roberts and Mitterer, 1992). The relative abundance of organic matter (maximum 4.8%) suggests that the Woodford was deposited in anoxic waters, however a recent study identified that the depositional environments of the Woodford Shale sediments vary between anoxic and suboxic (Romero and Philp, 2012). As stated previously, preservation of organic matter increases as oxygen concentrations decrease. The Woodford Shale consists of organic-rich bands that alternate between clay- and silica-rich. The silica-rich intervals can be attributed to the intensification of wind and upwelling episodes resulting in radiolarian and sponge productivity, which promoted organic-rich siliceous ooze (Roberts and Mitterer, 1992). In contrast, the more clay-rich shale intervals were deposited during long periods of low siliceous productivity and less dilution by organic matter (Roberts and Mitterer, 1992). The Woodford Shale is divided into three members: lower, middle, and upper.

Each member exhibits this alternating pattern of siliceous and clay intervals. It was suggested that the Lower Woodford Shale was deposited during the early stages of the Late Devonian – Early Mississippian transgression, while the Middle Woodford was deposited at the time of relative sea-level highstand and the Upper Woodford was deposited in the late stages when sea-level had already begun to fall (Lambert, 1993). On average, the clay content of the Woodford Shale decreases from the Lower to the Upper Woodford, which has an inverse relationship with the silica content (Lambert, 1993; Caldwell, 2011). On average, the TOC content of the Woodford Shale exhibits the greatest content in the Middle unit, while the Lower and Upper display lower percentages (Caldwell, 2011). It has been estimated that the entire Woodford Shale was deposited during a 10 to 15 million-year timespan and that sedimentation rates were faster for the siliceous layers than the argillaceous layers (Roberts and Mitterer, 1992).

During Woodford deposition, present-day North American continental platform (i.e., the southern Laurussian platform) was located in the southern tradewind belt (Figure 4). Figure 4 is a map after Ettensohn (2009) that shows the various rack types and facies that were deposited during late Devonian (Frasnian-Famennian). Woodford sediments were deposited during a major marine transgression that inundated the continental platform, facilitating widespread black shale deposition (Ettensohn, 2009; Over and Barrick, 1990). A stratified water column with oxygen-deficient bottom waters caused by the transgression during Woodford sedimentation was interpreted by Over and Barrick (1990) via conodont biofacies. Conodont, pyrite, and phosphate nodule concentrations are suggestive of a major transgressive event at or near the Frasnian-Famennian boundary (Over 1992).

During Woodford deposition, several topographic highs supplied the Anadarko basin with sediment. The Ouachita Embayment and the adjacent continental platform were topographic areas that received sediment from the central Kansas uplift (part of the Transcontinental Arch) the Chautauqua Arch, the St. Francois Mountains, and the Texas Arch (Johnson, 1989) (Figure 5).

Figure 4. Paleogeographic reconstruction map of present day North America during Late Devonian (Ettensohn, 2009). The study area is located approximately 30° south of the equator and circled in red. An epicontinental sea covers a majority of present day North America. Sedimentation was predominantly marine with little detrital influence. Figure adapted from Ettensohn (2009).

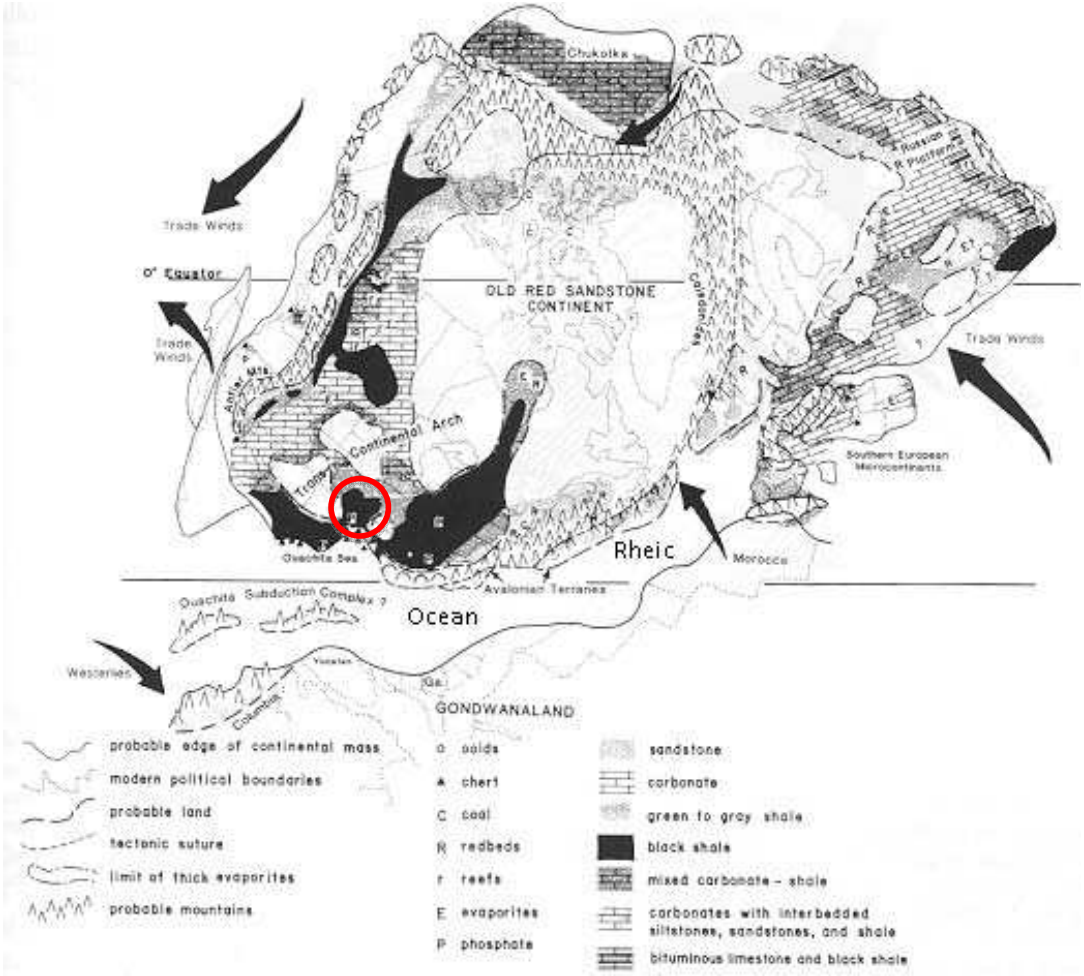

The SOA was apparently a major depocenter (Lambert 1993). During Woodford deposition, the SOA appears to have been tectonically quiescent. Major deformation of the SOA began during the Pennsylvanian (Morrowan). Crustal shortening occurred in the southeastern portion of the basin associated with Ouachita thrust belt and the Wichita Uplift (Cardott and Lambert, 1982; Johnson, 1989). Reverse faulting in the Wichita Uplift was directed principally northeastward

Figure 5. Map of south-central United States, showing approximate location of the Oklahoma Basin and other surrounding structures. Southern Oklahoma Aulacogen is dashed in red and correlates to the depocenter of the Anadarko basin with an axis trending northwest-southeast. Modified from Johnson (1989).

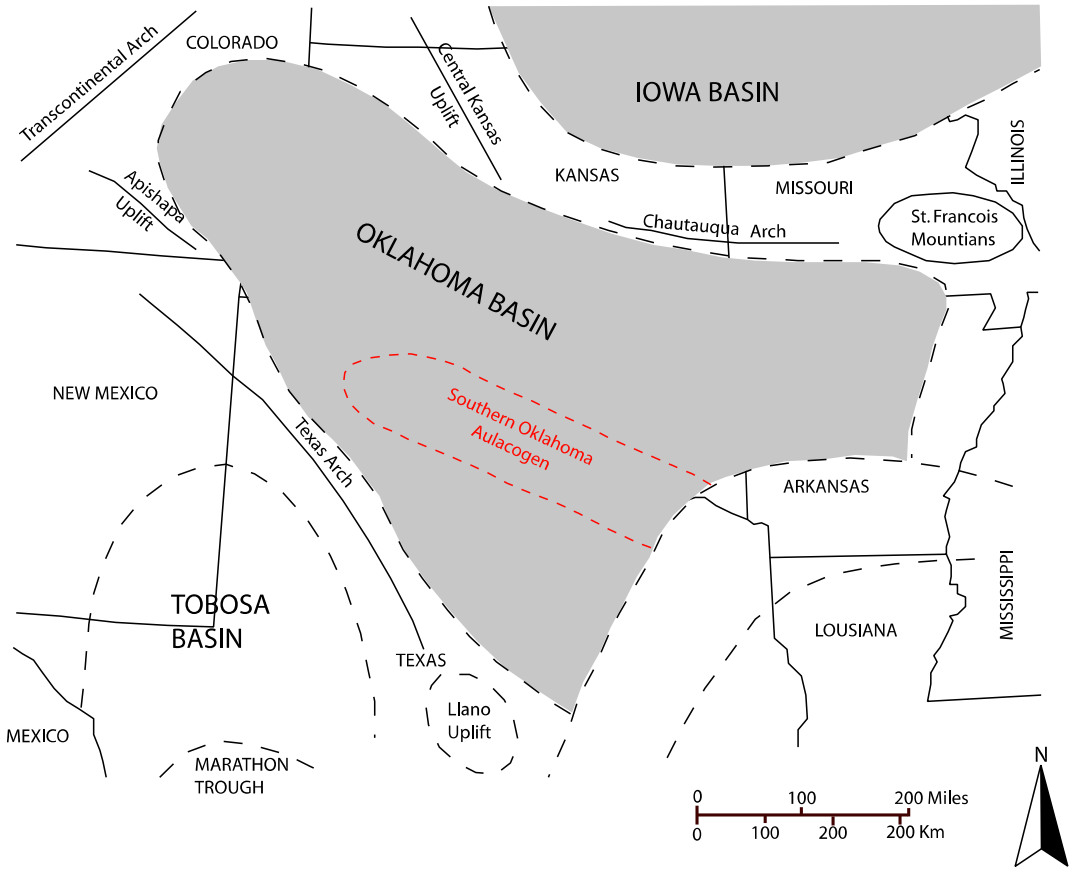

and was a major cause of subsidence of the Anadarko Basin (Figure 6; Johnson, 1989). The Cimarron Arch bounds the western portion of the Anadarko Basin and is thought to have formed near the end of the tectonic activity that produced the Wichita Uplift (Johnson,1989). Toward the end of the Paleozoic, the Ozark Plateau was uplifted (Brown, 2004), as tectonic activity continued through the Pennsylvanian to Early Permian (Johnson, 1989).

2.2 Geothermal History

In the Anadarko Basin, the Woodford shale is at a shallow depth on the shelf of the basin and dips to the depocenter, reaching a maximum depth of approximately 26,000 ft adjacent to the

Figure 6. Cross-section stretching from the Wichita Uplift to the Ozark Plateau (Johnson, 2008). As shown below, Cambrian through Pennsylvanian sediments have been subsided as a result of crustal shortening associated with the Wichita Uplift in the Pennsylvanian. Figure modified from Johnson (2008).

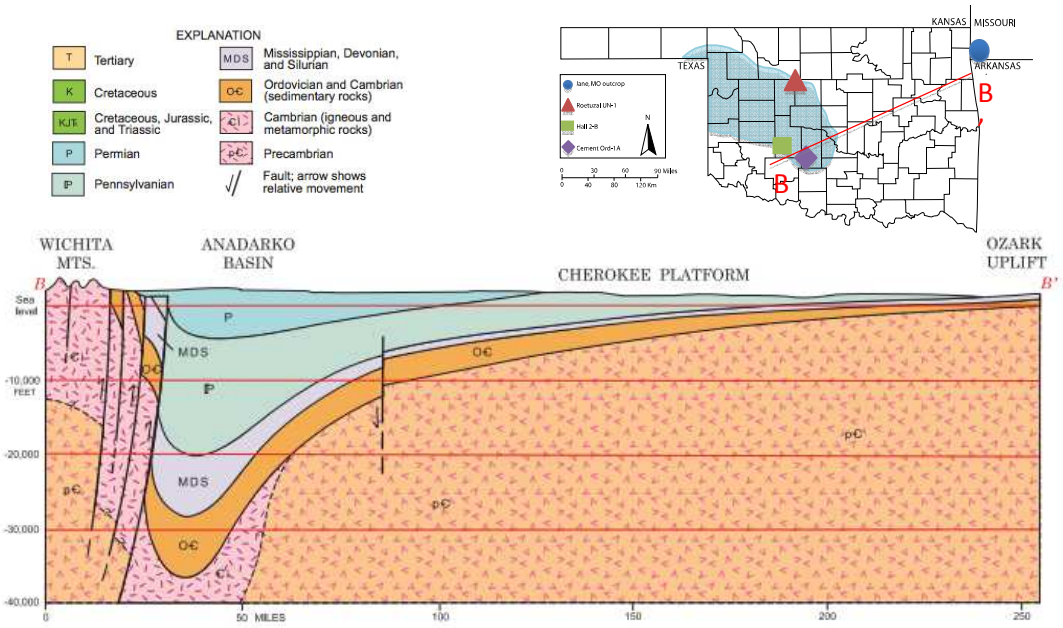

Wichita Uplift (Cardott and Lambert, 1982; Gallardo and Blackwell, 1999; Caldwell, 2011). Several techniques have been used to calculate the thermal maturity of the shale to assess hydrocarbon generation and reservoir properties. Vitrinite reflectance (R_o) is a method used to measure the percentage of light reflected by the vitrinite maceral in the shale. Vitrinite reflectance (R_o) of the Woodford Shale ranges from 0.5% in the shelf regions to 4.9% in the depocenter of the basin (Cardott and Lambert, 1982; Cardott, 1989, 2012) indicating that thermal maturity increases with depth. In the Arkoma Basin, R_o values range from 0.6% in the shelf regions in the north to greater the 4.0% in the depocenter of the basin near the Ouachita orogen (Cardott, 2012). R_o values from the Arkoma basin decrease as they approach the Ozark Plateau, indicating low R_o values for the samples gathered at the Jane, MO outcrop.

In locations where samples are inaccessible or unsampled, maturation values can be estimated conodont color-alteration index (CAI) (Epstein et al., 1977). CAI values from several studies suggest that conodonts darken to black as R_o values approach 3.6%, and then lighten to white/translucent as R_o values continue to increase (Epstein et al., 1977; Rejebian et al., 1987; Dean and Turner, 1995). However, no CAI values for the Woodford Shale in the Anadarko Basin and Ozark Plateau have been found in literature. Given the location of the JMOC outcrop, its present-day depth and geologic history, it is projected that CAI values would indicate vitrinite reflectance values equivalent to those just at the oil generation window.

2.3 Previous Work

Although little work has been done regarding the bulk sedimentary $\delta^{15}N$ values of the Woodford Shale in the Anadarko basin, a study comparing the Woodford shale to the Caney shale in the Arkoma basin showed relatively low bulk sedimentary $\delta^{15}N$ values for the Woodford Shale, ranging from -0.8 to 3.9 ‰ with an average of 1.6 ± 1.6 ‰ (Adigwe, 2012). The relatively low bulk sedimentary $\delta^{15}N$ values were attributed to anoxic conditions in the sediment-water column during deposition (Adigwe, 2012). The relative abundance of the bulk total nitrogen (TN) in the Woodford Shale in the Arkoma Basin exhibits relatively low values, ranging from 0.1 % to 0.8 % with an average of 0.3 % ± 0.2 % (Adigwe, 2012). The organic $\delta^{13}C$ values of the Woodford Shale in the Arkoma Basin range from -27.2 ‰ to -30.1 ‰ with an average of -28.7 ± 0.8 ‰ (Adigwe, 2012). The relative abundance of total organic carbon (TOC) of the Woodford Shale in the Arkoma Basin ranges from 1.4 % to 8.0 % with an average of 5.4 ± 1.8 ‰ (Adigwe, 2012).

CHAPTER III

ANALYTICAL METHODS

3.1 Sample Preparation

Samples were collected at various depths from each of the cores, depending on core quality and regulations of the Oklahoma Petroleum Information Center core library in Norman, Oklahoma. JMOC samples were collected at 9-inch intervals, ROETUN samples were collected at 1- to 3-feet intervals, CO1A samples were collected at 2.5- to 7-feet intervals, and H2B samples were collected at a range from 6- to 7-feet intervals. Because of incomplete core recovery, poor core quality, or missing intervals, some parts of the Woodford Shale are absent in each core and result in gaps in the data. Once the samples were collected, they were transported to the Noble Research Center (NRC) at Oklahoma State University (OSU) to prepare for analysis. Approximately 20-50 mg of rock was crushed and ground to a powder using an agate mortar and pestle except for the case of CO1A samples, where a ceramic ball and mill was used. The crushed samples were then oven-dried for 24 hours at approximately 60°C, and stored in vials.

3.2 Stable isotopic compositions and elemental concentrations

The powdered samples were analyzed for total organic carbon (TOC), total nitrogen (TN), bulk nitrogen isotopic compositions ($\delta^{15}N_{bulk}$), and organic carbon isotopic compositions ($\delta^{13}C_{org}$). The analysis was conducted at the Henry Bellman Research Center at Oklahoma State University where the nitrogen and carbon isotope ratios ($^{15}N/^{14}N$ and $^{13}C/^{12}C$, respectively) and elemental concentrations (TN and TOC, respectively) were determined using a Costech elemental

analyzer (EA) coupled with a ThermoFinnigan Delta Plus isotope ratio mass spectrometer (IRMS). The isotopic compositions are reported relative to Vienna Pee Dee Belemnite (VPDB) standard for $\delta^{13}C_{org}$ and air N_2 for $\delta^{15}N_{bulk}$. The isotopic compositions are expressed in delta (δ) notation in per mil (‰):

$$\delta(‰) = \left[\frac{R_{sample}}{R_{standard} - 1}\right] x\ 1000$$

where $R_{sample} = {}^{13}C/{}^{12}C_{sample}$ or ${}^{15}N/{}^{14}N_{sample}$ and $R_{standard} = {}^{13}C/{}^{12}C_{VPDB}$ or ${}^{15}N/{}^{14}N_{air}$.

The raw data were calibrated using standards of known isotopic composition to correct for any isotopic offset. Acetanilide, NIST N3 (KNO_3), and USGS 40 (L-glutamic acid) standards were used for nitrogen isotope calibrations, while urea and USGS 40 standards were used for carbon isotope calibrations. Replicates of the nitrogen standards KNO_3 and USGS 40 had standard deviations of ± 0.1 ‰ and ± 0.2 ‰, respectively. Replicates of the $\delta^{15}N_{bulk}$ samples for the JMOC, ROETUN, CO1A and H2B had standard deviations of ± 0.3 ‰, ± 0.2 ‰, ± 0.2 ‰ and ± 0.5 ‰, respectively. Replicates of the carbon standards urea and USGS 40 had standard deviations of ± 0.1 ‰. Replicates of the $\delta^{13}C_{org}$ samples for the JMOC, ROETUN, CO1A and H2B had standard deviations of ± 0.1 ‰, ± 0.3 ‰, ± 0.2 ‰ and ± 2.1 ‰, respectively. Standards were run every 10 samples to check for instrumental drift.

3.2.1 Total bulk nitrogen (TN) concentrations and $\delta^{15}N_{bulk}$ composition

To analyze for TN and $\delta^{15}N_{bulk}$, approximately 40 mg of each powdered sample was placed in tin boats. Minute amounts of the catalyst vanadium pentoxide were added to each sample to enhance combustion. The samples were then sealed and loaded into the autosampler to run through the Costech EA and ThermoFinnigan Delta Plus IRMS. As mentioned earlier, the acetanlide EA standard was used to calibrate for the elemental concentrations. The acetanilide EA standard produced a linear equation that was used to calibrate nitrogen and carbon elemental

concentrations of the samples. Acetanilide EA standard replicates had a standard deviation of ± 0.1 ‰. For each sample run, 3 samples were run in duplicates and 1 sample run in triplicate to estimate the precision, which was within the standard deviation of the average (± 0.5 ‰). Replicates of the TN samples for the JMOC, ROETUN, CO1A and H2B samples had standard deviations of ± 0.03 ‰, ± 0.2 ‰, ± 0.2 ‰ and ± 0.2 ‰, respectively. Replicates of the TOC samples for the JMOC, ROETUN, CO1A and H2B had standard deviations of ± 0.1 ‰, ± 0.2 ‰, ± 0.2 ‰ and ± 0.3 ‰, respectively.

3.2.2 Total organic carbon (TOC) concentrations and $\delta^{13}C_{org}$ compositions

To analyze for TOC and $\delta^{13}C_{org}$, approximately 40 mg of each sample was placed in silver boats. The samples were initially decarbonated using 25% HCl, then rinsed with ultrapure water (UHQ) to ensure no acid remained in the sediments. Subsequently, the samples were further decarbonated using concentrated HCl until the reaction ceased. Once the effervescence ceased, the samples were oven dried at approximately 60°C for approximately 3 days to ensure complete dryness. Once dried, the catalyst vanadium pentoxide was added to each of the decarbonated samples to enhance combustion, and then the samples were sealed. The samples were run through the Costech EA and ThermoFinnigan Delta Plus IRMS. As mentioned earlier, the Acetanlide EA standard was used to calibrate for the elemental concentrations.

3.3 Thermal maturity

Vitrinite reflectance (R_o) values were obtained for the sample locations using data and isoreflectance maps from both the Anadarko and Arkoma Basins from Cardott (2012). Cardott (2012) measured vitrinite reflectance from two of the cores in this study, ROETUN and H2B. For these samples, mean random vitrinite reflectance measurements were taken at different depth intervals throughout the Woodford Shale. The mean random vitrinite reflectance measurements were gathered from 81 wells in the Anadarko Basin and 117 wells from the Arkoma Basin, which

were used to construct the isoreflectance maps. Because vitrinite reflectance of the CO1A and JMOC locations was not directly measured on the actual samples, thermal maturity level of these locations was projected based on the isoreflectance maps of the Anadarko Basin for the CO1A and Arkoma Basin for the JMOC from Cardott (2012). Unfortunately, the location of the JMOC outcrop relative to the Arkoma Basin results in high uncertainty in the R_o projection; therefore a thermal maturity proxy was used to confirm projected values. The proxy used was conodont color alteration indices (CAI) for the JMOC outcrop samples.

3.4.1 Conodont color alteration index (CAI)

Conodont color alteration index (CAI) was used to analyze the thermal maturity of Woodford samples gathered from the Jane, MO (JMOC) outcrop. A wide variety of conodont species have been identified surrounding the Devonian – Carboniferous boundary within the Upper Woodford (Over, 1992), therefore samples were gathered from the top 1-meter of the JMOC outcrop at 10 cm intervals and labeled JMOC 1-C (top of measured section) through JMOC 10-C (bottom of measured section). A trench was dug to uncover fresh shale. 1-gallon Ziploc bags were filled with shale and brought back to the Hazardous Research Laboratory (HRL) at OSU. If rock samples were large, they were broken to roughly the size of a silver dollar. Approximately 1 kg of sample was placed in a 5-gallon bucket and treated with approximately 2 liters of 32% hydrogen peroxide (H_2O_2) to break it down. Once the reaction ceased, the sample was rinsed and sieved with a 35 mesh (425 μm) sieve stacked on top of a 120 mesh (125 μm) sieve. Samples greater than 35 mesh sieve were treated with H_2O_2 to further disaggregate the samples. This process was repeated until the entire sample passed through a 35-mesh sieve. Sample fractions larger than 120 mesh were gathered and dried in a Quincy Lab Inc. Model 40AF Lab Oven at a temperature of 100°C for 24 hours. Once dry, the samples were examined for conodonts using a McBain Systems Leica S6E binocular stereomicroscope equipped with a Leica L2 light. Conodonts were identified and separated to analyze for color

alteration analysis, based on the Epstein et al. (1977) color chart. Well-preserved conodont specimens were sent to the OSU Electron Microscopy Lab (OSUEML) for scanning electron microscope (SEM) imaging (Appendix A).

3.5 Trace element analysis

Trace element analysis was performed on individual samples using the Ultratrace-6 method performed by Activation Laboratories Ltd. The Ultractrace-6 method combines a four-acid digestion with the analysis of Fe and Mn using a Varian inductively coupled plasma (ICP) and analysis of V, U, Zn and Mo a Perkin Elmer Sciex ELAN inductively coupled plasma mass spectrometer (ICP-MS). Activation Laboratories Ltd. specifies, for the ICP portion of the analysis, that approximately 0.25 grams of each sample was first digested with hydrofluoric acid (HF), followed by a mixture of nitric (HNO_3) and perchloric acids. The samples were sequentially heated to incipient dryness. Next, samples were brought back into solution via aqua regia. It should be noted that with this digestion, certain minerals might only be partially dissolved, including zircon, monazite, sphene, gahnite, chromite, cassiterite, rutile, and barite. On the other hand, sulfide sulfur will be completely solubilized. The samples were subsequently analyzed using the Varian ICP. Quality control for each batch includes running 5 method reagent blanks, 10-in house controls, 10 sample duplicates, and 8 certified reference materials. An additional quality control was performed as a part of instrumental analysis to ensure quality in the areas of instrumental drift.

Additional elemental concentrations were determined by ICP-MS using the multi-acid digestion listed above. The samples were diluted and analyzed on the Perkin Elmer Sciex ELAN ICP-MS. A series of test runs was performed to ensure proper mechanical function, including one blank that is run for every 40 samples, an in-house control for every 20 samples, and digested standards for every 80 samples. In addition, a digestion duplicate was analyzed every 15 minutes, and instrument recalibration occurred every 80 samples.

A total of 60 trace elements were analyzed for various trace metals in each sample, including but not limited to Fe, V, U, Zn, Mo, and Mn. The assumption was made that all calcium (Ca) in each sample is in the inorganic form of calcium carbonate. Therefore, the trace element concentrations were corrected for carbonate. Samples also were normalized to Al to eliminate any detrital trace element input in order to exclusively analyze marine trace element concentrations. Therefore, correcting the trace element concentrations for the amount of terrigenous input and carbonate influence will produce trace element concentrations of marine carbonate-free samples.

CHAPTER IV

RESULTS

4.1 Jane, MO outcrop samples (JMOC)

The outcrop description indicates alternating silica- and clay-rich intervals in the Upper, Middle and Lower Woodford, however the Middle Woodford displayed more clay-rich than silica-rich intervals (Figure 7). The clay-rich intervals are generally more fissile than the silica-rich intervals. The more fissile shale intervals are dark grey to black in color, whereas the silica-rich intervals are grey to dark grey. Pyrite was identified in the Upper, Middle and Lower Woodford, however pyrite nodules ranging from 0.25 in to 1 in in diameter were identified in a thin layer within the Upper Woodford. During conodont identification, various fossils were found in the Upper Woodford, however the specific species were not identified. Horizontal burrows were identified in the Upper, Middle and Lower Woodford samples.

4.1.1 Total bulk nitrogen (TN) concentrations and $\delta^{15}N_{bulk}$ isotopic ratios for the Jane, MO outcrop (JMOC) samples

The nitrogen isotopic compositions of the bulk samples ($\delta^{15}N_{bulk}$) of the Woodford Shale intervals of the JMOC outcrop samples are presented in Table 1a. The range of the sedimentary $\delta^{15}N_{bulk}$ values for the Woodford Shale interval for the JMOC samples is of approximately 1.4 ‰, where the lowest concentration is 7.0 ‰ and the highest is 8.4 ‰. The average sedimentary $\delta^{15}N_{bulk}$ of all JMOC samples is 7.7 ‰ ± 0.3 ‰. The plot of the $\delta^{15}N_{bulk}$ values versus depth for the Woodford Shale intervals of the JMOC samples is shown in Figure 8a.

Figure 7. Stratigraphic columns and core descriptions of the Woodford Shale for the Roetzal UN-1 (ROETUN), Cement Ord 1-A (CO1A) and Hall 2-B (H2B) core. Notice that the H2B core only has the Middle and Lower Woodford, while the ROETUN and CO1A core has the three subdivisions. However, the quality of core covering the Middle Woodford in the ROETUN core was poor, therefore no samples were gathered. As for the H2B, the Lower Woodford was absent from the cored section.

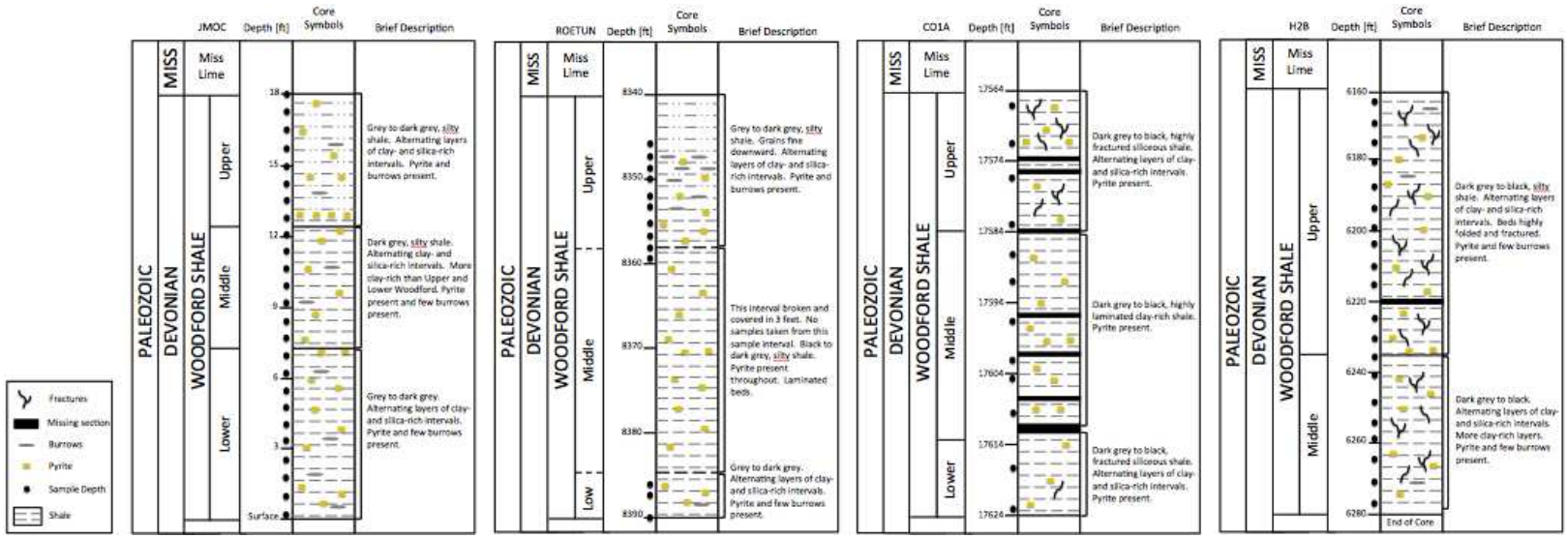

Table 1a. Bulk sedimentary nitrogen isotopic values ($\delta^{15}N_{bulk}$), organic carbon isotopic values ($\delta^{13}C_{org}$), bulk elemental nitrogen (TN) and total organic carbon (TOC) concentrations for the Woodford Shale samples of the Jane, MO outcrop (JMOC) samples. The solid grey line at the top of the first row = top of upper Woodford, dashed grey line = top of the middle Woodford, and dashed and dotted grey line = top of the lower Woodford.

Footage (ft)	Formation Name	$\delta^{15}N_{bulk}$ (‰)	$\delta^{13}C_{org}$ (‰)	TN (%)	TOC (%)
18	Upper Woodford	8.0	-29.9	0.09	1.1
17.25	Upper Woodford	7.7	-29.4	0.09	1.2
16.5	Upper Woodford	7.9	-29.5	0.08	1.2
15.75	Upper Woodford	7.6	-29.7	0.10	1.1
15	Upper Woodford	8.3	-30.4	0.09	1.2
14.25	Upper Woodford	7.5	-29.8	0.10	0.9
13.5	Upper Woodford	8.0	-29.9	0.07	0.8
12.75	Upper Woodford	7.8	-29.6	0.06	0.7
12	Middle Woodford	8.0	-28.3	0.07	0.9
11.25	Middle Woodford	7.3	-48.1*	0.08	1.1
10.5	Middle Woodford	7.8	-47.5*	0.13	1.2
9.75	Middle Woodford	7.2	-48.4*	0.12	1.4
9	Middle Woodford	7.7	-29.3	0.17	1.2
8.25	Middle Woodford	7.6	-29.4	0.12	1.3
7.5	Middle Woodford	8.4	-29.7	0.12	1.3
6.75	Lower Woodford	7.2	-29.7	0.14	1.2
6	Lower Woodford	7.5	-29.8	0.12	1.0
5.25	Lower Woodford	8.0	-29.4	0.10	1.0
4.5	Lower Woodford	7.5	-29.4	0.11	1.2
3.75	Lower Woodford	7.6	-29.8	0.09	1.1
3	Lower Woodford	7.0	-29.8	0.12	0.8
2.25	Lower Woodford	7.5	-29.9	0.13	1.4
1.5	Lower Woodford	7.7	-29.8	0.13	1.4
0.75	Lower Woodford	7.7	-28.0	0.10	1.3
0	Lower Woodford	7.7	-30.1	0.15	1.5
	Averages	7.7 ± 0.3	-29.6 ± 0.5	0.11 ± 0.03	1.1 ± 0.2
	Ranges	7.0 to 8.4	-30.4 to -28.0	0.1 to 0.2	0.7 to 1.5

* Anomalously low values

Table 1b. Bulk sedimentary nitrogen isotopic values ($\delta^{15}N_{bulk}$), organic carbon isotopic values ($\delta^{13}C_{org}$), bulk elemental nitrogen (TN) and total organic carbon (TOC) concentrations for the Woodford Shale samples of the Roetzal UN-1 (ROETUN) core samples. The solid grey line at the top of the first row = top of upper Woodford, dashed grey line = top of the middle Woodford, and dashed and dotted grey line = top of the lower Woodford. In this core, the entire middle Woodford was missing.

Depth (ft)	Formation Name	$\delta^{15}N_{bulk}$ (‰)	$\delta^{13}C_{org}$ (‰)	TN (%)	TOC (%)
-8346	Upper Woodford	9.2	-29.7	0.1	0.7
-8348	Upper Woodford	8.4	-28.3	0.0	0.5
-8349	Upper Woodford	9.6	-31.3	0.0	0.7
-8350	Upper Woodford	9.4	-30.7	0.1	1.3
-8353	Upper Woodford	7.9	-29.5	0.1	0.7
-8354	Upper Woodford	8.3	-31.9	0.4	1.2
-8356	Upper Woodford	7.0	-31.7	0.3	1.0
-8357	Upper Woodford	9.5	-29.7	0.3	0.4
-8358	Upper Woodford	8.2	-31.4	0.7	2.2
-8359	Upper Woodford	8.6	-31.2	0.6	2.1
-8386	Lower Woddford	8.9	-31.7	0.5	1.7
-8387	Lower Woddford	6.5	-31.4	0.6	2.3
-8390	Lower Woddford	7.7	-30.9	0.1	0.8
	Averages	8 ± 1	-31 ± 1	0.3 ± 0.3	1.2 ± 0.7
	Ranges	6.5 to 9.6	-31.9 to -28.3	0.0 to 0.7	0.4 to 2.3

The results of the elemental nitrogen concentrations (wt. %) of the bulk sedimentary nitrogen (TN) for the JMOC samples are presented in Table 1a. The wt. % TN of the Woodford Shale in the JMOC samples range from 0.06 % to 0.16 %, with an average of 0.11 ± 0.03 ‰. The plot of the wt. % TN versus depth for the JMOC samples is shown in Figure 8a. The wt. % TN of the Woodford Shale intervals increases from 0.08 % to 0.15 % as depth increases from the Upper Woodford to the Lower Woodford.

Table 1c. Bulk sedimentary nitrogen isotopic values ($\delta^{15}N_{bulk}$), organic carbon isotopic values ($\delta^{13}C_{org}$), bulk elemental nitrogen (TN) and total organic carbon (TOC) concentrations for the Woodford Shale samples of the Cement Ord 1-A (CO1A) core samples. The solid grey line at the top of the first row = top of upper Woodford, dashed grey line = top of the middle Woodford, and dashed and dotted grey line = top of the lower Woodford.

Depth (ft)	Formation Name	$\delta^{15}N_{bulk}$ (‰)	$\delta^{13}C_{org}$ (‰)	TN (%)	TOC (%)
-17567	Upper Woodford	4.4	-30.6	0.3	0.6
-17571	Upper Woodford	7.0	-30.3	0.2	0.5
-17576	Upper Woodford	7.0	-30.3	0.2	0.7
-17583	Upper Woodford	5.5	-30.7	0.4	1.2
-17588.5	Middle Woodford	3.8	-30.9	0.7	1.5
-17591	Middle Woodford	5.0	-30.6	0.9	2.1
-17596	Middle Woodford	2.1	-30.8	0.5	1.2
-17601	Middle Woodford	2.7	-30.8	0.5	1.4
-17605	Middle Woodford	4.2	-30.7	0.6	1.4
-17611	Middle Woodford	2.6	-30.7	0.5	2.4
-17617	Lower Woodford	4.2	-30.3	0.7	1.9
-17623	Lower Woodford	3.5	-31.0	0.6	1.5
	Averages	4 ± 2	-30.7 ± 0.2	0.5 ± 0.2	1.4 ± 0.6
	Ranges	2.1 to 7.0	-31.0 to -30.3	0.2 to 0.9	0.5 to 2.4

4.1.2 Total organic carbon (TOC) concentrations and $\delta^{13}C_{org}$ isotopic ratios for the Jane, MO outcrop (JMOC) samples

The stable carbon isotopic compositions ($\delta^{13}C_{org}$) are listed in Table 1a. The carbon isotope data denoted by asterisks (Figure 1a) exhibit anomalously low $\delta^{13}C_{org}$ values that are not within the range for the Woodford Shale (-28 ‰ to -32 ‰) in this study and other studies (Da Lewan, 1983; Wang and Philp, 1997; Adigwe, 2012). Though the cause is unknown at this time, these data will not be used in subsequent analyses until further evaluation. The $\delta^{13}C_{org}$ values with the asterisk are inaccurate measurements as a result of incomplete decarbonation, therefore these samples will not be considered in the subsequent evaluation of the JMOC location. The

Table 1d. Bulk sedimentary nitrogen isotopic values ($\delta^{15}N_{bulk}$), organic carbon isotopic values ($\delta^{13}C_{org}$), bulk elemental nitrogen (TN) and total organic carbon (TOC) concentrations for the Woodford Shale samples of the Hall 2-B (H2B) core samples. The solid grey line at the top of the first row = top of upper Woodford, dashed grey line = top of the middle Woodford, and dashed and dotted grey line = top of the lower Woodford.

Depth (ft)	Formation Name	$\delta^{15}N_{bulk}$ (‰)	$\delta^{13}C_{org}$ (‰)	TN (%)	TOC (%)
-6163	Upper Woodford	9.0	-31.9	0.2	1.5
-6169	Upper Woodford	9.2	-32.3	0.4	2.1
-6175	Upper Woodford	8.8	-32.4	0.8	2.7
-6181	Upper Woodford	8.9	-32.2	0.1	4.8
-6187	Upper Woodford	7.3	-31.2	0.2	1.5
-6193	Upper Woodford	8.0	-31.7	0.4	2.7
-6199	Upper Woodford	8.1	-32.1	0.3	2.6
-6205	Upper Woodford	8.3	-32.2	0.4	2.5
-6211	Upper Woodford	8.4	-31.9	0.5	2.8
-6217	Upper Woodford	7.7	-31.4	0.6	2.8
-6223	Upper Woodford	7.7	-31.1	0.6	3.6
-6229	Upper Woodford	6.2	-30.7	0.1	1.7
-6235	Upper Woodford	6.3	-30.7	0.1	1.7
-6241	Middle Woodford	7.9	-30.5	0.2	1.6
-6247	Middle Woodford	7.4	-30.9	0.3	2.0
-6253	Middle Woodford	6.1	-30.8	0.4	2.6
-6259	Middle Woodford	5.6	-31.6	0.6	3.2
-6265	Middle Woodford	5.3	-30.8	0.2	2.5
-6272	Middle Woodford	5.2	-31.0	0.3	3.1
-6278	Middle Woodford	5.2	-31.1	0.4	2.1
	Averages	7 ± 1	-31.4 ± 0.6	0.4 ± 0.2	2.5 ± 0.8
	Ranges	5.2 to 9.2	-32.4 to -30.5	0.1 to 0.8	1.5 to 4.8

Figure 8a. Cross-plots of bulk sedimentary nitrogen isotopic values ($\delta^{15}N_{bulk}$), organic carbon isotopic values ($\delta^{13}C_{org}$), bulk elemental nitrogen (Wt. N_{bulk}) and total organic carbon (TOC) concentrations with respect to depth for the Woodford Shale samples of the Jane, MO outcrop (JMOC) samples. The grey lines in this plot correspond to the grey lines in the Table 1.

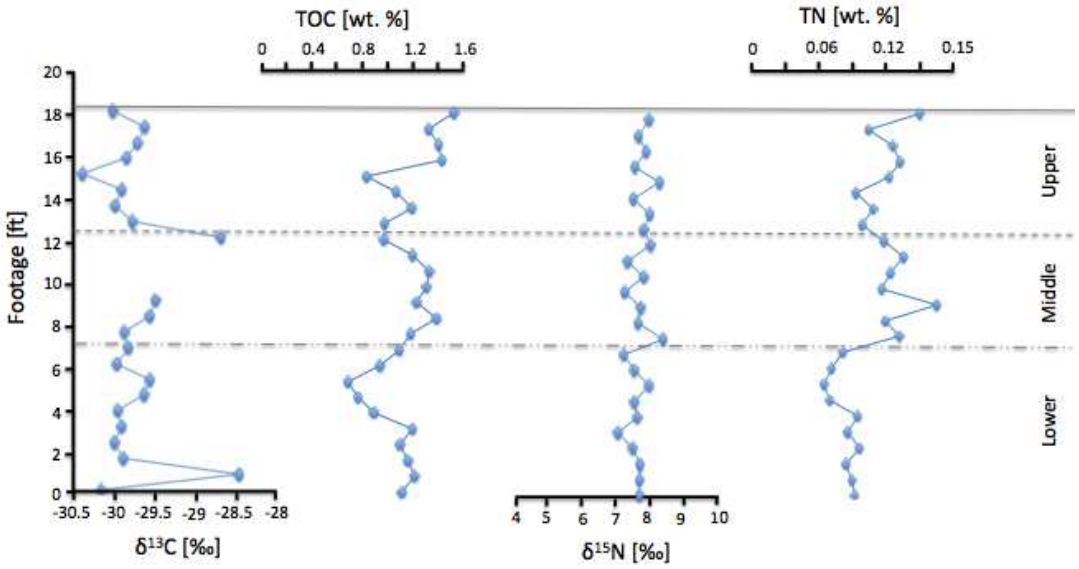

Figure 8b. Cross-plots of bulk sedimentary nitrogen isotopic values ($\delta^{15}N_{bulk}$), organic carbon isotopic values ($\delta^{13}C_{org}$), bulk elemental nitrogen (Wt. N_{bulk}) and total organic carbon (TOC) concentrations with respect to depth for the Woodford Shale samples of the Roetzal UN-1 (ROETUN) core samples. The grey lines in this plot correspond to the grey lines in the Table 1.

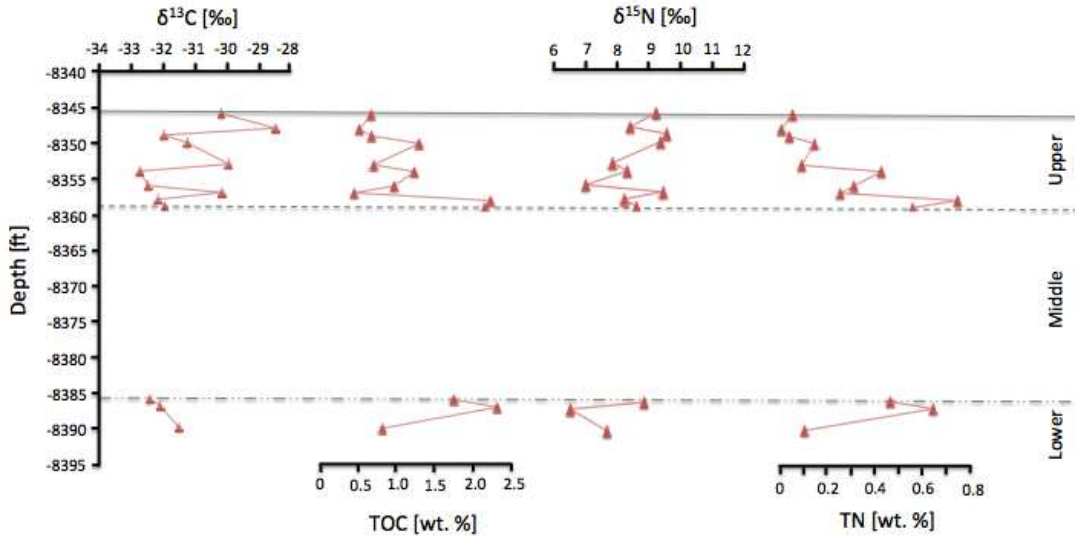

Figure 8c. Cross-plots of bulk sedimentary nitrogen isotopic values ($\delta^{15}N_{bulk}$), organic carbon isotopic values ($\delta^{13}C_{org}$), bulk elemental nitrogen (Wt. N_{bulk}) and total organic carbon (TOC) concentrations with respect to depth for the Woodford Shale samples of the Cement Ord 1-A (CO1A) core samples. The grey lines in this plot correspond to the grey lines in the Table 1.

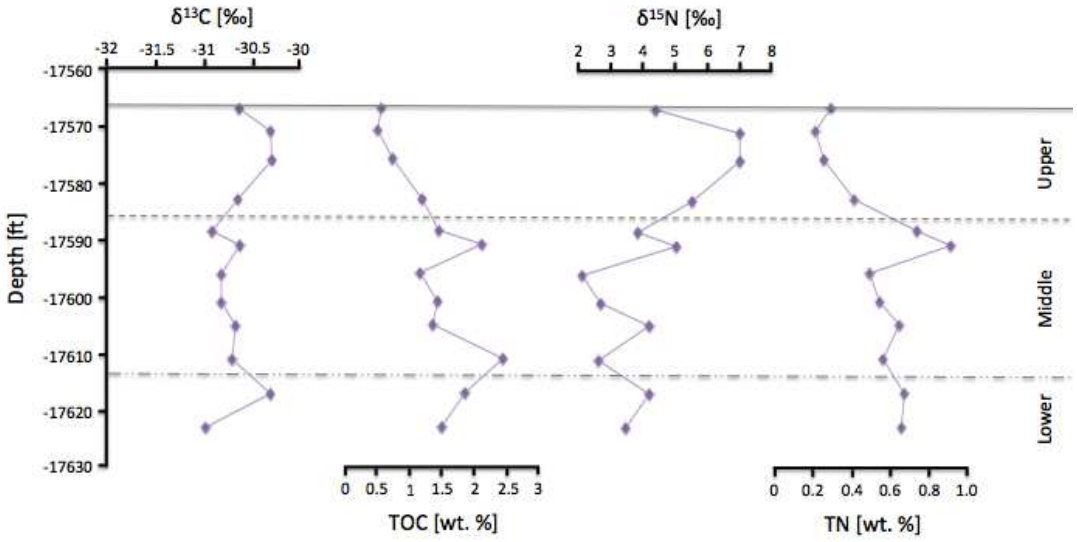

Figure 8d. Cross-plots of bulk sedimentary nitrogen isotopic values ($\delta^{15}N_{bulk}$), organic carbon isotopic values ($\delta^{13}C_{org}$), bulk elemental nitrogen (Wt. N_{bulk}) and total organic carbon (TOC) concentrations with respect to depth for the Woodford Shale samples of the Hall 2-B (H2B) core samples. The grey lines in this plot correspond to the grey lines in the Table 1.

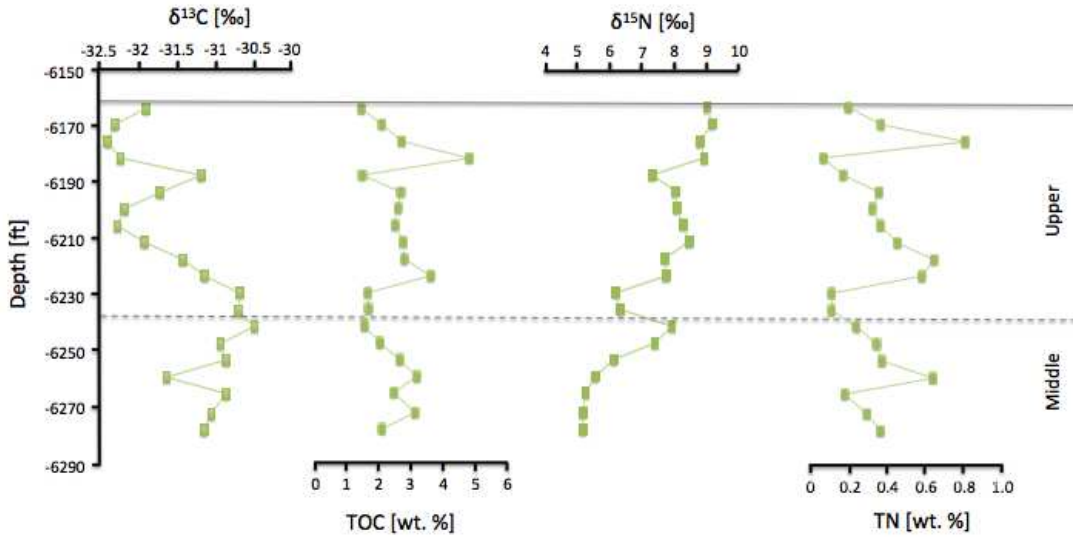

$\delta^{13}C_{org}$ values for the Woodford Shale in the JMOC outcrop samples are depleted relative to VPDB, ranging from -30.4 ‰ to -28.0 ‰ with an average of -29.6 ‰ ± 0.5 ‰. The $\delta^{13}C_{org}$ values of the JMOC samples display an increase from -29.9 ‰ in the Upper Woodford to -28.3 ‰ at the top of the Middle Woodford, then decrease to towards the bottom of the section where a significant peak is observed (Figure 8a).

The results of the elemental concentrations (wt. %) of the total organic carbon (TOC) for the JMOC samples are presented in Table 1a. The wt. % TOC of the Woodford Shale in the JMOC samples range from 0.7 % to 1.5 %, with an average of 1.1 ± 0.2 ‰. Plots of TOC versus depth are shown in Figures 8a, which display a general decrease with depth.

4.1.3 Conodont color alteration index (CAI) for the Jane, MO outcrop (JMOC) samples

Because the JMOC sample location was located out of the confines of the isoreflectance map of the Arkoma Basin (Figure 9b) from Cardott (2012), conodont CAI was used to identify the thermal maturity. Conodont species were identified in all but one sample interval, JMOC 9-C, and varied throughout. Though a variety of conodont species was recognizable within the sample intervals, only few were identifiable as the platform conodont Palmatoplepis gracilis. A Munsell soil chart was used to determine the color alteration of the different conodont species. The conodont color alterations ranged from very pale brown (10YR7/3) to dark brown (7.5YR3/2). The conodont color alteration index of these conodont species range from 1.5 to 2. Epstein et al. (1977) indicates that CAI 1.5 has a temperature range from 50 °C to 90 °C and CAI 2 has a temperature range from 60 °C to 140 °C. These temperature ranges are equivalent to oil mature source rocks with reflectance values ranging from 0.70 % to 1.3 % (Tables 2 and 3). Despite the large range, the majority of the samples are of lower maturity, which is consistent with thermal maturity values of the Woodford Shale in northern Arkansas (Carr, 1989). Therefore, the thermal maturity level 0.70 % will be used for the remainder of the study for the

Figure 9a. Isoreflectance map of the Anadarko Basin from Cardott (2012). The R_o values generally increase in value from north to south and the basin deepens. ROETUN and H2B cores have R_o values just inside the oil window, while the CO1A well has an R_o value within the gas window. These R_o values directly correlate to depth, where CO1A is the deepest, ROETUN is the intermediate and H2B is the shallowest. Note that CO1A is in the depocenter of the basin while ROETUN and H2B are on the shelf and basin margins.

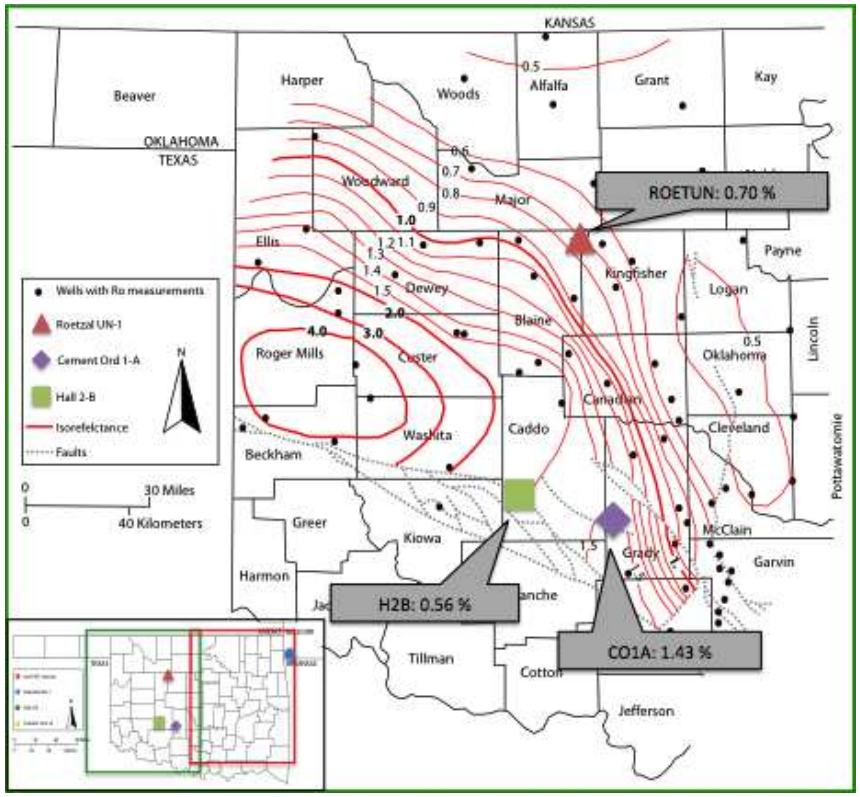

Figure 9b. Isoreflectance map of the Arkoma Basin from Cardott (2012). The R_o values generally increase from north to south. Unfortunately, the location of the JMOC results in great uncertainty when projecting the R_o value; therefore the R_o value cannot be projected using the Arkoma Basin isoreflectance map.

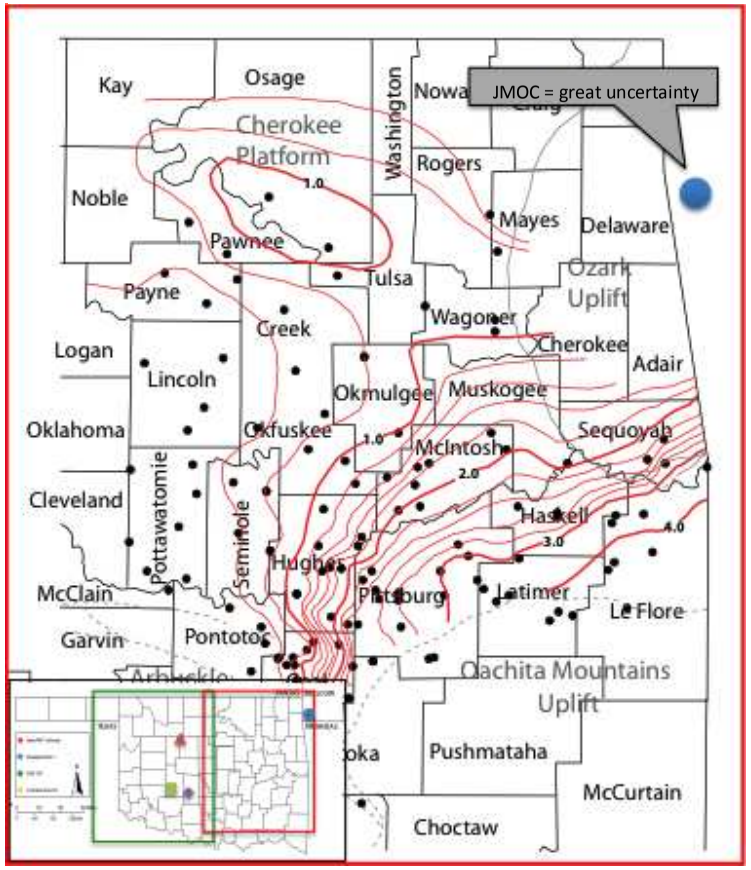

Table 2. Vitrinite reflectance values from Cardott R_o, conodont color alteration index (CAI) and vitrinite reflectance from CAI for the Woodford Shale intervals in the JMOC, ROETUN, CO1A, and H2B. The vitrinite reflectance value for the CO1A was projected using the isoreflectance map from the Anadarko Basin from Cardott (2012). CAI was only conducted on the JMOC samples.

Sample Location	Formation Name	Cardott Ro (%)	CAI	CAI Ro
JMOC	Woodford	-	1.5 - 2	0.7 - 1.3
ROETUN	Woodford	0.50 - 0.89	**	**
CO1A	Woodford	1.43 - 1.43*	**	**
H2B	Woodford	0.45 - 0.69	**	**

- Ro prediction(s) from Cardott (2012) high uncertainty

* Ro measurements predicted from Cardott (2012) isoreflectance maps

** CAI not evaluated

JMOC locations. These values are consistent with conodonts identified from Ordovician Everton and Cotter Formations of northern Arkansas and Mississippian Keokuk and Warsaw Formations of the Tri-State area (Missouri-Arkansas-Oklahoma boarders) (Sangster et al., 1994).

4.1.4 Trace element concentrations for the Jane, MO outcrop (JMOC) samples

Normalized and corrected trace element concentration for Fe, V, U, Zn, Mo, and Mn for the JMOC are presented in Table 4a, and their plots versus depth are shown in Figure 10a. These concentrations are normalized to aluminum (Al) and expressed as element/Al to evaluate the concentrations relative to the detrital fraction. Before normalizing the data to Al, element concentrations were corrected for calcium (Ca) content to adjust for inorganic substances with the

Table 3. Vitrinite reflectance values from conodont color alteration index (CAI), measurements from Cardott (2012), and isoreflectance maps from Cardott (2012) for the Woodford Shale intervals of the JMOC, ROETUN, CO1A and H2B samples. As mentioned earlier, the vitrinite reflectance value that will be used for the JMOC sample location is 0.70 %, ROETUN is 0.70 %, CO1A is 1.43 %, and H2B is 0.56 %. The vitrinite reflectance values indicate oil generation maturity for the JMOC, ROETUN and H2B, while the vitrinite reflectance values indicate gas generation maturity for the CO1A.

JMOC

Depth (ft)	Formation Name	Conodont CAI	CAI Ro (%)
18	Upper Woodford	1.5 to 2	0.70 to 1.30
17.25	Upper Woodford	1.5 to 2	0.70 to 1.30
16.5	Upper Woodford	1.5 to 2	0.70 to 1.30
15.75	Upper Woodford	1.5 to 2	0.70 to 1.30
15	Upper Woodford	1.5 to 2	0.70 to 1.30
14.25	Upper Woodford	1.5 to 2	0.70 to 1.30
13.5	Upper Woodford	1.5 to 2	0.70 to 1.30
12.75	Upper Woodford	1.5 to 2	0.70 to 1.30
12	Middle Woodford	1.5 to 2	0.70 to 1.30
0	Lower Woodford	1.5 to 2	0.70 to 1.30
	Average	1.5 to 2	0.70 to 1.30

ROETUN

Depth (ft)	Formation Name	Cardott Ro (%)
-8346	Upper Woodford	0.50
-8348	Upper Woodford	0.53
-8349	Upper Woodford	0.57
-8350	Upper Woodford	0.60
-8353	Upper Woodford	0.63
-8354	Upper Woodford	0.66
-8356	Upper Woodford	0.70
-8357	Upper Woodford	0.73
-8358	Upper Woodford	0.76
-8359	Upper Woodford	0.79
-8386	Lower Woddford	0.83
-8387	Lower Woddford	0.86
-8390	Lower Woddford	0.89
	Average	0.70

CO1A

Depth (ft)	Formation Name	Cardott Ro (%)
-17567	Upper Woodford	~ 1.43
-17571	Upper Woodford	~ 1.43
-17576	Upper Woodford	~ 1.43
-17583	Upper Woodford	~ 1.43
-17588.5	Middle Woodford	~ 1.43
-17591	Middle Woodford	~ 1.43
-17596	Middle Woodford	~ 1.43
-17601	Middle Woodford	~ 1.43
-17605	Middle Woodford	~ 1.43
-17611	Middle Woodford	~ 1.43
-17617	Lower Woodford	~ 1.43
-17623	Lower Woodford	~ 1.43
	Average	~ 1.43

H2B

Depth (ft)	Formation Name	Cardott Ro (%)
-6163	Upper Woodford	0.45
-6169	Upper Woodford	0.46
-6175	Upper Woodford	0.47
-6181	Upper Woodford	0.49
-6187	Upper Woodford	0.50
-6193	Upper Woodford	0.51
-6199	Upper Woodford	0.52
-6205	Upper Woodford	0.53
-6211	Upper Woodford	0.55
-6217	Upper Woodford	0.56
-6223	Upper Woodford	0.57
-6229	Upper Woodford	0.58
-6235	Upper Woodford	0.59
-6241	Middle Woodford	0.61
-6247	Middle Woodford	0.62
-6253	Middle Woodford	0.63
-6259	Middle Woodford	0.64
-6265	Middle Woodford	0.65
-6272	Middle Woodford	0.67
-6278	Middle Woodford	0.69
	Average	0.56

assumption that all of the calcium (Ca) in the samples was in the form of calcium carbonate. To evaluate the concentrations of trace element enrichment or depletion, the Post-Archean Average Shale from Australia (PAAS) standard reference (trace metal/Al ratios for the PAAS are presented in Appendix B) was used. PAAS provides an approximate baseline for the continental detrital mean (Cruse and Lyons, 2004) and is used to calculate the enrichment factors (EF) associated with each element.

The EF values were used to aid the interpretation of results. The individual EF values, the average EF values, and the range of the EF values for each sample location of the analyzed trace metals are presented in Tables 5a, b, c and d. For comparison, the average EF values are compiled in Table 6. EF is calculated as follows:

$$EF = \frac{\left(\frac{element}{AL}\right)sample}{\left(\frac{element}{AL}\right)shale}$$

where shale represents PAAS (Taylor and McClennan, 1985). The values for the various compositions and averages from PAAS are presented in the appendix. Element enrichment for each sample location relative to PAAS is expressed as EF > 1, and relative depletion is expressed as EF < 1 (Tribovillard et al., 2006; Brumsack, 2006).

High Al concentrations are observed in the Woodford intervals of the JMOC sample location and range from 4.04 % to 8.53 %, with an average of 6.6 % ± 0.8 %. Calcium concentrations are relatively low and are presented in the appendix. For the JMOC outcrop samples, Fe, V, U, Zn, Mo and Mn concentrations are significantly enriched relative to the PAAS standards (Figure 9a). To get a complete list of all the trace element concentrations analyzed, refer to Appendix C.

Fe concentrations of the JMOC outcrop samples decrease from the Upper Woodford to the Middle Woodford, where they become relatively consistent throughout the rest of the core

except for sample JMOC 10 (11.25 ft above surface (abs)). From top to bottom of the outcrop, the Fe concentration at sample JMOC 10 decreases significantly to 0.83 wt. %, but increases to the background concentration of approximately 1.65 %. From the top of the outcrop, V concentrations display a general and gradual increase from the top of the Upper Woodford (163.05 ppm) to the Lower Woodford (169.48 ppm), with few significant shifts. The first shift occurs at the top of the section between JMOC 1 (18 ft abs) and JMOC 2 (17.25 ft abs), where the V concentrations decrease from 163.05 ppm to 78.81 ppm, respectively. The other dramatic shift occurs at the top of the Lower Woodford between JMOC 18 (5.25 ft abs) and JMOC 19 (4.5 ft abs), where the V concentrations decrease from 116.19 ppm to 94.85 ppm, respectively. U and Mo concentrations mirror one another, where the Middle Woodford concentrations are enriched compared to the Upper and Lower Woodford intervals. Zn concentrations of the JMOC outcrop samples decrease from the top of the Upper Woodford (78.63 ppm) to the top of the Middle Woodford (58.35 ppm) and become constant throughout the remainder of the outcrop with a two significant spikes. These spikes occur at the base of the middle Woodford and at the top of the Lower Woodford. Mn concentrations decrease continuously from top of the outcrop (457.86 ppm) to the bottom of the outcrop (189.54).

4.2 Roetzal UN-1 (ROETUN) core samples

A core description of the ROETUN core (Figure 7) indicates that the Woodford contains alternating silica-rich and clay-rich intervals in the Upper, Middle and Lower Woodford, where the clay-rich intervals are generally more fissile than the silica-rich intervals. The more fissile shale intervals are laminated and dark grey to black in color, whereas the silica-rich intervals weakly laminated and grey. Approximately 25 ft of the Woodford Shale was covered by 3 ft, therefore no samples were collected from depths 8360 ft to 8385 ft. However, the sediments in this depth range were dark grey to black, silty shale. Clay clasts were identified in the Upper Woodford, while pyrite, and burrows are distributed sparingly throughout the core.

Table 4a. Concentrations of Fe, V, U, Zn, Mo and Mn for the Woodford Shale intervals of the JMOC outcrop samples, which were corrected for $CaCO_3$ influences and normalized to Al to disregard detrital influence. The horizontal grey lines represent the tops of the Woodford subdivisions.

Depth (ft)	Formation Name	Fe (%)	V (ppm)	U (ppm)	Zn (ppm)	Mo (ppm)	Mn (ppm)
18	Upper Woodford	2.15	163.05	7.29	78.63	9.35	457.86
17.25	Upper Woodford	1.88	78.81	11.88	74.62	0.51	383.37
16.5	Upper Woodford	1.70	131.61	7.53	65.73	4.61	298.01
15.75	Upper Woodford	1.89	143.59	6.43	62.39	5.81	310.93
15	Upper Woodford	1.65	111.93	4.99	69.03	2.45	233.60
14.25	Upper Woodford	1.65	133.80	6.08	53.79	8.04	449.65
13.5	Upper Woodford	1.54	132.04	5.79	70.01	11.88	506.66
12.75	Upper Woodford	1.59	126.00	5.03	58.35	4.00	378.56
12	Middle Woodford	1.76	163.97	5.99	82.89	5.78	266.82
11.25	Middle Woodford	0.83	158.85	6.56	56.54	8.38	248.77
10.5	Middle Woodford	1.57	132.88	8.94	47.94	18.49	360.92
9.75	Middle Woodford	1.72	142.11	10.98	52.85	26.03	394.40
9	Middle Woodford	1.54	150.03	9.37	72.78	14.78	309.36
8.25	Middle Woodford	1.70	156.86	8.01	131.60	9.43	245.59
7.5	Middle Woodford	1.76	171.09	8.83	57.80	10.55	289.05
6.75	Lower Woodford	1.69	169.48	7.43	58.65	10.58	266.53
6	Lower Woodford	1.66	166.08	6.33	50.52	8.58	286.80
5.25	Lower Woodford	1.61	116.19	4.29	187.33	1.53	220.81
4.5	Lower Woodford	1.41	94.84	4.09	110.11	1.53	211.70
3.75	Lower Woodford	1.61	131.89	4.94	54.93	2.32	189.12
3	Lower Woodford	1.52	144.69	5.14	58.56	6.04	172.74
2.25	Lower Woodford	1.64	145.93	5.95	57.94	3.83	200.11
1.5	Lower Woodford	1.76	151.51	6.33	58.36	6.27	223.00
0.75	Lower Woodford	1.62	140.32	6.47	56.50	9.31	194.67
0	Lower Woodford	1.55	135.21	5.76	59.71	5.66	189.54
	Averages	1.64 ± 0.22	139.71 ± 22.56	6.82 ± 1.96	71.50 ± 30.55	7.83 ± 5.72	291.54 ± 93.20
	Ranges	1.62 to 3.70	5.25 to 11.41	13.18 to 38.33	5.94 to 15.48	5.12 to 260.29	1.92 to 5.63

(-) = non-detect

Table 4b. Concentrations of Fe, V, U, Zn, Mo and Mn for the Woodford Shale intervals of the Roetzal UN-1 (ROETUN) samples, which were corrected for $CaCO_3$ influences and normalized to Al to disregard detrital influence. The horizontal grey lines represent the tops of the Woodford subdivisions.

Depth (ft)	Formation Name	Fe (%)	V (ppm)	U (ppm)	Zn (ppm)	Mo (ppm)	Mn (ppm)
-8346	Upper Woodford	0.59	57.53	3.53	48.47	1.33	101.89
-8348	Upper Woodford	0.11	25.94	1.30	29.42	0.50	75.47
-8349	Upper Woodford	0.52	48.89	3.30	48.69	0.90	159.78
-8350	Upper Woodford	-	166.17	5.98	102.97	0.91	130.10
-8353	Upper Woodford	-	81.63	2.90	42.40	1.00	319.20
-8354	Upper Woodford	1.48	734.14	8.52	1364.71	70.46	133.47
-8356	Upper Woodford	1.66	201.98	8.42	206.96	9.83	131.13
-8357	Upper Woodford	0.95	93.79	11.50	43.46	2.70	184.20
-8358	Upper Woodford	0.55	418.67	67.31	325.52	193.18	89.25
-8359	Upper Woodford	1.33	430.32	15.93	661.77	29.33	95.63
-8386	Lower Woddford	1.29	988.34	32.52	284.23	114.43	99.40
-8387	Lower Woddford	-	406.71	66.57	353.20	205.05	108.20
-8390	Lower Woddford	0.48	404.35	11.76	127.84	29.52	56.14
	Averages	0.89 ± 0.52	312.19 ± 294.74	18.43 ± 22.99	297.97 ± 373.27	50.70 ± 74.07	129.53 ± 66.52
	Ranges	0.21 to 3.25	1.73 to 65.89	4.19 to 217.14	3.46 to 160.55	5.00 to 2050.49	0.62 to 3.55

(-) = non-detect

Table 4c. Concentrations of Fe, V, U, Zn, Mo and Mn for the Woodford Shale intervals of the Cement Ord 1-A (CO1A) samples, which were corrected for $CaCO_3$ influences and normalized to Al to disregard detrital influence. The horizontal grey lines represent the tops of the Woodford subdivisions.

Depth (ft)	Formation Name	Fe (%)	V (ppm)	U (ppm)	Zn (ppm)	Mo (ppm)	Mn (ppm)
-17567	Upper Woodford	0.27	643.30	74.49	192.20	9.69	74.59
-17571	Upper Woodford	0.31	916.17	14.84	882.76	50.35	24.50
-17576	Upper Woodford	0.34	936.40	17.22	1005.61	51.05	37.99
-17583	Upper Woodford	0.36	935.77	21.99	1402.64	90.07	35.96
-17588.5	Middle Woodford	0.39	523.06	41.78	314.28	152.84	68.09
-17591	Middle Woodford	-	340.22	78.97	352.21	178.57	154.33
-17596	Middle Woodford	0.64	233.89	52.07	248.84	241.87	71.11
-17601	Middle Woodford	0.54	239.90	48.90	188.72	170.62	63.76
-17605	Middle Woodford	0.71	232.83	40.19	236.84	128.31	51.62
-17611	Middle Woodford	-	228.66	57.28	237.72	120.69	74.11
-17617	Lower Woodford	0.47	230.93	82.79	232.97	198.35	102.42
-17623	Lower Woodford	1.40	499.01	57.36	214.48	85.59	62.43
	Averages	0.54 ± 0.33	496.68 ± 294.78	48.99 ± 23.11	459.11 ± 404.38	123.17 ± 68.67	68.41 ± 34.20
	Ranges	0.53 to 2.75	15.24 to 62.43	47.87 to 267.05	22.20 to 165.02	96.93 to 2418.70	0.27 to 1.71

(-) = non-detect

Table 4d. Concentrations of Fe, V, U, Zn, Mo and Mn for the Woodford Shale intervals of the Hall 2-B (H2B) samples, which were corrected for $CaCO_3$ influences and normalized to Al to disregard detrital influence. The horizontal grey lines represent the tops of the Woodford subdivisions.

Depth (ft)	Formation Name	Fe (%)	V (ppm)	U (ppm)	Zn (ppm)	Mo (ppm)	Mn (ppm)
-6163	Upper Woodford	0.35	245.63	3.23	283.45	5.24	131.84
-6169	Upper Woodford	0.39	275.47	20.68	315.04	11.29	91.51
-6175	Upper Woodford	0.51	956.33	17.69	1155.00	52.68	70.78
-6181	Upper Woodford	0.17	81.38	1.64	130.10	3.81	30.32
-6187	Upper Woodford	0.21	884.36	7.90	1889.74	39.84	15.98
-6193	Upper Woodford	0.21	565.25	45.64	492.91	14.58	25.95
-6199	Upper Woodford	0.25	610.01	39.37	329.58	11.39	291.67
-6205	Upper Woodford	0.42	356.06	18.98	318.47	12.89	104.42
-6211	Upper Woodford	0.48	955.41	16.42	4212.54	115.61	40.01
-6217	Upper Woodford	0.57	518.20	7.35	292.78	13.69	54.27
-6223	Upper Woodford	0.82	376.89	8.40	337.71	20.69	182.05
-6229	Upper Woodford	0.19	890.60	4.20	2038.15	42.48	47.78
-6235	Upper Woodford	0.25	748.44	15.41	436.10	55.90	34.95
-6241	Middle Woodford	0.33	918.34	11.14	570.71	39.44	29.06
-6247	Middle Woodford	0.48	951.99	17.26	877.87	71.24	35.09
-6253	Middle Woodford	0.48	757.09	31.29	286.08	115.47	47.95
-6259	Middle Woodford	0.51	605.10	19.58	318.90	123.25	508.77
-6265	Middle Woodford	0.29	906.75	14.42	452.91	41.65	22.01
-6272	Middle Woodford	0.10	518.24	26.54	108.91	58.39	675.91
-6278	Middle Woodford	0.50	428.63	25.72	141.48	69.36	61.43
	Averages	0.38 ± 0.17	627.51 ± 273.64	17.64 ± 11.68	749.42 ± 976.79	45.95 ± 37.59	125.09 ± 174.89
	Ranges	0.33 to 1.61	16.38 to 63.76	5.29 to 147.23	12.31 to 495.59	38.10 to 1232.54	0.18 to 7.51

(-) = non-detect

Figure 10a. Normalized trace element concentrations versus depth of the Woodford Shale intervals of the JMOC outcrop samples. Plotted are values for Fe, V, U, Zn, Mo and Mn. Dashed grey vertical lines indicate element/Al concentration ratios for PAAS standard (Table 6; Taylor and McClennan, 1985), while the horizontal grey lines represent the tops of the Woodford subdivisions. Ratios are calculated as wt. % element/wt. % Al for Fe, and ppm element/wt. % Al. for V, U, Zn, Mo and Mn.

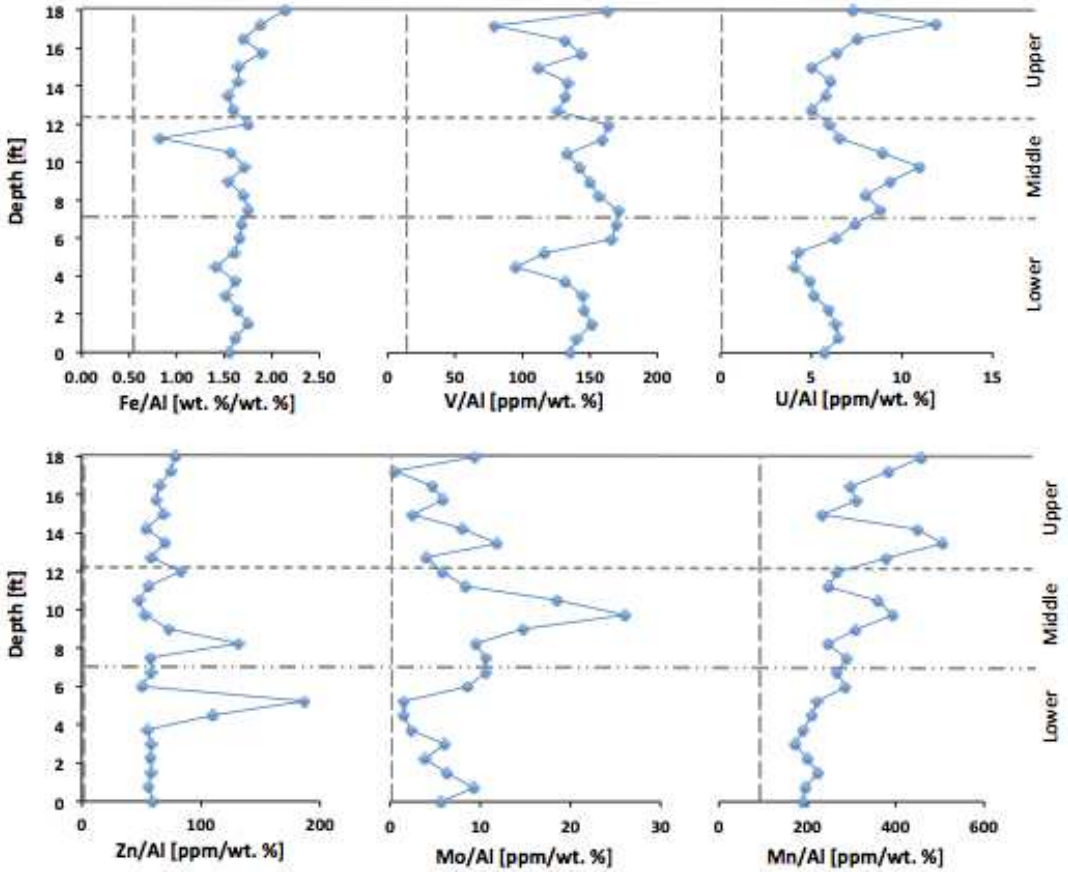

Figure 10b. Normalized trace element concentrations versus depth of the Woodford Shale intervals of the Roetzal UN-1 (ROETUN) outcrop samples. Plotted are values for Fe, V, U, Zn, Mo and Mn. Dashed grey vertical lines indicate element/Al concentration ratios for PAAS standard (Table 6; Taylor and McClennan, 1985), while the horizontal grey lines represent the tops of the Woodford subdivisions. Ratios are calculated as wt. % element/wt. % Al for Fe, and ppm element/wt. % Al. for V, U, Zn, Mo and Mn.

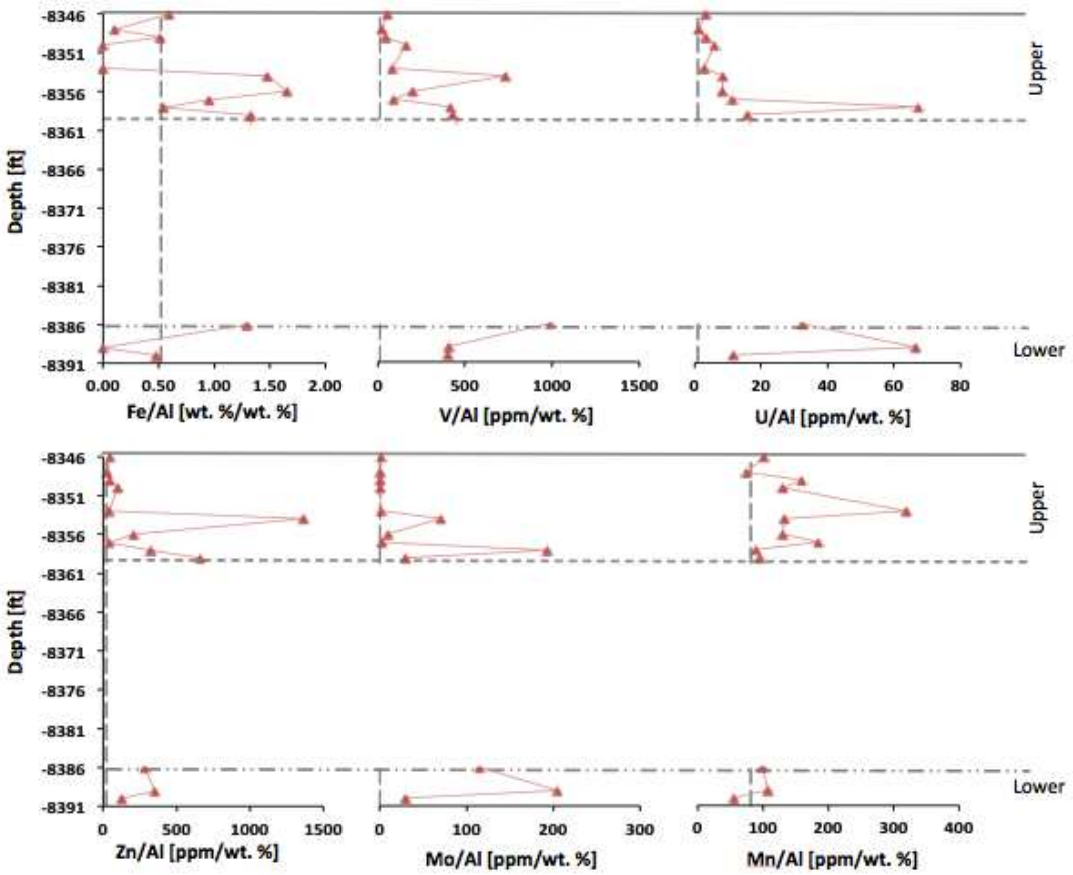

Figure 10c. Normalized trace element concentrations versus depth of the Woodford Shale intervals of the Cement Ord 1-A (CO1A) outcrop samples. Plotted are values for Fe, V, U, Zn, Mo and Mn. Dashed grey vertical lines indicate element/Al concentration ratios for PAAS standard (Table 6; Taylor and McClennan, 1985), while the horizontal grey lines represent the tops of the Woodford subdivisions. Ratios are calculated as wt. % element/wt. % Al for Fe, and ppm element/wt. % Al. for V, U, Zn, Mo and Mn.

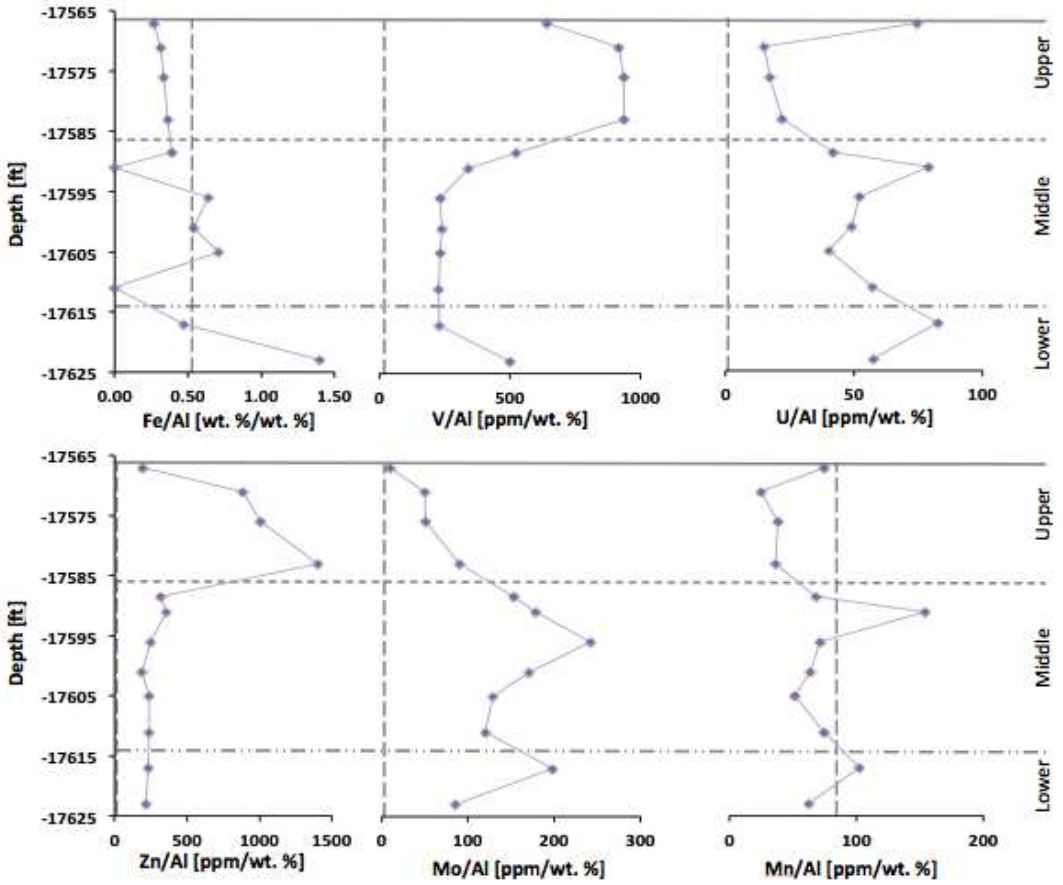

Figure 10d. Normalized trace element concentrations versus depth of the Woodford Shale intervals of the Hall 2-B (H2B) outcrop samples. Plotted are values for Fe, V, U, Zn, Mo and Mn. Dashed grey vertical lines indicate element/Al concentration ratios for PAAS standard (Table 6; Taylor and McClennan, 1985), while the horizontal grey lines represent the tops of the Woodford subdivisions. Ratios are calculated as wt. % element/wt. % Al for Fe, and ppm element/wt. % Al. for V, U, Zn, Mo and Mn.

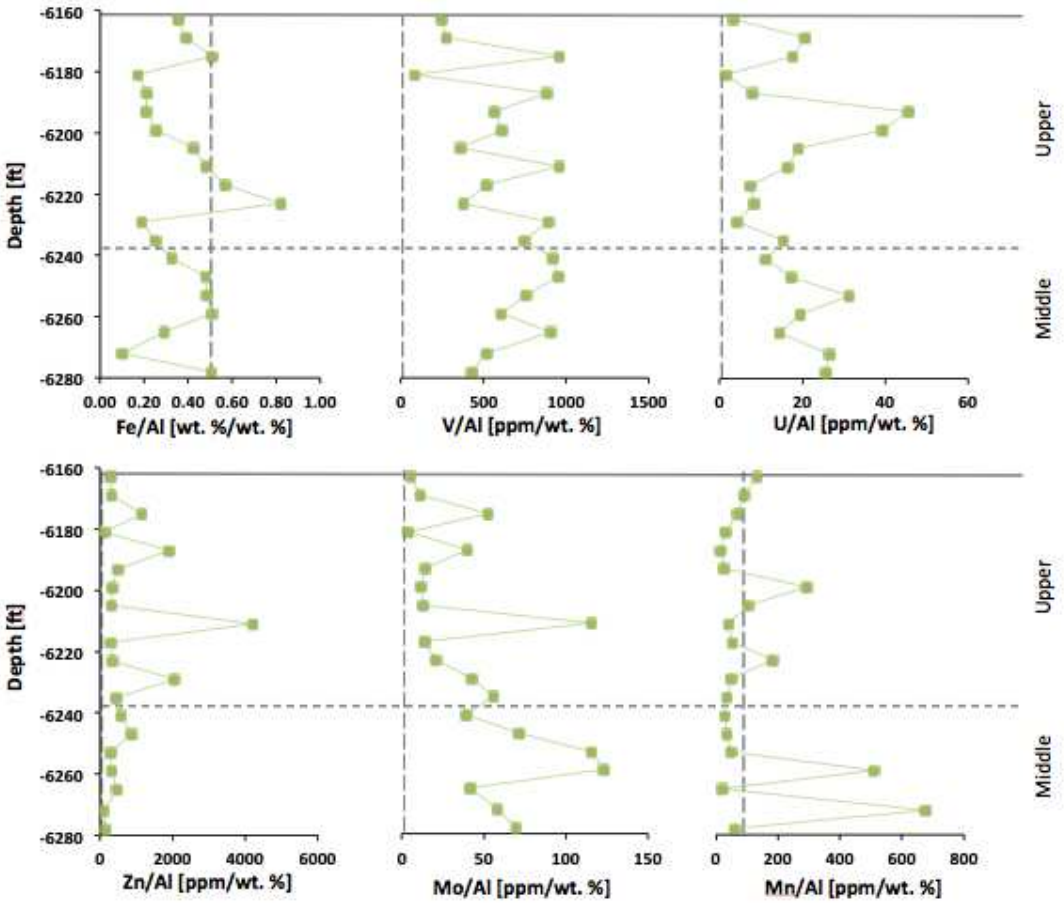

Table 5a. EF values of Fe, V, U, Zn, Mo and Mn for the Woodford Shale intervals of the JMOC outcrop samples. The horizontal grey lines represent the tops of the Woodford subdivisions.

Depth (ft)	Formation Name	Fe (%)	V (ppm)	U (ppm)	Zn (ppm)	Mo (ppm)	Mn (ppm)
18	Upper Woodford	4.21	10.87	23.53	9.25	93.48	5.09
17.25	Upper Woodford	3.70	5.25	38.33	8.78	5.12	4.26
16.5	Upper Woodford	3.33	8.77	24.29	7.73	46.10	3.31
15.75	Upper Woodford	3.71	9.57	20.73	7.34	58.15	3.45
15	Upper Woodford	3.23	7.46	16.11	8.12	24.46	2.60
14.25	Upper Woodford	3.24	8.92	19.63	6.33	80.43	5.00
13.5	Upper Woodford	3.02	8.80	18.67	8.24	118.85	5.63
12.75	Upper Woodford	3.11	8.40	16.22	6.86	40.03	4.21
12	Middle Woodford	3.45	10.93	19.31	9.75	57.82	2.96
11.25	Middle Woodford	1.62	10.59	21.16	6.65	83.75	2.76
10.5	Middle Woodford	3.07	8.86	28.85	5.64	184.93	4.01
9.75	Middle Woodford	3.37	9.47	35.43	6.22	260.29	4.38
9	Middle Woodford	3.02	10.00	30.23	8.56	147.80	3.44
8.25	Middle Woodford	3.33	10.46	25.84	15.48	94.32	2.73
7.5	Middle Woodford	3.44	11.41	28.48	6.80	105.52	3.21
6.75	Lower Woodford	3.30	11.30	23.95	6.90	105.79	2.96
6	Lower Woodford	3.26	11.07	20.43	5.94	85.79	3.19
5.25	Lower Woodford	3.16	7.75	13.83	22.04	15.31	2.45
4.5	Lower Woodford	2.77	6.32	13.18	12.95	15.32	2.35
3.75	Lower Woodford	3.16	8.79	15.94	6.46	23.20	2.10
3	Lower Woodford	2.98	9.65	16.57	6.89	60.42	1.92
2.25	Lower Woodford	3.22	9.73	19.19	6.82	38.32	2.22
1.5	Lower Woodford	3.45	10.10	20.42	6.87	62.70	2.48
0.75	Lower Woodford	3.17	9.35	20.88	6.65	93.06	2.16
0	Lower Woodford	3.04	9.01	18.59	7.02	56.62	2.11
	Averages	3.21 ± 0.44	9.31 ± 1.50	21.99 ± 6.33	8.41 ± 3.59	78.30 ± 57.17	3.24 ± 1.04
	Ranges	1.62 to 3.71	5.25 to 11.41	13.18 to 38.33	5.64 to 22.04	5.12 to 260.29	1.92 to 5.63

(-) = non-detect

Table 5b. EF values of Fe, V, U, Zn, Mo and Mn for the Woodford Shale intervals of the Roetzal UN-1 (ROETUN) outcrop samples. The horizontal grey lines represent the tops of the Woodford subdivisions.

Depth (ft)	Formation Name	Fe (%)	V (ppm)	U (ppm)	Zn (ppm)	Mo (ppm)	Mn (ppm)
-8346	Upper Woodford	1.16	3.84	11.39	5.70	13.30	1.13
-8348	Upper Woodford	0.21	1.73	4.19	3.46	5.00	0.84
-8349	Upper Woodford	1.01	3.26	10.64	5.73	9.00	1.78
-8350	Upper Woodford	-	11.08	19.29	12.11	9.12	1.45
-8353	Upper Woodford	-	5.44	9.35	4.99	10.00	3.55
-8354	Upper Woodford	2.90	48.94	27.48	160.55	704.60	1.48
-8356	Upper Woodford	3.25	13.47	27.17	24.35	98.27	1.46
-8357	Upper Woodford	1.87	6.25	37.09	5.11	27.00	2.05
-8358	Upper Woodford	1.07	27.91	217.14	38.30	1931.76	0.99
-8359	Upper Woodford	2.60	28.69	51.38	77.86	293.26	1.06
-8386	Lower Woodford	2.53	65.89	104.90	33.44	1144.30	1.10
-8389	Lower Woodford	-	27.11	214.74	41.55	2050.49	1.20
-8390	Lower Woodford	0.94	26.96	37.92	15.04	295.15	0.62
	Averages	1.75 ± 1.12	20.81 ± 19.52	59.44 ± 74.17	32.94 ± 43.91	507.02 ± 740.73	1.44 ± 0.74
	Ranges	- to 3.25	1.73 to 65.89	4.19 to 217.14	3.46 to 160.55	5.00 to 2050.49	0.62 to 3.55

(-) = non-detect

Table 5c. EF values of Fe, V, U, Zn, Mo and Mn for the Woodford Shale intervals of the Cement Ord 1-A (CO1A) outcrop samples. The horizontal grey lines represent the tops of the Woodford subdivisions.

Depth (ft)	Formation Name	Fe (%)	V (ppm)	U (ppm)	Zn (ppm)	Mo (ppm)	Mn (ppm)
-17567	Upper Woodford	0.53	42.89	240.28	22.61	96.93	0.83
-17571	Upper Woodford	0.61	61.08	47.87	103.85	503.50	0.27
-17576	Upper Woodford	0.66	62.43	55.55	118.31	510.47	0.42
-17583	Upper Woodford	0.71	62.38	70.95	165.02	900.74	0.40
-17588.5	Middle Woodford	0.76	34.87	134.79	36.97	1528.45	0.76
-17591	Middle Woodford	-	22.68	254.74	41.44	1785.67	1.71
-17596	Middle Woodford	1.25	15.59	167.97	29.28	2418.70	0.79
-17601	Middle Woodford	1.05	15.99	157.75	22.20	1706.24	0.71
-17605	Middle Woodford	1.40	15.52	129.65	27.86	1283.13	0.57
-17611	Middle Woodford	-	15.24	184.77	27.97	1206.88	0.82
-17617	Lower Woodford	0.93	15.40	267.05	27.41	1983.53	1.14
-17623	Lower Woodford	2.75	33.27	185.03	25.20	855.90	0.69
	Averages	1.06 ± 0.66	33.11 ± 19.65	158.03 ± 74.54	54.01 ± 47.58	1231.68 ± 686.66	0.76 ± 0.638
	Ranges	- to 2.75	15.24 to 62.43	47.87 to 267.05	22.20 to 165.02	96.93 to 2418.70	0.27 to 1.71

(-) = non-detect

Table 5d. EF values of Fe, V, U, Zn, Mo and Mn for the Woodford Shale intervals of the Hall 2-B (H2B) outcrop samples. The horizontal grey lines represent the tops of the Woodford subdivisions.

Depth (ft)	Formation Name	Fe (%)	V (ppm)	U (ppm)	Zn (ppm)	Mo (ppm)	Mn (ppm)
-6163	Upper Woodford	0.69	16.38	10.41	33.35	52.41	1.46
-6169	Upper Woodford	0.77	18.36	66.69	37.06	112.93	1.02
-6175	Upper Woodford	1.00	63.76	57.05	135.88	526.78	0.79
-6181	Upper Woodford	0.33	5.43	5.29	15.31	38.10	0.34
-6187	Upper Woodford	0.42	58.96	25.48	222.32	398.43	0.18
-6193	Upper Woodford	0.41	37.68	147.23	57.99	145.84	0.29
-6199	Upper Woodford	0.50	40.67	127.01	38.77	113.89	3.24
-6205	Upper Woodford	0.83	23.74	61.23	37.47	128.91	1.16
-6211	Upper Woodford	0.94	63.69	52.97	495.59	1156.10	0.44
-6217	Upper Woodford	1.12	34.55	23.71	34.45	136.89	0.60
-6223	Upper Woodford	1.61	25.13	27.09	39.73	206.88	2.02
-6229	Upper Woodford	0.37	59.37	13.55	239.78	424.80	0.53
-6235	Upper Woodford	0.49	49.90	49.70	51.31	559.00	0.39
-6241	Middle Woodford	0.64	61.22	35.92	67.14	394.44	0.32
-6247	Middle Woodford	0.94	63.47	55.67	103.28	712.41	0.39
-6253	Middle Woodford	0.95	50.47	100.95	33.66	1154.74	0.53
-6259	Middle Woodford	0.99	40.34	63.17	37.52	1232.54	5.65
-6265	Middle Woodford	0.57	60.45	46.50	53.28	416.45	0.24
-6272	Middle Woodford	0.19	34.55	85.60	12.81	583.90	7.51
-6278	Middle Woodford	0.99	28.58	82.97	16.64	693.62	0.68
	Averages	0.74 ± 0.34	41.83 ± 18.24	56.91 ± 37.68	88.17 ± 114.92	459.45 ± 375.87	1.39 ± 1.94
	Ranges	0.19 to 1.61	5.43 to 63.76	5.29 to 147.23	12.81 to 495.59	38.10 to 1232.54	0.18 to 7.51

(-) = non-detect

Table 6. Averages of the bulk sedimentary nitrogen isotopic values ($\delta^{15}N_{bulk}$), organic carbon isotopic values ($\delta^{13}C_{org}$), bulk elemental nitrogen (TN), total organic carbon (TOC) concentrations and the enrichment factors of iron (Fe), vanadium (V), uranium (U), zinc (Zn), molybdenum (Mo) and manganese (Mn) concentrations relative to PAAS (Post Archean Average Shale) for the Woodford Shale intervals in the JMOC, ROETUN, CO1A and H2B sample locations.

Sample Location	Formation Name	$\delta^{15}N_{bulk}$ (‰)	$\delta^{13}C_{org}$ (‰)	TN (%)	TOC (%)	Fe (ppm)	V (ppm)	U (ppm)	Zn (ppm)	Mo (ppm)	Mn (ppm)
JMOC	Woodford	7.7 ± 0.3	-29.6 ± 0.5	0.1 ± 0.0	1.1 ± 0.2	1.64 ± 0.22	139.71 ± 22.56	6.82 ± 1.96	71.50 ± 30.55	7.83 ± 5.72	291.54 ± 93.20
ROETUN	Woodford	8.41 ± 0.95	-30.7 ± 1.1	0.3 ± 0.3	1.2 ± 0.7	0.89 ± 0.52	312.19 ± 294.74	18.43 ± 22.99	297.97 ± 373.27	50.70 ± 74.07	129.53 ± 66.52
CO1A	Woodford	4.4 ± 1.6	-30.7 ± 0.2	0.51 ± 0.21	1.36 ± 0.59	0.54 ± 0.33	496.68 ± 294.78	48.99 ± 23.11	459.11 ± 404.38	123.17 ± 68.67	68.41 ± 34.20
H2B	Woodford	7.3 ± 1.4	-31.4 ± 0.6	0.35 ± 0.20	2.51 ± 0.81	0.38 ± 0.17	627.51 ± 273.64	17.64 ± 11.68	749.42 ± 976.79	45.95 ± 37.59	125.09 ± 174.89

Sample Location	Formation Name	$\delta^{15}N_{bulk}$ (‰)	$\delta^{13}C_{org}$ (‰)	TN (%)	TOC (%)	Fe (ppm)	V (ppm)	U (ppm)	Zn (ppm)	Mo (ppm)	Mn (ppm)
JMOC	Upper Woodford	7.8 ± 0.3	-29.8 ± 0.3	0.08 ± 0.01	1.01 ± 0.21	1.76 ± 0.20	127.60 ± 24.54	6.88 ± 2.22	66.57 ± 8.26	5.83 ± 3.75	377.33 ± 92.46
JMOC	Middle Woodford	7.7 ± 0.4	-29.2 ± 0.6	0.12 ± 0.03	1.21 ± 0.15	1.55 ± 0.33	153.68 ± 13.07	8.38 ± 1.71	71.77 ± 29.03	13.35 ± 7.00	302.13 ± 56.99
JMOC	Lower Woodford	7.6 ± 0.3	-29.6 ± 0.6	0.12 ± 0.02	1.19 ± 0.23	1.61 ± 0.10	139.61 ± 22.19	5.67 ± 1.05	75.26 ± 42.86	5.57 ± 3.25	215.50 ± 35.97
ROETUN	Upper Woodford	8.6 ± 0.8	-30.6 ± 1.2	0.26 ± 0.25	1.08 ± 0.64	0.90 ± 0.55	225.91 ± 230.78	12.87 ± 19.65	287.44 ±427.25	31.01 ± 61.13	142.01 ± 70.55
ROETUN	Lower Woodford	7.7 ± 1.2	-30.3 ± 0.4	0.40 ± 0.27	1.62 ± 0.75	0.88 ± 0.57	599.80 ± 336.49	36.95 ± 27.67	255.09 ± 115.47	116.33 ± 87.78	87.91 ± 27.87
CO1A	Upper Woodford	6.0 ± 1.3	-30.5 ± 0.2	0.28 ± 0.09	0.75 ± 0.31	0.32 ± 0.04	857.91 ± 143.38	32.14 ± 28.39	870.80 ± 503.87	50.29 ± 32.82	43.26 ± 21.71
CO1A	Middle Woodford	3.4 ± 1.1	-30.8 ± 0.1	0.63 ± 0.15	1.66 ± 0.50	0.57 ± 0.14	299.76 ± 117.44	53.20 ± 14.14	263.10 ± 59.38	165.48 ± 43.77	80.50 ± 37.01
CO1A	Lower Woodford	3.8 ± 0.5	-30.6 ± 0.5	0.64 ± 0.01	1.68 ± 0.25	0.94 ± 0.65	364.97 ± 189.56	70.07 ± 17.98	223.72 ± 13.07	141.97 ± 79.73	82.43 ± 28.28
H2B	Upper Woodford	8.0 ± 0.9	-31.7 ± 0.6	0.35 ± 0.23	2.54 ± 0.93	0.37 ± 0.19	574.16 ± 295.68	15.91 ± 13.43	940.89 ± 1166.75	30.78 ± 31.12	86.27 ± 78.01
H2B	Middle Woodford	6.1 ± 1.1	-31.0 ± 0.3	0.35 ± 0.15	2.45 ± 0.59	0.38 ± 0.15	726.59 ± 211.31	20.85 ± 7.25	393.84 ± 268.06	74.12 ± 33.31	197.17 ± 274.53

4.2.1 Total bulk nitrogen (TN) concentrations and $\delta^{15}N_{bulk}$ isotopic ratios for the Roetzal UN-1 (ROETUN) core samples

The bulk sedimentary samples $\delta^{15}N_{bulk}$ of the Woodford Shale intervals of the ROETUN core samples are presented in Table 1b, along with the averages and ranges. The bulk sedimentary $\delta^{15}N_{bulk}$ values for the Woodford Shale interval for the ROETUN samples has a range of approximately 3.1 ‰, where the lightest isotopic values is 6.5 ‰ and the heaviest isotopic value is 9.6 ‰. The average bulk sedimentary $\delta^{15}N_{bulk}$ of all ROETUN samples is 8 ‰ ± 1 ‰, which is larger than the JMOC (7.7 ± 0.3 ‰), CO1A (4 ± 2 ‰), and H2B (7 ± 1 ‰). The plot of the $\delta^{15}N_{bulk}$ values versus depth for the Woodford Shale intervals of the ROETUN samples are shown in Figure 8b.

The results of the elemental nitrogen concentrations (wt. %) of the bulk sedimentary nitrogen (TN) are presented in Table 1b, along with the averages and ranges. The wt. % TN of the Woodford Shale in the ROETUN samples vary from 0.0 % to 0.7 %, with a range of approximately 0.7 %. The average TN for the ROETUN core samples is 0.3 ± 0.3 ‰. The plot of the wt. % TN versus depth for the ROETUN core samples is shown in Figure 8b. The wt. % TN of the Woodford Shale intervals for the ROETUN core samples increases from 0.0 % to 0.7 %.

4.2.2 Total organic carbon (TOC) concentrations and $\delta^{13}C_{org}$ isotopic ratios for the Roetzal UN-1 (ROETUN) core samples

The stable organic carbon isotopic compositions ($\delta^{13}C_{org}$) for the ROETUN core samples are listed in Table 1b, along with the averages and ranges. The $\delta^{13}C_{org}$ values for the Woodford Shale in the ROETUN outcrop samples are depleted relative to VPDB, ranging from -31.9 ‰ to -28.3 ‰ with an average of -31 ‰ ± 1 ‰. The $\delta^{13}C_{org}$ values of the ROETUN samples display a general decrease from the top of the measured section to the bottom of the measured section. The

range of the $\delta^{13}C_{org}$ values observed in the ROETUN samples (3.6 ‰) is larger than the scatter observed in the JMOC (2.4 ‰), CO1A (0.7 ‰) and H2B (1.9 ‰) samples.

The results of the elemental concentrations (wt. %) of the total organic carbon (TOC) are presented in Table 1b, along with the averages and ranges. The wt. % TOC of the Woodford Shale in the ROETUN samples ranges from 0.4 % to 2.3 %, with an average of 1.2 ± 0.7 ‰. Plots of TOC versus depth are shown in Figure 8b, which display a general increase with depth.

4.2.3 Trace element concentrations for the Roetzal UN-1 (ROETUN) core samples

Normalized and corrected trace element concentration for Fe, V, U, Zn, Mo, and Mn for the ROETUN are presented in Table 4b and their variations versus depth are shown in Figure 10b. Al concentrations observed in the Woodford intervals of the ROETUN sample location range from 1.08 % to 6.84 %, with an average of 4 % ± 2 %. Calcium concentrations are relatively low and are presented in the appendix. For the ROETUN outcrop samples, V, U, Zn, Mo and Mn concentrations are significantly enriched relative to the PAAS standards (Figure 10b), whereas Fe is intermittently enriched and depleted within the Upper and Lower Woodford. EF values were used to aid the interpretation of results. The individual EF values, the average EF values, and the range of the EF values for each sample location of the analyzed trace metals are presented in Tables 5a, b, c and d. For comparison, the average EF values are compiled in Table 6. To get a complete list of all the trace element concentrations analyzed, refer to Appendix C.

Unlike the JMOC outcrop samples, the trace element concentrations for the ROETUN core samples exhibit similar shifts for the Upper Woodford and Lower Woodford Shale intervals, which are intermittently enriched and depleted relative to PAAS standards (Figure 10b). Fe, V, U, Zn and Mo concentrations exhibit a positive shift in the lower portion of the Upper Woodford interval. The Fe, V, U, Zn and Mo concentrations in the Upper Woodford interval are enriched relative to PAAS standards. As for Mn from top to bottom, the Upper Woodford initially exhibits

an increase in concentrations, then a decrease in concentrations to the lower portion of the Upper Woodford interval, but remain enriched relative to PAAS standards. As for the Lower Woodford interval, U, Zn, Mo and Mn concentrations display an initial positive shift and enrichment relative to PAAS standards, immediately followed by negative shift. Regarding Fe and V concentrations, the Lower Woodford interval is marked by an initial depletion followed by an immediate enrichment. Fe and Mn concentrations in the Lower Woodford interval decrease to depleted concentrations relative to PAAS standards.

4.3 Cement Ord 1-A (CO1A) core samples

A core description of the CO1A core (Figure 7) indicates that the Woodford has alternating silica-rich and clay-rich intervals, where the clay-rich intervals are generally more fissile than the silica-rich intervals. The more fissile shale intervals were highly laminated and black in color, while the silica-rich intervals were fracture oriented and dark grey. On average, the sediments in the CO1A core were darker than the JMOC, ROETUN and H2B sediments. The Upper, Middle, and Lower Woodford intervals were present in the cored section and the Middle Woodford Shale was generally more fissile and clay-rich than the Upper and Lower Woodford. Pyrite was present throughout the entire core, however burrows and fossils were not identified in this core.

4.3.1 Total bulk nitrogen (TN) concentrations and $\delta^{15}N_{bulk}$ isotopic ratios for the Cement Ord 1-A (CO1A) core samples

The nitrogen isotopic compositions of the bulk sedimentary samples ($\delta^{15}N_{bulk}$) of the Woodford Shale intervals of the CO1A core samples are presented in Table 1c, along with the averages and ranges. The sedimentary $\delta^{15}N_{bulk}$ values for the Woodford Shale interval for the CO1A samples has a range of approximately 4.9 ‰, where the lightest composition is 2.1 ‰ and the heaviest is 7.0 ‰. The average sedimentary $\delta^{15}N_{bulk}$ of all CO1A samples is 4 ‰ ± 2 ‰,

which is less than the average sedimentary $\delta^{15}N_{bulk}$ JMOC (7.7 ± 0.3 ‰), ROETUN (8.4 ± 1.0 ‰) and H2B (7.3 ± 1.4 ‰) samples. The plot of the $\delta^{15}N_{bulk}$ values versus depth for the Woodford Shale intervals of the CO1A samples are shown in Figure 8c.

The results of the elemental nitrogen concentrations (wt. %) of the bulk sedimentary nitrogen (TN) for the CO1A core samples are presented in Table 1c, along with the averages and ranges. The wt. % TN of the Woodford Shale in the CO1A samples vary from 0.2 % to 0.9 %, with a range of approximately 0.7 %. The average TN for the CO1A core samples is 0.5 ± 0.2 ‰. The plot of the wt. % TN versus depth for the CO1A core samples is shown in Figure 7c. The wt. % TN of the Woodford Shale intervals for the CO1A core samples increases to a maximum from the top of the Upper Woodford (0.2 %) to the top of the Middle Woodford (0.9 %). After the maximum value, the wt. % TN significantly decreases (0.5 %), then increases gradually to the Lower Woodford (0.6 %).

4.3.2 Total organic carbon (TOC) concentrations and $\delta^{13}C_{org}$ isotopic ratios for the Cement Ord 1-A (CO1A) core samples

The stable carbon isotopic compositions ($\delta^{13}C_{org}$) for the CO1A core samples are listed in Table 1c, along with the averages and ranges. The plot of the $\delta^{13}C_{org}$ versus depth for the CO1A core samples is shown in Figure 8c. The $\delta^{13}C_{org}$ values for the Woodford Shale in the CO1A outcrop samples are depleted relative to VPDB, ranging from -31.0 ‰ to -30.3 ‰ with an average of -30.7 ‰ ± 0.2 ‰. The $\delta^{13}C_{org}$ values of the CO1A samples remain relatively consistent throughout the entire Woodford Shale interval. The range of the $\delta^{13}C_{org}$ values observed in the CO1A samples (0.7 ‰) is relatively smaller than the range observed in the JMOC (2.4 ‰), ROETUN (3.6 ‰) and H2B (1.9 ‰) samples.

The results of the elemental concentrations (wt. %) of the total organic carbon (TOC) for the CO1A core samples are presented in Table 1c, along with the averages and ranges. The wt. %

TOC of the Woodford Shale in the CO1A samples range from 0.5 % to 2.4 %, with an average of 1.4 ± 0.6 ‰. Plots of TOC versus depth are shown in Figure 8c, which display a general increase with depth.

4.3.3 Trace element concentrations for the Cement Ord 1-A (CO1A) core samples

Normalized and corrected trace element concentration for Fe, V, U, Zn, Mo, and Mn for the CO1A are presented in Table 4c and their plots versus depth are shown in Figure 10c. Al concentrations observed in the Woodford intervals of the CO1A sample location range from 1.27 % to 6.47 %, with an average of 3 % ± 2 %. Calcium concentrations are relatively low and are presented in the appendix. For the CO1A outcrop samples, V, U, Zn and Mo concentrations are significantly enriched relative to the PAAS standards (Figure 9c), whereas Fe and Mn both exhibit intermittent enrichment and depletion. EF values were used to aid the interpretation of results. EF values for the analyzed trace metals are presented in Tables 5a, b, c and d, their ranges are shown in Table 1, and their averages are shown in Table 6. To get a complete list of all the trace element concentrations analyzed, refer to Appendix C.

Similar to the ROETUN core samples, the trace element concentrations for the CO1A core samples exhibit intermittent enrichments and depletions relative to PAAS standards (Figure 10c). From the Upper Woodford to the Middle Woodford, Fe concentrations become enriched relative to PAAS from the initial concentrations. At the top Lower Woodford, Fe concentrations then display a positive shift, resulting in enriched values relative to PAAS standards. In the lower portions of the sampled section, Fe concentrations are depleted relative to PAAS standards until the onset of the Lower Woodford interval, where they become enriched. Similar shifts in U, Mo and Mn concentrations are observed throughout the measured section, though a majority of the samples are depleted in Mn relative to PAAS standards. These elemental concentrations increase from the Upper Woodford interval to a maximum in the Middle Woodford interval, then

decreases to the Lower Woodford. The onset of the Lower Woodford interval marks an additional spike in U, Mo, and Mn concentrations. V and Zn concentrations display similar shifts and are both enriched relative to PAAS standards. The concentrations of these elements in the Upper Woodford interval exhibits a positive shift, then changes to a negative shift at the Middle Woodford interval and remains relatively constant till the end of the section.

4.4 Hall 2-B (H2B) core samples

A core description of the H2B core (Figure 7) indicates the Woodford as alternating silica-rich and clay-rich shale, where the clay-rich intervals are generally more laminated than the silica-rich intervals. The sediments in this core are highly deformed, where the clay-rich intervals are folded and the silica-rich intervals are fractured. Bedding planes were visible in the clay-rich layers despite the deformation. The clay-rich intervals were black in color, while the silica-rich intervals were dark grey. The upper and middle Woodford intervals were present in the cored section. Pyrite and burrows were identified throughout the core, however fossils were not observed.

4.4.1 Total bulk nitrogen (TN) concentrations and $\delta^{15}N_{bulk}$ isotopic ratios for the Hall 2-B (H2B) core samples

The nitrogen isotopic compositions of the bulk sedimentary samples ($\delta^{15}N_{bulk}$) of the Woodford Shale intervals of the H2B core samples are presented in Table 1d, along with the averages and ranges. The sedimentary $\delta^{15}N_{bulk}$ values for the Woodford Shale interval for the H2B samples has a range of approximately 4.0 ‰, where the lightest composition is 5.2 ‰ and the heaviest is 9.2 ‰. The H2B $\delta^{15}N_{bulk}$ duplicate and triplicate samples have a standard deviation of 0.5 ‰ and the average bulk sedimentary $\delta^{15}N_{bulk}$ of all H2B samples is 7 ‰ ± 1 ‰. This average is less than the average bulk sedimentary $\delta^{15}N_{bulk}$ of the JMOC (7.7 ± 0.3 ‰) and the ROETUN (8 ± 1 ‰), but greater than the average bulk sedimentary $\delta^{15}N_{bulk}$ of the CO1A (4 ±

2 ‰). The plot of the $\delta^{15}N_{bulk}$ values versus depth for the Woodford Shale intervals of the H2B samples are shown in Figure 8d.

The results of the elemental nitrogen concentrations (wt. %) of the bulk sedimentary nitrogen (TN) for the H2B core samples are presented in Table 1d, along with the averages and ranges. The wt. % TN of the Woodford Shale in the H2B samples vary between 0.1 % to 0.8 %, with a range of approximately 0.8 %. The average TN for the H2B core samples is 0.4 ± 0.2 ‰. The plot of the wt. % TN versus depth for the H2B core samples is shown in Figure 8d. The wt. % TN of the Woodford Shale intervals for the H2B core samples exhibits three different cycles resulting in three different peaks: one at the top of the upper Woodford (0.8 %), the second near the bottom of the upper Woodford (0.7 %), and the third near the middle of the middle Woodford (0.6 %). After each peak, the wt. % TN drastically decreases where it then gradually increases to the following peak, 0.1 % following the first, 0.1 % following the second, and 0.2 % following the third (Figure 8d).

4.4.2 Total organic carbon (TOC) concentrations and $\delta^{13}C_{org}$ isotopic ratios for the Hall 2-B (H2B) core samples

The stable carbon isotopic compositions ($\delta^{13}C_{org}$) for the Hall 2-B core samples are listed in Table 1d, along with the averages and ranges. The $\delta^{13}C_{org}$ values for the Woodford Shale in the H2B outcrop samples are depleted relative to VPDB, ranging from -32.4 ‰ to -30.5 ‰ with an average of -31.4 ‰ ± 0.6 ‰. The $\delta^{13}C_{org}$ values of the H2B samples generally increase from the Upper Woodford (-31.9 ‰) to the Middle Woodford (-30.5 ‰), then decreases to the bottom of the Middle Woodford (-31.1 ‰). The variation of the $\delta^{13}C_{org}$ values observed in the H2B samples (1.9 ‰) is smaller than the range observed in the JMOC (2.4 ‰) and ROETUN (3.6 ‰) samples and relatively larger than the ranges observed in the CO1A samples. The plot of the

$\delta^{13}C_{org}$ values versus depth for the Woodford Shale intervals of the H2B samples are shown in Figure 8d.

The results of the elemental concentrations (wt. %) of the total organic carbon (TOC) for the H2B core samples are presented in Table 1d, along with the averages and ranges. The wt. % TOC of the Woodford Shale in the H2B samples range from 1.5 % to 4.8 %, with an average of 2.5 ± 0.8 ‰. Plots of TOC versus depth are shown in Figure 7d, which exhibit three different cycles resulting in two main peaks: one at the top of the upper Woodford (4.8 %) and the second near the bottom of the upper Woodford (3.6 %). Though not significant peaks, two positive shifts are observed in the lower Woodford (Figure 7d). After each peak, the wt. % TN drastically decreases where it then gradually increases to the following peak, 1.50 % following the first and 1.68 % following the second (Figure 8d).

4.4.3 Trace element concentrations for the Hall 2-B (H2B) core samples

Normalized and corrected trace element concentration for Fe, V, U, Zn, Mo, and Mn for the H2B are presented in Table 4d and their plots versus depth are shown in Figure 10d. Al concentrations observed in the Woodford intervals of the H2B sample location range from 0.68 % to 3.53 %, with an average of 1.6 % ± 0.7 %. Calcium concentrations are relatively low and are presented in the appendix. For the H2B outcrop samples, V, U, Zn and Mo concentrations are significantly enriched relative to the PAAS standards (Figure 10d), whereas Fe and Mn concentrations become intermittently enriched and depleted. EF values were used to aid the interpretation of results. EF values for the analyzed trace metals are presented in Tables 5a, b, c and d, their ranges are shown in Table 1, and their averages are shown in Table 6. To get a complete list of all the trace element concentrations analyzed, refer to Appendix C.

Trace metal concentrations for the H2B core samples are variable throughout the core and fluctuate between enrichment and depletion relative to PAAS standards (Figure 10d).

Although a majority of the Fe concentrations are depleted relative to PAAS standards, several samples display positive shifts that are equivalent to or enriched relative to PAAS standards. V concentrations display significant positive and negative shifts throughout the core. However, the profile of V increases from Upper Woodford (16.38 ppm) to Middle Woodford (61.22 ppm), where the concentrations then decrease. U and Mo concentrations display similar profiles to one another. The Upper Woodford exhibits two prominent positive shifts in both U and Mo. As for the Lower Woodford, one prominent peak in U and Mo is observed. A majority of the Zn concentrations are consistent, with the exception of several anomalously high values in the Upper Woodford. As for the Mn concentrations, a majority of the values are depleted relative to PAAS standards. Four anomalously high positive shifts of Mn concentrations occur in the core, two in the Upper Woodford and two in the Lower Woodford.

CHAPTER V

DISCUSSION

5.1 Depositional environment influences on the bulk sedimentary $\delta^{15}N$ values

In order to evaluate the effects of thermal maturity on the average bulk sedimentary $\delta^{15}N$ values for each sample location, we made the assumption that the sedimentary organic matter of the Woodford Shale was deposited under similar redox conditions and depositional environments. However, when looking at the average $\delta^{15}N_{bulk}$ values of the Woodford Shale interval for each sample location superimposed on Figure 2, the data suggests that this assumption was incorrect. Instead, the bulk sedimentary $\delta^{15}N_{bulk}$ values are a product of two populations deposited under different redox states (Figure 11). The two separate populations are divided into (1) a more depleted population incorporating CO1A and (2) a relatively more enriched population incorporating JMOC, ROETUN and H2B. In fact, the average bulk sedimentary $\delta^{15}N_{bulk}$ values of the enriched population in this study are similar to the findings for organic matter subjected to denitrification and deposited under suboxic conditions (Altabet et al., 1995; Ganeshram et al., 1995; Altabet et al., 1999; Pride et al., 2010; Adigwe et al., 2012), while the average bulk sedimentary $\delta^{15}N_{bulk}$ values of the depleted population in this study are similar to the findings for organic matter subjected to nitrogen fixation and deposited under anoxic conditions (Karl et al., 1997; Adigwe, 2012).

The evidence of the suboxic nature of the JMOC, ROETUN and H2B locations and the

Figure 11. Average $\delta^{15}N$ values for the JMOC, ROETUN, CO1A and H2B superimposed on $\delta^{15}N$ versus O_2 concentrations plot. The values indicate two different populations that could be the result of two different depositional environments, suboxic and anoxic. The JMOC (blue circle), ROETUN (red triangle), and H2B (green square) are enriched relative to the CO1A (purple diamond) sediments. The three enriched locations are suggested to being deposited under suboxic environments while the depleted location is suggested of being deposited under anoxic environments. Note: the $\delta^{15}N$ values in this figure are projected estimates and do not represent the initial $\delta^{15}N$ values for organic matter at these sites.

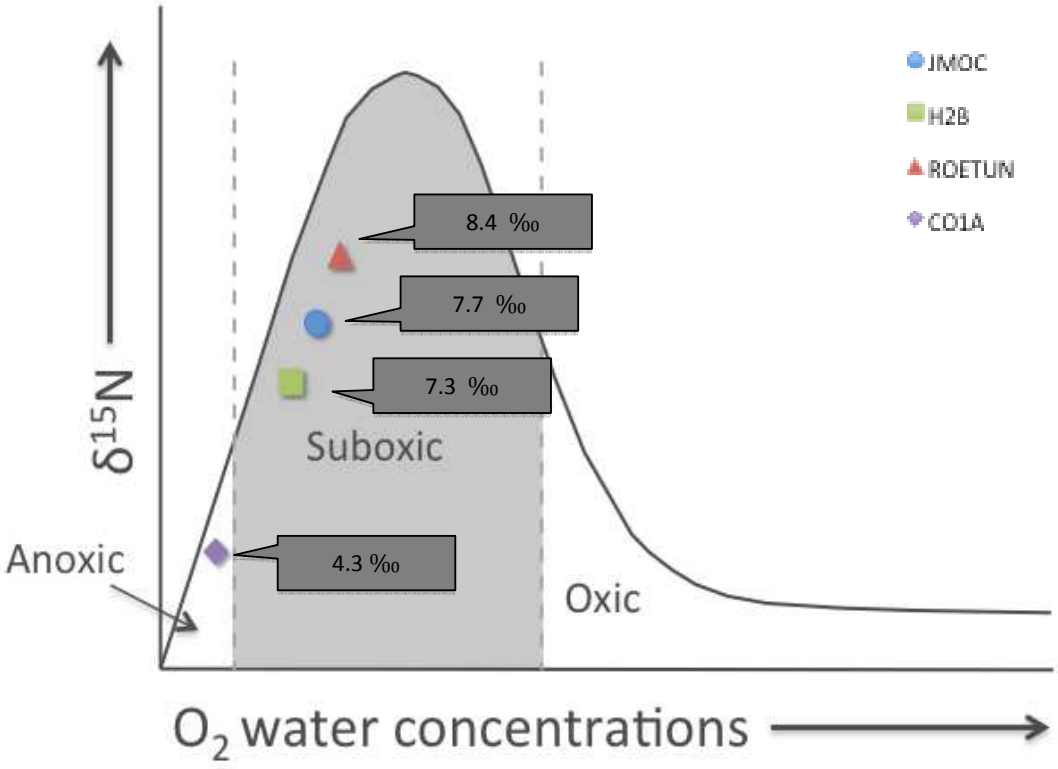

anoxic nature of the CO1A location lies within the core descriptions, as well as the redox sensitive trace metal concentrations. The burrows identified in the JMOC, ROETUN and H2B, as well as fossils in the Upper Woodford in the JMOC sediments, suggest that oxygen concentrations in the water column at these locations must be high enough to facilitate life, which supports the findings that sediments and organic matter at these locations were deposited under suboxic environments. On the contrary, the lack of fossils and burrows in the CO1A sediments suggests water column oxygen concentrations at this location were too low to promote life, which

supports the findings that sediments and organic matter at this location were deposited under anoxic environments. Also, reduced forms U and Mo are easily diffused from the water column to the sediments under anoxic environments enriching the concentrations within the sediments, thus making U and Mo useful water column redox states proxies (Calvert and Pederson, 1993; Mumford and Emerson, 1999; Brumsack, H.J, 2006; Tribovillard et al., 2006). On average, U and Mo concentrations in the CO1A sediments are greater than the U and Mo concentrations in the JMOC, ROETUN and H2B sediments (Table 6). Therefore, the initial assumption that the sedimentary organic matter of the Woodford Shale was deposited under similar redox conditions and depositional environments is invalid. In fact, the sediments at the different locations are products of two different water column redox states, where the JMOC, ROETUN and H2B sediments and organic matter were deposited under suboxic environments and the CO1A sediments and organic matter were deposited under anoxic environments.

The different depositional environments indicated by the average bulk sedimentary $\delta^{15}N_{bulk}$ values may be related to depth within the basin. Therefore, to evaluate whether or not the previously observed bulk sedimentary $\delta^{15}N_{bulk}$ populations are a product of depth within the basin, the average sedimentary bulk $\delta^{15}N_{bulk}$ values of the Woodford Shale interval for each sample location are plotted against depth (Figure 12). Similar to Figure 11, this plot indicates two separate populations of data, a population with greater bulk sedimentary $\delta^{15}N_{bulk}$ values incorporating JMOC, ROETUN and H2B and a population with less bulk sedimentary $\delta^{15}N_{bulk}$ values incorporating CO1A. Not only does this demonstrate that the JMOC, ROETUN and H2B sediments were deposited under different depositional environments than the CO1A sediments, but that depth may play a role. The relatively shallow sediments have higher bulk sedimentary $\delta^{15}N_{bulk}$ values than the deep sediments, which indicate that the shallow sediments were deposited under suboxic environments and the deep sediments were deposited under anoxic environments. These depths at which the Woodford Shale is located and the geographic positions of the sample

Figure 12. A cross-plot of the $\delta^{15}N$ values versus depth. The values posted are the average $\delta^{15}N$ values of the specific sample locations. The large blue circle represents the average for the JMOC, the large green square represents the average for the H2B, the large red triangle represents the average for the ROETUN and the large purple diamond represents the average for the CO1A. The enriched $\delta^{15}N$ values observed in the JMOC, H2B and ROETUN indicate suboxic water column conditions, whereas the depleted $\delta^{15}N$ values of the CO1A indicate anoxic water column conditions.

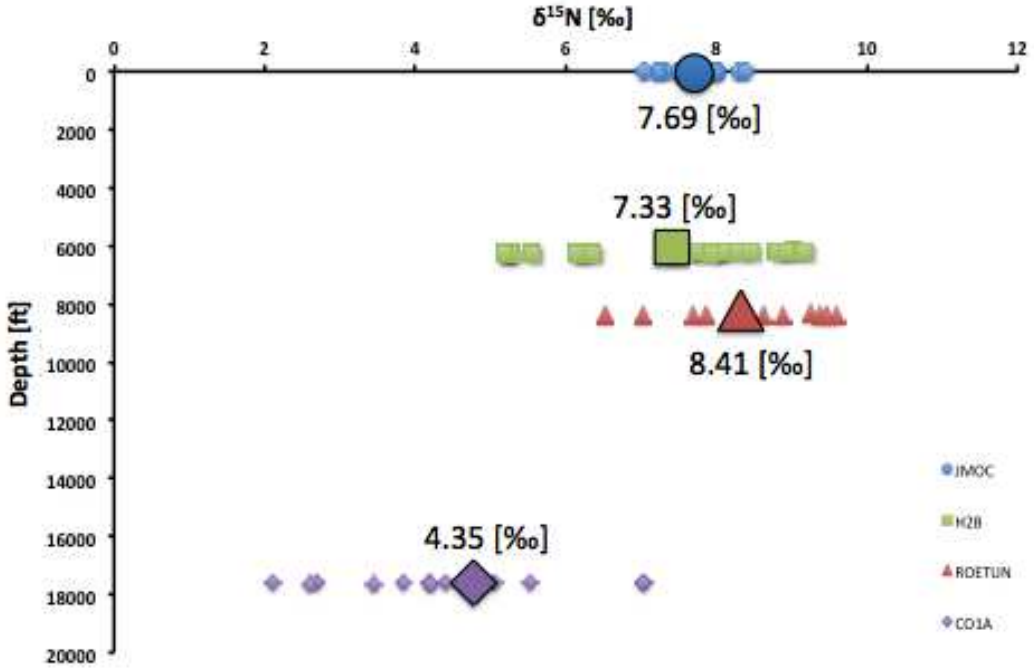

locations implies that the JMOC, ROETUN and H2B sediments were deposited at either the basin margin or basin shelf, and the CO1A sediments were deposited at the depocenter of the basin (Cardott and Lambert, 1982, Da Wang and Philp, 1997; Carter et al., 1998; Johnson, 2008). The bulk sedimentary $\delta^{15}N_{bulk}$ values of these sample locations reflect the depositional environments rather than thermal maturity effects.

As previously mentioned, a positive shift of the bulk sedimentary $\delta^{15}N_{bulk}$ values should be observed with the increase of thermal maturity from the oil window to the gas window (Boudou et al., 1984a; Zhu et al., 2000; Oldenburg et al., 2007; Boudou et al., 2008; Schimmelmann and Lis, 2012). However, when evaluating the cross-plot of the bulk sedimentary

Figure 13. Cross-plot of bulk sedimentary $\delta^{15}N_{bulk}$ values versus the R_o values for all of the sample locations in each sample location. The projected vitrinite reflectance values for the JMOC and CO1A samples were assumed to represent the entire Woodford Shale at these locations, thus the R_o values are the same for each sample at these locations. This results in the vertical lines observed for these locations. As for the ROETUN and H2B cores, the bulk sedimentary $\delta^{15}N_{bulk}$ values decrease with the increase of vitrinite reflectance, which is opposite of what was expected.

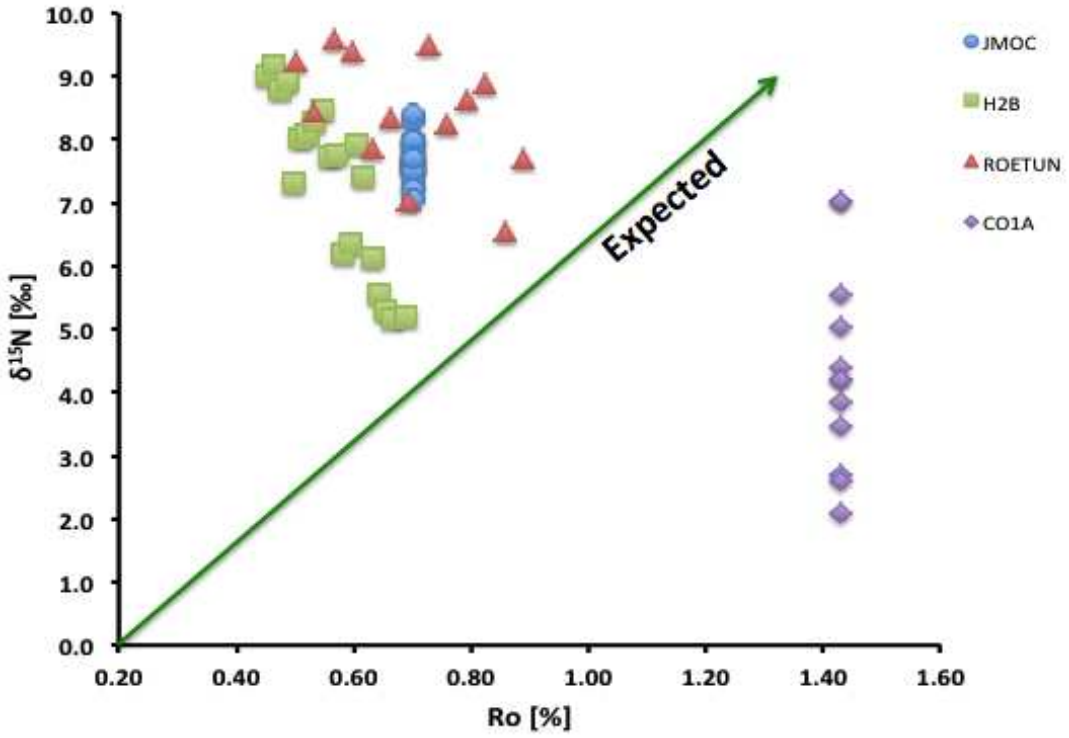

$\delta^{15}N_{bulk}$ values against the various R_o values (Figure 13) for each location, what is observed is a decrease in bulk sedimentary $\delta^{15}N_{bulk}$ values with the increase of vitrinite reflectance. This is contrary to what is expected (shown by the green arrow), where the sample locations with less average vitrinite reflectance values have relatively greater average bulk sedimentary $\delta^{15}N_{bulk}$ values than those with greater average vitrinite reflectance values.

In this figure, the data can be separated into two populations similar to what was previously observed. One population, represented by JMOC, ROETUN and H2B sediments, has higher bulk sedimentary $\delta^{15}N_{bulk}$ values than the other, represented by CO1A sediments. The population with higher bulk sedimentary $\delta^{15}N_{bulk}$ values has an average of 7.8 ‰ ± 0.6 ‰,

whereas the population with lower bulk sedimentary $\delta^{15}N_{bulk}$ values has an average of 4 ‰ ± 2 ‰. Also, the population with greater bulk sedimentary $\delta^{15}N_{bulk}$ values lies within the oil window (R_o below 1.3 %) and the population with less bulk sedimentary $\delta^{15}N_{bulk}$ values lies within the gas window (R_o above 1.3%). If thermal maturity had indeed affected the initial $\delta^{15}N_{bulk}$ values of the sediments at the sample locations, what we expect to see are higher bulk sedimentary $\delta^{15}N_{bulk}$ values for the population in the gas window compared to the population in the oil window. However, that is not the case, which suggests that thermal maturity did not affect the bulk sedimentary $\delta^{15}N_{bulk}$ values as previously expected. Instead, the bulk sedimentary $\delta^{15}N_{bulk}$ values seem to be more strongly influenced by the redox state of the water column during sediment and organic matter deposition. The higher bulk sedimentary $\delta^{15}N_{bulk}$ values observed at the JMOC, ROETUN and H2B sample locations suggest that sediments and organic matter at these locations were deposited under suboxic environments, which are within the $\delta^{15}N$ range (7 – 10 ‰) for organic matter resulting from denitrification (Altabet et al., 1998; Altabet et al., 1999; Voss et al., 2001; Altabet et al., 2002; Hendy et al., 2004; Robinson et al., 2006). On the other hand, the lower bulk sedimentary $\delta^{15}N_{bulk}$ values observed at the CO1A sample location suggest that sediments and organic matter at this location were deposited under anoxic environments (Figure 11).

The redox conditions during sediment and organic matter deposition at each sample location suggest that the depositional environments impose greater influence on the bulk sedimentary $\delta^{15}N_{bulk}$ values than thermal maturity. Looking at the average bulk sedimentary $\delta^{15}N_{bulk}$ values of each Woodford subdivision from each location (Table 6), it is apparent that redox conditions have changed throughout Woodford deposition. The average bulk sedimentary $\delta^{15}N_{bulk}$ values increase from older to younger sediments at the sample locations indicating a change in the water column redox states geographically over time. For the CO1A, the average

$\delta^{15}N$ values for the Lower and Middle Woodford (3 ‰ ± 1 ‰ and 3.8 ‰ ± 0.5 ‰, respectively) are significantly more depleted than the Upper Woodford (6 ‰ ± 1 ‰), indicating anoxic bottom waters during Lower and Middle Woodford deposition. Over time, the oxygen concentrations of the bottom waters increased from anoxic to suboxic at this location, resulting in an increase of water column denitrification and subsequently enriching the average $\delta^{15}N$ values. As for the ROETUN sediments, the average bulk sedimentary $\delta^{15}N$ values for the Lower Woodford (8 ‰ ± 1 ‰) are relatively more depleted than the Upper Woodford (8.6 ‰ ± 0.8 ‰). Similar to ROETUN, the average bulk sedimentary $\delta^{15}N$ values for Middle Woodford (6 ‰ ± 1 ‰) at the H2B location are relatively more depleted than the Upper Woodford (8.0 ‰ ± 0.9 ‰). Over time, the oxygen concentrations in the bottom waters during Upper Woodford deposition at the ROETUN and H2B locations increased, which resulted in an increase of the degree of denitrification in the Upper Woodford. It is important to note that the increase of the oxygen concentrations over time does not result in a completely oxic water column. Regarding the subdivisions of the JMOC, the average $\delta^{15}N$ values remain consistent throughout the entire Woodford and throughout time. Therefore, the suboxic redox conditions throughout time at this location remain constant. Overall, the enriched average $\delta^{15}N$ values observed in the JMOC, ROETUN, and upper H2B are attributed to the deposition of sediments in OMZs, where the denitrification process is predominant. The depleted average $\delta^{15}N$ value observed in the CO1A is attributed to the deposition of sediments under prevailing anoxic environments. However, the stratigraphic variations in the average $\delta^{15}N$ values observed in the Woodford subdivisions of ROETUN, H2B and CO1A are attributed to the water column redox states changing throughout Woodford deposition.

As mentioned earlier, we made an assumption that the sedimentary organic matter of the Woodford Shale is from a similar source to reduce the variables that could possibly affect the bulk sedimentary $\delta^{15}N_{bulk}$. To test whether or not the sedimentary organic matter is from the

same source, a plot of the $\delta^{13}C$ values versus depth for all sample locations is evaluated (Figure 14). If the sedimentary organic matter from each sample locations is from a similar source, then what is expected is an overlap of $\delta^{13}C$ values because same sources of organic matter will exhibit similar $\delta^{13}C$ values (Beier and Hayes, 1989; Schubert and Calvert, 2000; Koppelmann et al., 2009; Bonn and Rounds, 2010). In fact, the organic $\delta^{13}C$ values of this plot overlap, which indicate a common source for organic matter. This interpretation agrees with the results from the study by Beier and Hayes (1989), which reports organic $\delta^{13}C$ values in the range of -28.8 ‰ to -30.0 ‰ for the New Albany Shale. They suggest that this range indicates a common source for organic matter for the sample intervals of the New Albany Shale.

5.2 Evidence of thermal maturity

Unlike the bulk sedimentary $\delta^{15}N_{bulk}$ values, the organic $\delta^{13}C$ values may reflect thermal maturity effects (Lewan, 1983) and can be explained by analyzing the cross-plot of the $\delta^{13}C$ values versus R_o (Figure 16). Since the organic $\delta^{13}C_{org}$ values indicate common source of organic matter, the ranges may be caused by thermal maturity, which can be explained by evaluating the cross-plot of the organic $\delta^{13}C_{org}$ values versus R_o. Figure 15 shows no direct relationship between the $\delta^{13}C_{org}$ values and thermal maturity. H2B sediments seem to exhibit an increase in $\delta^{13}C_{org}$ values with the increase of thermal maturity. In contrast to H2B, ROETUN sediments exhibit a decrease of organic $\delta^{13}C$ values with the increase of thermal maturity. If thermal maturation affects the sediments in both of these sites, then the organic $\delta^{13}C$ values should be affected proportionately and positively (Lewan, 1983). In fact this is not the case. Therefore, the arrangement of the organic $\delta^{13}C$ values observed in Figure 14 suggests a common source for the organic matter in the sediments at each sample location rather than the product of different organic matter sources.

Figure 14. A plot of the depth versus $\delta^{13}C$. The values represent the averages of the $\delta^{13}C$ values. Notice how the ranges overlap, indicating similar source material of organic matter, in this case marine. The average $\delta^{13}C$ values for each location are represented by the large symbols.

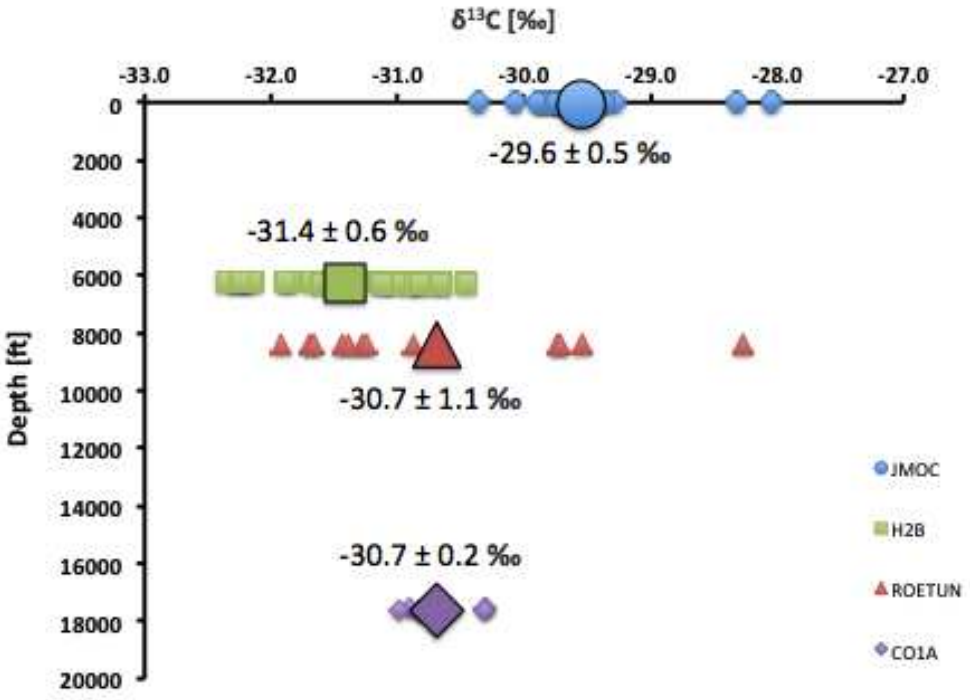

Studies have shown that alterations of elemental concentrations and isotopic compositions are associated with the increase of thermal maturity from the oil generation window to the gas generation window (Boudou et al., 1984a; Zhu et al., 2000; Oldenburg et al., 2007; Boudou et al., 2008). However, the observed nitrogen isotopic compositions of the samples in this study do not show thermal maturation effects. Even though the nitrogen isotopic signals do not show the effects of thermal maturity, it may still be observed in the elemental concentrations. In order to examine thermal maturity affects, cross-plots of weight % TN and TOC versus R_o were constructed (Figures 16 and 17). Because nitrogen and carbon are lost from kerogen during the expulsion of hydrocarbons (Boudou et al., 1984a; Barth et al., 1986; Vandenbroucke et al., 2007; Boudou et al., 2008; Schimmelman and Lis, 2010), cross-plots of weight % TN and TOC

Figure 15. A cross-plot of the $\delta^{13}C_{org}$ values versus R_o values for each sample from the JMOC, ROETUN, CO1A and H2B samples. The projected vitrinite reflectance values from CAI for the JMOC and isoreflectance maps from the Anadarko Basin for the CO1A samples were assumed to represent the entire Woodford Shale at these locations, thus the R_o values are the same for each sample at these locations. This results in the vertical lines observed for these locations. For the H2B samples, an increase in $\delta^{13}C_{org}$ values is observed with an increase of R_o, however for the ROETUN the opposite is observed.

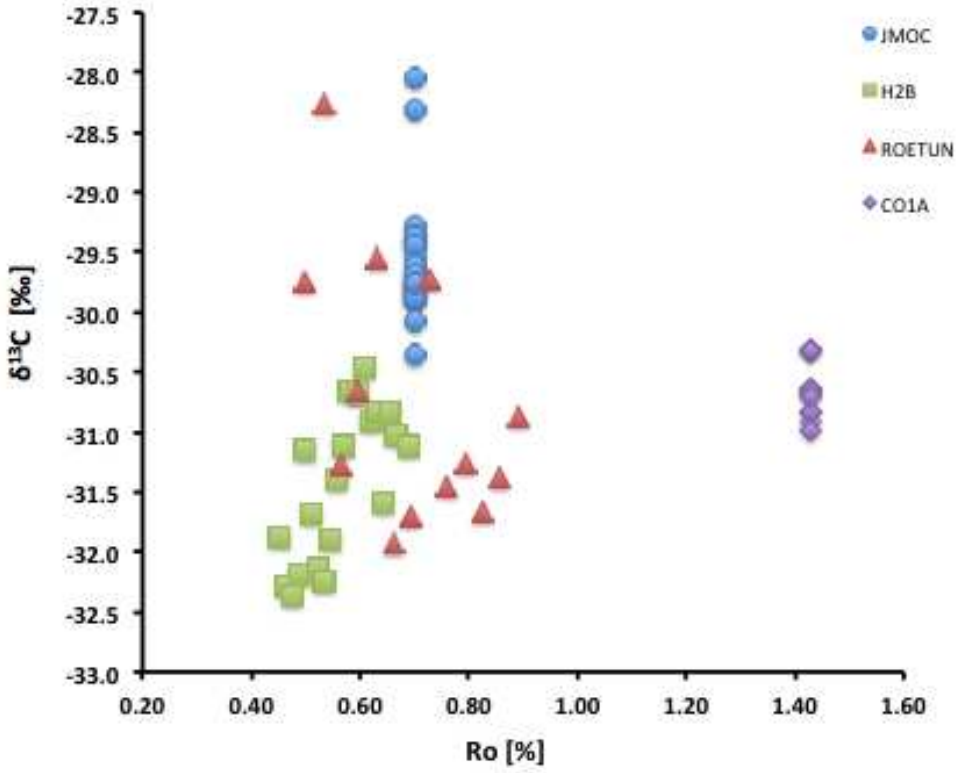

versus R_o should display a relative decrease in weight % of TN and TOC with increasing R_o.

Contrary to what is expected, the cross-plot of weight % TN versus R_o displays an increase of weight % TN with the increase of R_o values (Figure 16). Similar to the TN concentrations, TOC concentrations should exhibit an increase with the increase of thermal maturity, however this is not what is observed (Figure 17). Since Figures 16 and 17 do not exhibit a relationship between TN and TOC with thermal maturity, other post-depositional alterations may be the cause. TN concentrations of sediments reflect nitrogen preservation, via

Figure 16. Cross-plot of weight % TN versus R_o for the Woodford Shale interval for JMOC, ROETUN, CO1A and H2B. Contrary to the expected (green arrow) decrease of TN with increasing R_o, what is observed is a relative increase of TN from JMOC to CO1A. This is attributed to preservation.

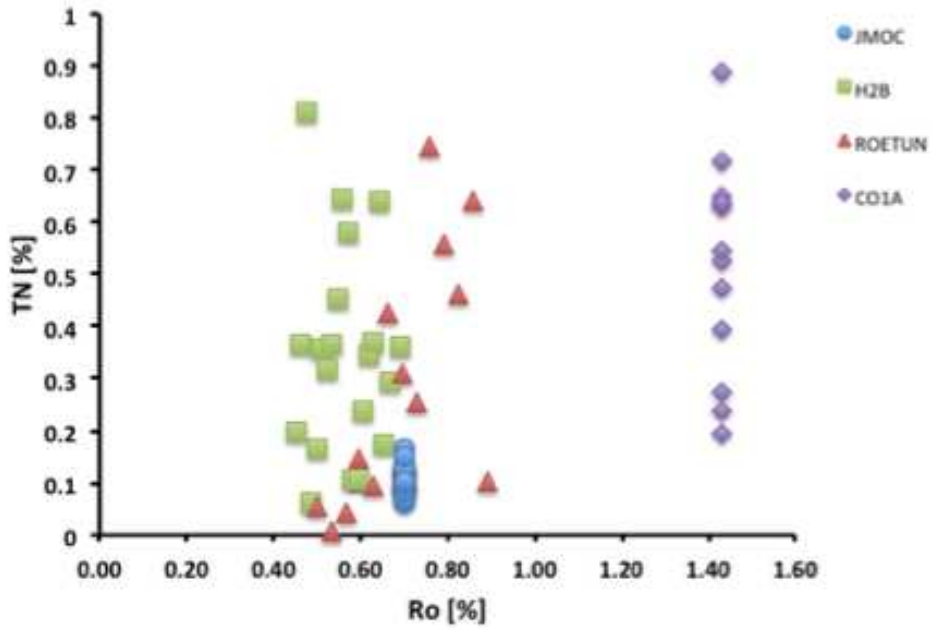

Figure 17. Cross-plot of weight % TOC versus R_o for the Woodford Shale interval for JMOC, ROETUN, CO1A and H2B. Contrary to the expected (green arrow) decrease of TOC with increasing R_o, what is observed is a relative increase of TN from JMOC to CO1A with a drastic increase from JMOC to H2B. The relative increase from JMOC to CO1A is attributed to preservation, whereas the dramatic increase from JMOC to H2B is attributed to PP.

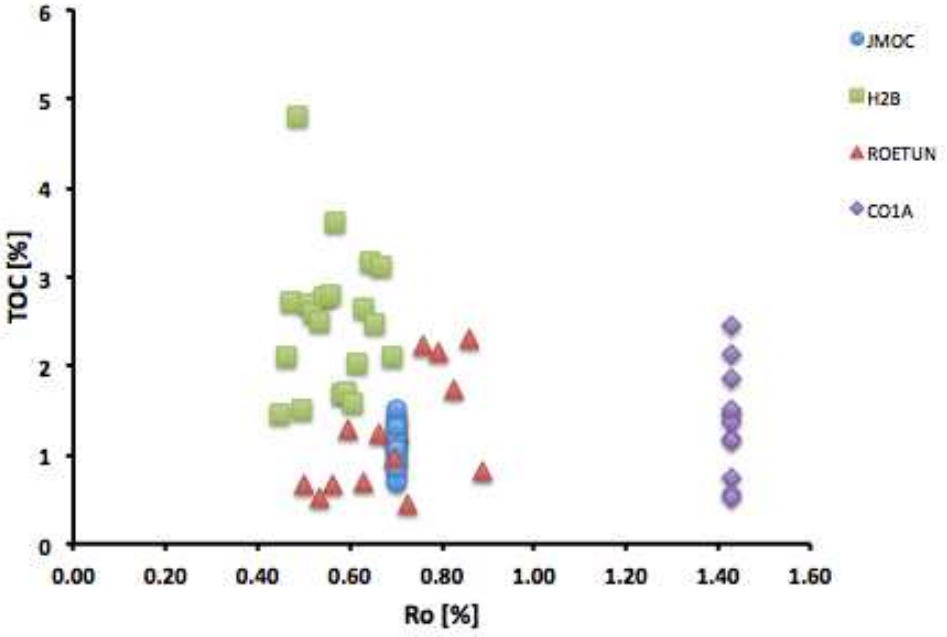

lattice-bound nitrogen in clay (Mingram et al., 2003, Knies et al., 2007) and initial concentrations based on locality and source (Knies et al., 2007; Mobius et al., 2010; Schneider-Mor et al., 2012), or degradation (Mingram and Brauer, 2001; Lehmann et al., 2002; Zonneveld et al., 2010). TOC concentrations in sediments reflect primary production (Mobius et al., 2010; Schneider-Mor et al., 2012), preservation (Schwart and Frimmel, 2004; Mobius et al., 2010), and decomposition (Mingram and Brauer, 2001; Mobius et al., 2010). The TN and TOC values are lower in the younger sediments at the sample locations (Figure 6). This may indicate that over time organic matter degradation increased as oxygen increased, which would suggest that the TN concentrations at the sample locations are strongly related to organic matter degradation and preservation. Therefore, in this study, the TN and TOC concentrations of the sediments at the sample locations seem to reflect degradation and preservation.

5.3 Trace element record of the Woodford Shale for paleoredox proxies

Trace elements are present in marine water in two different semblances: 1) soluble form, or 2) adsorbed onto particles. These trace metals are transferred to sediments by either biotic or abiotic processes (Tribovillard et al., 2006). The deposition of trace elements into the sediments is strongly influenced by the redox state of the water column, biological activity, and location of the chemocline relative to the basin (Cruse and Lyons, 2004; Tribovillard et al., 2006). The effects of these influences result in the variations of enrichment and depletion within the sedimentary record (Cruse and Lyons, 2004; Brumsack, 2006; Tribovillard et al., 2006). Oxygen concentrations of the water column predominantly control the aforementioned influences, though in the case of anoxic environments, the reduced forms of the trace metals are easily diffused into the sediments (Cruse and Lyons, 2004; Brumsack, 2006; Tribovillard et al., 2006). Amongst the trace elements measured, Fe, V, U, Zn, Mo and Mn (Table 6) concentrations were evaluated for this study.

As mentioned earlier, U and Mo concentrations are redox sensitive trace metals (Calvert and Pederson, 1993; Mumford and Emerson, 1999; Cruse and Lyons, 2004; Brumsack, 2006; Tribovillard et al., 2006), where U and Mo concentrations are enriched in sediments deposited in anoxic bottom waters due to the reduced forms diffusion from the water column, diffusion reactions and adsorption or precipitation (Calvert and Pederson, 1993; Mumford and Emerson, 1999; Brumsack, 2006; Tribovillard et al., 2006). The concentrations of U and Mo exhibit strong correlations with one another because U and Mo concentrations depend on the accumulation rate and the oxygen penetration depth within the sediments (Mumford and Emmerson, 1999; Tribovillard et al., 2006). Slower sedimentation rates allow more time for diffusion from the water column to the sediments. For sediments deposited in anoxic bottom waters, it is expected that the U and Mo concentrations of the sample locations be relatively enriched compared to PAAS. The average U concentrations for the JMOC (7 ± 2pm/wt. %), ROETUN (18 ± 23 ppm/wt. %), CO1A (49 ± 23 ppm/wt. %), and H2B (8 ±12 ppm/wt.%) and the average Mo concentrations for the JMOC (8 ± 6), ROETUN (51 ± 74), CO1A (123 ± 69) and H2B (46 ± 38) are all enriched relative to PAAS (U = 0.31 ppm/wt. %; Mo = 0.10 %). The enrichment of U and Mo observed in the CO1A relative to JMOC, ROETUN and H2B indicate anoxia for the CO1A sediments and suboxia for the JMOC, ROETUN and H2B sediments. The depositional environments concluded from the trace metals supports the depositional environments concluded from the bulk sedimentary $\delta^{15}N_{bulk}$ values.

Iron is generally enriched in black shales due to its reduction under anoxic conditions and subsequent fixation as pyrite (Cruse and Lyons, 2004). The Fe/Al ratio enrichment relative to PAAS (Figures 10a, b, c and d) may be indicative of anoxic environments (Cruse and Lyons, 2004). However, initial Fe concentrations within the water column may differ from location to location as a result of water column processes (i.e. upwelling zones; Chase et al. (2005)), and the presence of different Fe forms (i.e. particulate and dissolved Fe; Cruse and Lyons (2004); Chase

et al. (2005)), and thus may not be a direct response to redox conditions. Therefore, the variation of initial Fe between the sample locations may be the cause of several processes, which cannot be explained by the observed Fe concentrations in the sample locations. Regarding the presence of pyrite, Fe fixation can occur in situ in euxinic bottom waters or in euxinic pore water in the sediments (Cruse and Lyons, 2004). The bulk sedimentary $\delta^{15}N_{bulk}$ values suggest suboxia and anoxia rather than euxinia. Therefore, pyrite mineralization in the sample locations of this study is most likely confined to pore water in the sediments.

Vanadium is relatively unreactive in marine water as is generally concentrated in sediments overlain by anoxic or near-anoxic bottom waters (Emerson and Huested, 1991; Mumford and Emerson, 1999; Tribovillard et al., 2006) due to the direct interaction with organic matter (Cruse and Lyons, 2004). The average V concentrations for the JMOC (140 ± 23 ppm/wt. %), ROETUN (310 ± 290 ppm/wt. %), CO1A (500 ± 290 ppm/wt. %), and H2B (630 ± 270 ppm/wt.%) display a strong correlation with organic matter, where the average TOC concentrations show an increase from JMOC (1.1 ± 0.2 %) to H2B (2.5 ± 0.8). Zinc concentrations, like V, are associated with organic matter (Robinson et al., 2002; Tribovillard et al., 2006). This correlation between Zn and TOC is observed in the sample locations, where the average Zn concentrations increase from the JMOC (72 ± 31 ppm/wt. %), ROETUN (300 ± 370 ppm/wt. %), CO1A (460 ± 400 ppm/wt. %), to H2B (750 ± 980 ppm/wt. %) and the average TOC concentrations increase from JMOC to H2B, as previously noted (Table 6). This indicates that for the sample locations, V and Zn concentrations are strongly correlated with organic matter concentrations rather than redox states.

Manganese concentrations in sediments are depleted in suboxic to anoxic sediments (Cruse and Lyons, 2004), as it is highly mobile in its reduced state (Brumsack, H.J., 2006). The average Mn concentrations for the JMOC (292 ± 93 %), ROETUN (130 ± 67), and H2B (125 ± 170) are enriched relative to PAAS, whereas the average Mn concentration for the CO1A (68 ±

34) is depleted relative to PAAS. The depletion of Mn concentrations in the CO1A relative to PAAS are indicative of anoxic water column, where the average and majority Mn concentrations are depleted relative to PAAS. However, the enriched Mn concentrations observed in the JMOC, ROETUN and H2B could be explained by the reductive leaching into the sediments from oxygen minimum zone waters (Bender et al., 1977; Calvert and Pederson, 1993; Lewis and Luther, 2000; Brumsack, 2006). The average Mn concentrations seem to correlate with the $\delta^{15}N$ values. It has been suggested that the electron acceptor MnO_2 may oxidize NH_4^+ to produce NO_3^-, which can then be denitrified (Hulth, 2005). However, this indirect relationship of the $\delta^{15}N$ values with Mn has yet to be observed and may be more complicated. Further investigation is required to uncover the relationship observed between sedimentary $\delta^{15}N$ values and Mn in these sample locations.

5.4 Depositional evolution of the Woodford Shale at JMOC, ROETUN, CO1A and H2B locations

The data in this study indicates that the redox states of the water column during sediment and organic matter deposition at the sample locations more strongly influenced the bulk sedimentary $\delta^{15}N_{bulk}$ values than the thermal maturity. The redox states of the bottom waters during deposition varied temporally and spatially throughout the basin. In the shelf and basin margins (JMOC, ROETUN and H2B), suboxic bottom waters prevail, while anoxic bottom waters prevail in the depocenter of the basin (CO1A). Over time, the redox states of the water column at these locations have changed due to the increase of oxygen in the bottom waters. Based on the bulk sedimentary $\delta^{15}N_{bulk}$ isotopic ratios and the U and Mo concentrations, the water column at the ROETUN and H2B locations remained suboxic despite the increase of oxygen, while the CO1A changed from anoxic to suboxic. This increase of oxygen resulted in an increase in incomplete denitrification from the lower and/or Middle Woodford to the Upper Woodford in each section: Lower Woodford for the ROETUN, the Middle Woodford for the H2B, and the Middle and Lower Woodford for the CO1A. The TN and TOC concentrations observed at the

sample locations show no direct relationship with thermal maturity, and in fact reflect organic matter degradation and preservation. The TN and TOC concentrations in all of the samples have decreased over time from the older sediments to the younger sediments. These concentrations indicate that over time, as oxygen concentrations increased, organic matter degradation increased. The organic matter content is primarily derived from the same marine source. The pore waters of the sediments within the basin at all of the sample locations were sulfate reducing at some point in time, which resulted in abundant pyrite mineralization.

CHAPTER VI

CONCLUSIONS

6.1 Conclusions

In this thesis, the results of the nitrogen isotopic compositions of bulk samples and the carbon isotopic compositions of acidified samples from three cores of the Woodford Shale from the Anadarko Basin and one outcrop exposing the Woodford Shale from the Ozark Plateau were presented. The results reveal the JMOC (7.7 ‰ ± 0.3 ‰), ROETUN (8 ‰ ± 1 ‰) and H2B (7 ‰ ± 1 ‰) sediments have relatively more enriched average $\delta^{15}N$ values, whereas the CO1A (4 ‰ ± 2 ‰) sediments have relatively more depleted average $\delta^{15}N$ values. Despite the variability observed in the $\delta^{15}N$ values, the organic $\delta^{13}C$ ranges for the JMOC (-51.7 ‰ to -29.5 ‰), ROETUN (-45.8 ‰ to -42.5 ‰), CO1A (-31.0 ‰ to -30.3 ‰) and H2B (-45.5 ‰ to -31.2 ‰) overlap indicating the same source of organic matter. When the data were cross-plotted with vitrinite reflectance data for the sample locations, the results of the bulk sedimentary $\delta^{15}N$ values did not coincide with what was expected for $\delta^{15}N$ values affected by increased thermal maturity. In fact, the results indicated two different populations.

The average TN concentrations reveal the JMOC (0.11 % ± 0.03 %), ROETUN (0.3 % ± 0.3 %), H2B (0.4 % ± 0.2 %) have relatively more depleted average TN values than the CO1A (0.5 % 0.2 %) sediments. The results of the average total organic carbon for the JMOC (1.14 % ± 0.21%), ROETUN (1.21 % ± 0.68 %), and CO1A (1.36 % ± 0.59 %) sediments have relatively more depleted values than the H2B (2.51 % ± 0.81 %) sediments. The higher average TN and

TOC concentrations observed in the older sediments in the sample locations reflects greater organic matter preservation than in the lower sediments, where the lower TN and TOC concentrations are attributed to greater organic matter degradation. The observed decrease of TN and TOC concentrations at the sample locations correlates with the increased oxygen concentrations over time. Therefore, the isotopic composition and elemental concentrations suggest that the initial depositional environment has greater influence on the bulk sedimentary $\delta^{15}N$ values than catagenesis.

The difference in $\delta^{15}N$ values is attributed to the sedimentation of the Woodford Shale in two different depositional environments, anoxic for the CO1A sediments and suboxic for the JMOC, ROETUN and H2B sediments. The JMOC, ROETUN and H2B sediments were deposited under suboxic bottom waters while the CO1A sediments were deposited under anoxic bottom waters. However, the upper Woodford interval in the CO1A was deposited under suboxic environments. Incomplete denitrification was predominant in the water column during the deposition of the JMOC, ROETUN and H2B sediments resulting in the relatively enriched average bulk sedimentary $\delta^{15}N$ values. On the other hand, nitrogen fixation was predominant in the water column during the deposition of the CO1A sediments producing the relatively depleted average bulk sedimentary $\delta^{15}N$ values observed. The suboxic environment that the upper Woodford was deposited in the CO1A, resulted in denitrification. The suboxic environments during JMOC and ROETUN sediment deposition are further supported by the low V, U, MO and Zn concentrations and high Mn concentrations. The low V, U, Mo and Zn concentrations are attributed to the suboxic nature of the water column during sedimentation. The low Mn concentrations in the CO1A is attributed the anoxic environments, while the high Mn concentrations are attributed to the reductive leaching into sediments deposited under suboxic environments. The anoxic environment during CO1A sediment and organic matter deposition is further supported by the high V, U, Mo and Zn concentrations. The Fe concentration enrichments

observed in the sample locations are attributed to euxinic pore waters and the mineralization of pyrite taking place in the sediments. As for the H2B, the relatively low V and U concentrations support the suboxic environments during sediment deposition.

6.2 Recommendations

The present study was based on three subsurface locations and one outcrop location to address a regional study. Future studies should incorporate more sample locations including core and outcrop locations as well as increase the data gathered. To increase the data, bulk and clay mineralogy should be analyzed. It has been speculated the bulk and clay mineralogy may affect the bulk sedimentary $\delta^{15}N$ values (Mingram and Brauer, 2001; Mingram et al., 2003). With the interaction of formation fluids, NH_3 can be lost and reincorporated back into organic matter, and/or be incorporated into clay minerals in the form of NH_4 (Mingram et al., 2003). Clay minerals in organic-rich shales have a high potential to absorb inorganic NH_4 and preserve it in the mineral lattice during post-depositional alterations (Mingram and Brauer, 2001; Mingram et al., 2003). Also, NH_4 is substituted for potassium in minerals including illite, muscovite, biotite and feldspar due to its equal charge and similar ionic radius to potassium (K) (Mingram and Brauer, 2001). The $\delta^{15}N$ values of the NH_4 species bound in the minerals are dependent on the parent nitrogen (i.e. organic matter) (Mingram et al., 2003). Therefore, the $\delta^{15}N$ values of the NH_4 bound in the clay lattice or incorporated in minerals would reflect that of the parent specie, which could possibly be the initial $\delta^{15}N$ values.

Another possibility to increase the data gathered, future studies could measure vitrinite reflectance on the same samples. For this study, vitrinite reflectance data was based on isoreflectance maps and data gathered from Cardott (2012) and conodont color alteration indices. For the samples that vitrinite reflectance measurements were projected, direct measurements would increase the accuracy and precision of the thermal maturity at the JMOC and CO1A. Also,

the vitrinite reflectance data interpreted from the isoreflectance maps, however generally accurate, are speculative and may not be the precise vitrinite reflectance for the sample location. Conodont color alteration indices have been used to identify the relative thermal maturity of a formation (Epstein et al., 1977), however it provides a general range for thermal maturity and thus accompanied by discrepancies. Therefore, vitrinite reflectance measurements for future studies should be conducted on the same samples as the isotopic and elemental data was analyzed to cut down any associated error.

REFERENCES

Adigwe, E., 2012. Nitrogen isotopes as indicators of depositional environments: case of the Caney and Woodford Shales in the Arkoma Basin, Oklahoma, USA. MS Thesis, Oklahoma State University.

Altabet, M., and Francois, R., 1994. Sedimentary nitrogen isotopic ratio as a recorder for surface ocean nitrate utilization. Global Biogeochemical Cycles, 8, 103-116.

Altabet, M., Francois, R., Murray, D.W., and Prell, W.L., 1995. Climate- related variations in denitrification in the Arabian Sea from sediment $^{15}N/^{14}N$ ratios. Nature, 373, 506-509.

Altabet, M.A., Pilskaln, C., Thunell, R., Pride, C., Sigman, D., Chavez, F., and Francois, R., 1999. The nitrogen isotope biogeochemistry of sinking particles from the margin of the Eastern North Pacific. Deep-Sea Research I, 46, 655-679.

Altabet, M., Higgins, M.J., and Murray, D.W., 2002. The effect of millennial-scale changes in Arabian Sea denitrification on atmospheric CO_2. Nature, 415, 159-162.

Barth, T., Rist, K., Huseby, B., and Ocampo, R., 1996. The distribution of nitrogen between bitumen, water and residue in hydrous pyrolysis of extracted Messel oil shale. Organic Geochemistry, 24, 889 – 895.

Beier, .A., and Hayes, J.M., 1989. Geochemical and isotopic evidence for paleoredox conditions during deposition of the Devonian-Mississippian New Albany Shale, Southern Indiana: Geological Society of America Bulletin, 101, 774-782.

Bender, M.L., Klinkhammer, G.P., and Spencer, D.W., 1977. Manganese in seawater and marine manganese balance. Deep-Sea Research 24, 799 – 812.

Bonn, B.A., and Rounds, S.A., 2012. Use of stable isotopes of carbon and nitrogen to identify sources of organic matter to bed sediments of the Tualatin River, Oregon. United States Geological Survey, Scientific Investigations Report 2010-5154, 1 – 58.

Boudou, J.P., Mariotti, A., and Oudin, J.L., 1984. Unexpected enrichment of nitrogen during the diagenetic alteration of sedimentary organic matter. Fuel, 63, 1508-1510. doi: 10.1016/0016-2361(84)90215-1.

Boudou, J.P., Schimmelmann, A., Ader, M., Mastalerz, M., Sebilo, M., and Gengembre, L., 2008. Organic nitrogen chemistry during low-grade metamorphism. Geochimica et Cosmochimica Acta, 72, 1199-1221.

Bowen, R., 1988. *Isotopes in the Earth Sceinces:Environmental Isotopes in the Atmosphere and Hydrosphere*. New York, NY: Elsevier Publishing Company, Inc.

Brumsack, H.J., 2006. The trace metal content of recent organic carbon-rich sediments: Implications for Cretaceous black shale formation. Paleogeography, Paleoclimatology, Paleoecology, 232, 344-361.

Caldwell, C. D., 2011. Lithostratigraphy of the Woodfrod Shale, Anadarko Basin, West-Central Oklahoma. *American Association of Petroleum Geologists Mid-Con meeting*, Oklahoma City, OK, October 1-4, 2011.

Calvert, S.E., and Pedersen, T.F., 1993. Geochemistry of recent oxic and anoxic marine sediments: Implications for the geologic record. Marine Geology, 113, 67-88.

Calvert, S.E., Bustin, R.M., and Ingall, E.D., 1996. Influence of water column anoxia and sediment supply on burial and preservation of organic carbon in marine shales. Geochimica et Cosmochimica Acta, 60, 1577-1593.

Canfield, D.E., Kristensen, E., and Thamdrup, B., "The nitrogen cycle," in Advances in Marine Biology. Aquatic Geomicrobiology, A. Southward, P. A. Tyler, C. M. Young, and L. A. Fuiman, Eds., vol. 48, chapter 7, pp. 205–267, Elsevier, London, UK, 2005.

Cardott, B.J. and Lambert, M.W., 1982. Thermal maturation by vitrinite reflectance of Woodford Shale, Anadarko Basin, Oklahoma. The American Association of Petroleum Geologists Bulletin 69, 1982-1998.

Cardott, B.J., 1989. Thermal maturation of the Woodford Shale in the Anadarko Basin. Oklahoma Geological Survey Circular, 90, 32-46.

Cardott, B.J., 2012. Thermal maturity of the Woodford Shale gas and oil plays , Oklahoma, USA. International Journal of Coal Geology, 103, 109-119.

Carr III, J.L., 1989. The thermal maturity of the Chattanooga Formation along a transect from the Ozark Uplift to the Arkoma Basin. Oklahoma City Geological Society Shale Shaker, 12, 161 – 169.

Checkley, D.M., Jr., and Miller, C.A., 1989. Nitrogen isotope fractionation by oceanic zooplankton. Deep-Sea Research, 36, 1449-1456.

Cruse, A.M., and Lyons, T.W., 2004. Trace metal records of regional paleoenvironmental variability in Pennsylvanian (Upper Cretaceous) black shales. Chemical Geology, 206, 319-345.

Da Wang, H., and Philp, R.P., 1997. Geochemical study of potential source rocks and crude oils in the Anadarko Basin, Oklahoma. American Association of Petroleum Geologists Bulletin, 81, 240 – 275.

Dalsgaard, T., Canfield, D.E., Peterson, J., Thamdrup, B., and Acuna-Gonzalez, J., 2003. N_2 production by the anammox reaction in the anoxic water column of Golfo Dulce, Costa Rica. Nature, 422, 606-608.

Dean, M.T., and Turner, N., 1995. Conodont color alteration index (CAI) values for the Carboniferous of Scotland. Transactions of the Royal Society of Edinburg: Earth Science, 85, 211-220.

Emerson, S.R., and Huested, S.S., 1991. Ocean anoxia and ocean concentrations of molybdenumand vanadium in seawater. Marine Chemistry, 34, 177-196.

Epstein, A.G., Epstein, J.B., and Harris, L.D., 1977. Conodont color alteration – an index to organic metamorphism. Geologic Survey Professional Paper, 995, 1-27.

Ettensohn, F.R., Lierman, R.T., and Mason, C.E., 2009. Upper Devoian – Lower Mississippian clastic rocks in northeastern Kentucky: Evidence for Acadian alpine glaciation and models for source-rock and reservoir-rock development in the eastern United States, Spring Field Trip, April 18, 2009: Lexington, American Institute of Professional Geologists – Kentucky Section, 52 p. (contains 7 articles coauthored by F.R. Ettensohn).

Faure, G., and Mensing, T., 2005. *Isotopes: Principles and Applications* (third edition). Hoboken, NJ: John Wiley Sons, Inc.

Franseen, E.K., Byrnes, A.P., Cansler, J.R., Steinhauff, D.M., and Carr, T.R., 2004. The Geology of Kansas, Arbuckle Group. Current Research in in Earth Sciences Bulletin, 250, 43.

Galbraith, E.D., Kienast, M., Pederson, T.F., and Calvert, S.E., 2004. Glacial-interglacial modulation of marine nitrogen cycle by high-latitude O_2 supply to the golbal thermocline. Paleoceanography. 19, PA4007.

Gallardo, J., and Blackwell, D.D., 1999. Thermal structure of the Anadarko Basin. American Association of Petroleum Geologists Bulletin, 83, 333-361.

Galloway, J.N., 2005. The global nitrogen cycle: past, present and future. Science in China. Series C, Life sciences/Chinese Academy of Sciences, 48 Special No., 669 – 677.

Ganeshram, R.S., Pederson, T.F., Calvert, S.E., and Murray, J.W., 1995. Large changes in oceanic nutrient inventories from glacial to interglacial periods. Nature, 376, 755-758.

Godfrey, L.V., and Glass, J.B., (2011), The geochemical record of the ancient nitrogen cycle, nitrogen isotopes and metal co-factors. Methods in Enzymology, 486, 483-506.

Gondwe, M., Guilford, S., and Hecky, R., 2008. Planktonic nitrogen fixation in Lake Malawi/Nyasa. Hydrobiologia 596, 251-267.

Granger et al., 2008. Nitrogen isotope fractionation during dissimilatory nitrate reduction by denitrifying bacteria. Limnology and Oceanography, 53, 2533-2545.

Gruber, N., 2008. The marine nitrogen cycle: overview and challenges. In *Nitrogen in the Marine Environment*, ed. DG Capone, DA Bronk, MR Mulholland, EJ Carpenter, 1-50. Amsterdam: Elsevier. 2nd edition.

Hendy, I.L., Pederson, T.F., Kennet, J.P., and Tada, R., 2004. Intermittent existence of a southern California upwelling cell during submillennial climate change of the last 60kyr. Paleoeanography 19 (3).

Holmes, E.M., Müller, P.J., Schneider, R.R., Segl, M., Pätzold, J., and Wefer, G., 1996. Stable nitrogen isotopes in Angola Basin surface sediments. Marine Geology, 134, 1-12.

Hulth, S., Aller, R.C., Canfield, D.E., Dalsgaard, T., Engstrom, P., Gilbert, F., Sundback, K., and Thamdrup, B., 2005. Nitrogen removal in marine environments: recent findings and future research challenges. Marine Chemistry, 94, 125-145.

Jasper, J.P., and Gagosian, R.B., 1990. The source and deposition of organic matter in the Late Quaternary Pigmy Basin, Gulf of Mexico. Geochimica et Cosmochimica Acta, 54, 1117 – 1132.

Jetten, M.S.M., Wagner, M., Fuerst, J., van Loosdrecht, M., Kuenen, G., and Strous, M., 2001. Microbiology and application of the anaerobic ammoniu oxidation (anammox) process. Current Opinion in Biotechnology, 12, 283-288.

Johnson, K.S., 1989. Geologic evolution of the Anadarko Basin, *in* Kenneth S. Johnson (ed.), Anadarko Symposium: Oklahoma Geological Survey, Norman, Circular, 90, 3-12.

Johnson, K.S., 2008. Geologic history of Oklahoma. Oklahoma Geological Survey Educational Publication, 9, 3 – 8.

Karl et al., 1997. The role of nitrogen fixation in biogeochemical cycling in the subtropical North Pacific Ocean. Nature, 388, 533-538.

Karl, D.M., and Michaels, A.F., 2001. *Encyclopedia of Ocean Sciences: Nitrogen Cycle* (v. 4). San Diego, CA: Academic Press, ed. Steele, J., Turekian, K., and Thorpe, S.

Killops, S., and Killops, V., 2005. Introduction to Organic Geochemistry Blackwell, Oxford.

Klinkhammer, G.P., and Bender, M.L., 1980. The distribution of manganese in the Pacific Ocean. Earth Planetary Science Letters, 46, 361-384.

Knies, J., Brookes, S., and Schubert, C.J., 2007. Re-assessing the nitrogen signal in continental margin sediments: New insights from the high northern latitudes. Earth and Planetary Science Letters, 253, 471-484.

Koppelmann, R., Böttger-Schnack, R., Möbius, J., and Weikert, H., 2009. Trophic relations of zooplankton in the eastern Mediterranean based on stable isotope measurements. Journal of Plankton Research, 31, 669 – 686.

Kritee et al., 2012. Reduced isotope fractionation by denitrification under conditions relevant to the ocean. Geochimica et Cosmochimica Acta, 92, 243-259.

Kuramoto, T., and Minagawa, M., 2001. Stable carbon and nitrogen isotopic characterization of organic matter in a Mangrove ecosystem on the southwestern coast of Thailand. Journal of Oceanography, 57, 421 – 431.

Kuykendall, M.D., and Fritz, R.D., 2001. Misener sandstone of Oklahoma. Search and Discovery Article #10018, 74 pp.

Kuypers, M.M.M., Sliekers, A.O., Lavik, G., Schmid, M., Jergensen, B.B., Kuenen, J.G., Sinninghe Damsté, J.S., Strous, M., and Jetten, M.S.M., 2003. Anaerobic ammonium oxidation by annamox bacteria in the Black Sea. Nature, 422, 608-611.

Kuypers, M.M.M., Lavik, G., Woebken, D., Schmid, M., Fuchs, B.M., Amann, R., Jorgensen, B.B., and Jetten, M.S.M., 2005. Massive nitrogen loss from the Benguela upwelling system through anaerobic ammonium oxidation. Procecedings of the National Academy of Sciences of the United States of America, 102, 6478-6483.

Lambert, M.W., 1993. Internal stratigraphy and organic facies of the Devonian-Mississippian Chattanooga (Woodford) Shale in Oklahoma and Kansas, in B.J. Katz and L.M. Pratt, eds., Source rocks in a sequence stratigraphic framework: AAPG Studies in Geology, 13, 163-176.

Lehmann, M.F., Bernasconi, S.M., Barbieri, A., and McKenzie, J.A., 2002. Preservation of organic matter and alteration of its carbon and nitrogen isotope composition during simulated and in situ early sedimentary diagenesis. Geochimica et Cosmochimica Acta, 66, 3573-3584.

Lewan, M.D., 1983. Effects of thermal maturation on stable organic carbon isotopes as determined by hydrous pyrolysis of Woodford Shale. Geochimica et Cosmochimica Acta., 47, 1471-1479.

Lewis, B.L., and Luther, G.W., 2000. Processes controlling the distribution and cycling of manganese in oxygen minimum zones of the Arabian Sea. Deep-Sea Research II, 47, 1541 – 1561.

Littke, R., Kroos, B., Idiz, E., and Frienlingsdorf, J., 1995. Molecular nitrogen in gas accumulations: generations for sedimentary organic matter at high temperatures. American Association of Petroleum Geologists Bulletin, 79, 410-430.

Mariotti, A., Germon, J.C., Hubert, P., Kaiser, P., Letolle, R., Tardieux, A., and Tardieux, P., 1981. Experimental dertemination of nitrogen kinetic fractionation:some principles; illustration for the denitrification and nitrification processes. Plant and Soil 62, 413-430.

Martin, J.H., and Knauer, G.A., 1984. VERTEX: manganese transport through oxygen minima. Earth Planetary Science Letters, 67, 35-47.

Mingram, B., and Bräuer,K., 2001. Ammonium concentration and the nitrogen isotope concentrations in metasedimentary rocks from different tectonometamorphic units of the European Variscan Belt. Geochimica et Cosmochimica Acta, 65, 273-287.

Mingram, B., Hoth, P., and Harlov, D.E., 2003. Nitrogen potential of Namurian shales in the North German Basin. Journal of Geochmeical Exploration, 78-79, 405-408.

Mobius, J., Gaye, B., Lahajnar, N., Bahlmann, E., and Emeis, K., 2011. Influence of diagenesis on sedimentary $\delta^{15}N$ in the Arabian Sea over the last 130 kyr. Marine Geology 284, 127-138.

Mumford, J.L., and Emerson, S., 1999. The geochemistry of redox sensitive trace metals in sediments. Geochimica et Cosmochimica Acta, 63, 1735-1750.

Oldenburg, T.B.P., Larter, S.R., and Huang, H., 2007. Nitrogen isotope systematics of petroleum fractions of differing polarity – Neutral versus basic compounds. Organic Geochemistry, 38, 1789-1794.

Over, D.J., and Barrick, J.E., 1990. The Devonian/Carboniferous boundary in the Woodford Shale, Lawrence Uplift, Southcentral Oklahoma. Oklahooma Geological Survey Guidebook, 27, 63-73.

Over, D.J., 1992. Conodonts and the Devonian – Mississippian boundary in the Upper Woodford Shale, Arbuckle Mountains, South-Central Oklahoma. Journal of Paleontology, 66, 293 – 311.

Peters, K.E., Sweeney, R.E., and Kaplan, .R., 1978. Correlation of carbon and nitrogen stable isotope ratios in sedimentary organic matter. Limnology and Oceanography, 23, 598 – 604.

Pride, C., Thunell, R., Sigman, D., Keigwin, L., Altabet, M., and Tappa, E., 2010. Nitrogen isotopic variations in the Gulf of California since the last deglaciation: response to global climate change. Paleoceanography, 14, 397-409.

Quan, T.M., Adigwe, E., and Puckette, J., (submitted). Evaluating nitrogen isotopes as proxies for depositional environmental conditions in shales: comparing Caney and Woodford Shales in the Arkoma Basin, Oklahoma. Chemical Geology.

Quan, T.M., and Falkowski, P.G., 2009. Redox control of N:P ratios in aquatic ecosystems. Geobiology, 7, 124-139.

Quan, T.M., van de Schootbrugge, B., Field, M.P., Rosenthal, Y., and Falkowski, P.G., 2008. Nitrogen isotope and trace metal analyses from the Mingolsheim core (Germany): Evidence for redox variations across the Triassic-Jurassic boundary. Global Biogeochemical Cycles, 22, GB2014, doi: 1029/2007GB002981.

Rechlin, K.J., 2003. Reservoir quality of the Frisco Formation, Hunton Group, Seminole County, Oklahoma. MS Thesis, Oklahoma State University.

Rejebian, V.A., Harris, A.G., and Huebner, J.S., 1987. Conodont color and textural alteration: an index to regional metamorphism , contact metamorphism and hydrothermal alteration. Geological Society of America Bulletin, 99, 471-479.

Roberts, C.T., and Mitterer, R.M., 1992. Laminated black shale-bedded chert cyclicity in the Woodford Formation, Southern Oklahoma. Oklahoma Geological Survey Circular 93, 330-336.

Robinson, R.S., Meyers, P.A., and Murray R.W., 2002. Geochemical evidence for variations in delivery and deposition of sediment in Pleistocene light-dark color cycles under the Benguela Current Upwelling System. Marine Geology, 180, 249-270.

Robinson, R.S., Mix, A., and Martinez, P., 2006. Southern ocean control on the extent of denitrification in the southeast Pacific over the last 70 ka. Quaternary Science Reviews 26, 201-212.

Robinson, R.S., Kienast, M., Albuquerque, A.L., Altabet, M., Contreras, S., De Pol Holz, R., Dubois, N., Francois, R., Galbraith, E., Hsu, T., Ivanchko, T., Jaccard, S., Kao, S., Keifer, T., Kienast, S., Lehmann, M., Martinez, P., McCarthy, M., Mobius, J., Pederson, P., Quan, T.M., Ryabenko, E., Schmittner, A., Schneider, R., Schneider-Mor, A., Shigemitsu, M., Sinclair, D., Somes, C., Studer, A., Thunell, R., and Yang, J., 2012. A review of nitrogen isotopic alteration in marine sediments. Paleoceanography, 27, PA4203, doi:10.1029/2012PA002321.

Romero, A.M., and Philp, R.P., 2012. Organic geochemistry of the Woodford Shale, southeastern Oklahoma: How variable can shales be?, American Association of Petroleum Geologists Bulletin, 96, 493 – 517.

Sangster, D.F., Nowlan, G.S., and McCracken, A.D., 1994. Thermal Comparisonn of Mississippi Valley-Type lead-zinc deposits and their host rocks using fluid inclusions and conodont color alteration index data. Economic Geology, 89, 493 – 514.

Schimmelmann, A., and Lis,G.P., 2010. Nitrogen isotopic change during maturation of organic matter. Organic Geochemistry, 41, 63 – 70.

Schlessinger, W.H., 1997. *Biogeochemistry: An Analysis of Global Change* (second edition). San Diego, CA: Academic Press.

Schmoker, J.W., 1986. Oil generation in the Anadarko Basin, Oklahoma and Texas: Modeling using Lopatin's Method. Oklahoma Geological Survey Special Publication, 86-3, 1-40.

Strapoć, D., Mastalerz, M., Schimmelmann, A., Drobniak, A., and Hasenmueller, N., 2010. Geochemical constraints on the origin and volume of gas in the New Albany (Devonian-Mississippian), eastern Illinois Basin. American Association of Petroleum Geologists Bulletin 94, 1713-1740.

Taylor, S.R., and McClennan, S.M., 1985. The continental crust: Its composition and evolution Blackwell, Oxford.

Tribovillard, N., Algeo, T.J., Lyons, T., and Riboulleau, A., 2006. Trace metals as paleoredox and paleoproductivity proxies: An update. Chemical Geology, 232, 12-32.

Vandenbroucke, M., and Largeau, C., 2007. Kerogen origin, evolution and structure. Ogranic Geochemistry, 38, 719 – 833.

Voss, M., Dippner, J.W., and Montoya, J.P., 2001. Nitrogen isotope patterns in the oxygen-deficient waters of the Eastern Tropical North Pacific Ocean. Deep-Sea Research, 48, 1905-1921.

Wada, E., 1980. Nitrogen isotope fractionation and its significnce in biogeochemical processes occurring in marine environments. In:E. D. Goldberg and Y. Horibe, Eds., *Isotope Marine Chemistry*. Uchida Rokakuho Publ. Co. Ltd., Tokyo.

Wada, E., Minagawa, M., Mizuntani, H., Tsuji, T., Imaizumi, R., and Karasawa, K., 1987. Biogeochemical studies on the transport of organic matter along the Otsuchi River Watershed, Japan. Estuarine and Coastal and Shelf Science, 25, 321 – 336.

Watson, B.P., 2005. Internal stratigraphy, composition, and depositional setting of the Woodford Shale n Southern Seminole County, Oklahoma. MS Thesis, Oklahoma State University.

Whittaker, S., Bidle, K., Kustka, A., and Falkowski, P., 2011. Quantification of nitrogenase in *Trichodesmium* IMS 101: implications for iron limitation of nitrogen fixation in the ocean. Environmental Microbiology reports 3(1), 54-58.

Williams, L.B., Ferrell Jr., R.E., Hutcheon, I., Bakel, A.J., Walsh, M.M., and Krouse, H.R., 1995. Nitrogen isotope geochemistry of organic matter and minerals during diagenesis and hydrocarbon migration. Geochimica et Cosmochimica Acta, 59, 765-779.

Zhu, Y., Buqing, S., and Fang, C., 2000. The isotopic compositions of molecular nitrogen: implications on their origins in natural gas accumulations. Chemical Geology, 164, 321-330.

Zonneveld, K.A.F., Versteegh, G.J.M., Kasten, S., Elinton., T.I., Emeis, K.-C., Huguet, C., Koch, B.P., de Lange, G.J., de Leeuw, J.W., Middelburg, J.J., Mollenhauer, G., Prahl, F.G., Rethemeyer, J., and Wakeham, S.G., 2010. Selective preservation of organic matter in marine environments, processe and impact on the sedimentary record. Biogeosciences, 7, 483-511.

Zumf, W.G., 1997. Cell biology and molecular basis of denitrification. Microbiology and Molecular Biology Reviews, 61, 533-616.

APPENDIX A

Platform conodonts, Palmatoplepis gracilis, were the majority of the conodont species identified, which are confined to the Devonian. This implies that no Mississippian Woodford exists at the JMOC location.

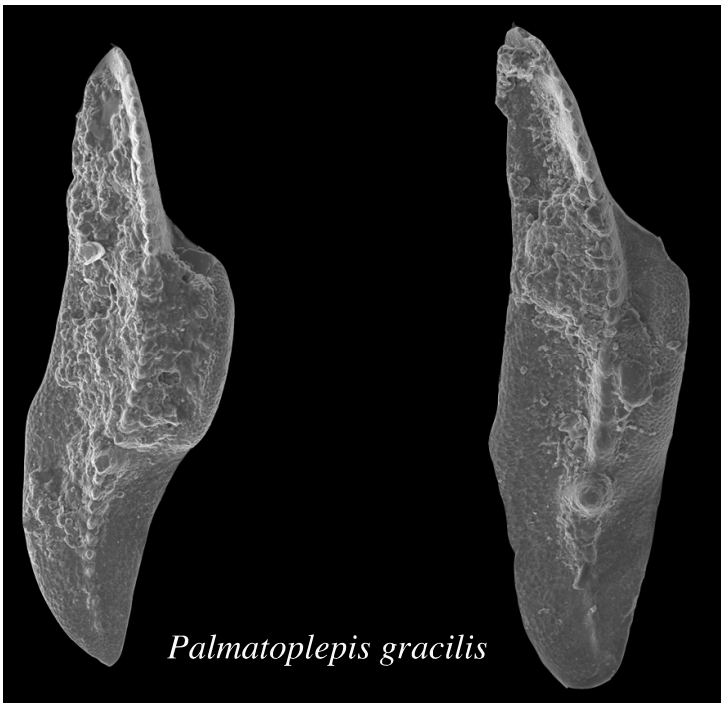

APPENDIX B

Trace element/Al ratios in most Post-Archean Average Shale standard (PAAS) (Taylor and McClennan, 1985).

Trace Element	Element/Al
wt. % / wt. %	
Fe	0.51
ppm / wt. %	
V	15
U	0.31
Zn	8.5
Mo	0.10
Mn	90

APPENDIX C

Additional trace metal concentrations provided by ActLabs, Inc. Note: these concentrations have not been normalized to Al or corrected for $CaCO_3$.

Report'Date:'3/20/2013

Analyte Symbol	Li	Na	Mg	Al	K
Unit Symbol	ppm	%	%	%	%
Detection Limit	0.5	0.01	0.01	0.01	0.01
Analysis Method	TD-MS	TD-MS	TD-MS	TD-MS	TD-MS
JM1	47	0.14	2.16	8.53	> 5.00
JM2	45.2	0.13	1.98	7.77	4.71
JM3	43.2	0.12	1.84	7.79	4.86
JM4	41.8	0.12	1.81	7.59	4.84
JM5	35.7	0.11	1.62	6.54	4.23
JM6	41.4	0.12	1.68	7.78	4.92
JM7	36.1	0.1	2.01	6.45	4.27
JM8	35.4	0.1	2.09	6.35	4.16
JM9	36.2	0.1	1.81	6.27	4.03
JM10	43.1	0.12	1.61	6.94	4.54
JM11	38.2	0.11	1.32	4.04	3.03
JM12	38.9	0.12	1.62	5.53	3.93
JM13	40.5	0.1	1.61	6.77	4.03
JM14	38.8	0.1	1.6	6.76	4.32
JM15	39	0.1	1.6	6.76	4.32
JM16	37.1	0.1	1.52	6.79	4.4
JM17	37.6	0.11	1.63	7.08	4.61
JM18	35.4	0.1	1.57	6.58	4.34
JM19	38	0.11	1.65	6.78	4.44
JM20	35.5	0.1	1.65	6.53	4.29
JM21	36	0.1	1.66	6.42	4.22
JM22	30.9	0.09	1.57	5.78	2.71
JM23	34.4	0.1	1.62	6.61	4.2
JM24	32.4	0.09	1.61	5.79	3.85
JM25	33.9	0.1	1.5	6.06	3.95
JM26	36.2	0.1	1.64	6.68	3.59
JM27	35	0.1	1.68	6.64	2.87
JM28	35.6	0.1	1.62	6.45	4.07
JM29	33.8	0.09	1.64	6.27	2.35
CO1	18.8	0.14	0.53	1.36	0.5
CO2	22.3	0.08	0.13	1.27	0.33
CO3	21	0.1	0.25	1.52	0.64
CO4	18.9	0.13	0.25	1.53	0.79
CO5	20.8	0.26	0.56	3.69	2.15
CO6	29.8	0.61	1.15	6.11	3.89
CO7	17.5	0.29	1.28	3.27	1.96
CO8	18.5	0.43	0.65	3.38	1.95
CO9	20.7	0.56	0.74	4.28	2.39
CO10	24.9	0.1	0.15	1.48	0.38

Report'Date:'3/20/2013

Analyte Symbol	Li	Na	Mg	Al	K
Unit Symbol	ppm	%	%	%	%
Detection Limit	0.5	0.01	0.01	0.01	0.01
Analysis Method	TD-MS	TD-MS	TD-MS	TD-MS	TD-MS
CO11	20.4	0.61	0.77	4.36	2.48
CO12	18.4	0.58	0.93	4.49	2.51
CO13	26.2	0.61	1.55	5.41	3.32
CO14	30.2	0.63	1.19	6.47	4.12
CO15	18.5	0.44	0.67	3.48	2.03
CO16	27.9	0.11	0.17	1.63	0.42
RU1	24.2	0.37	1.57	2.52	1.39
RU2	25.1	0.19	1.02	1.08	0.57
RU3	22.4	0.34	2.07	2.13	1.18
RU4	162	0.34	1.23	2.6	2.4
RU5	141	0.19	4.57	1.82	1.84
RU6	52.1	0.29	1.46	5.73	4
RU7	37.6	0.3	1.03	4.99	3.34
RU8	46.6	0.34	1.3	6.61	4.54
RU9	37.1	0.32	1.6	4.28	2.54
RU10	47.6	0.28	1.23	5.6	3.92
RU11	53.9	0.28	1.21	5.75	4.04
RU12	22.6	0.32	1.41	2.27	1.26
RU13	50.4	0.28	1.46	5.8	3.4
RU14	47.4	0.3	1.24	6	4.28
RU15	33.4	0.13	0.52	1.91	1.23
RU16	50.9	0.39	1.42	6.84	4.76
RU17	24.6	0.33	1.48	2.35	1.29
HB1	31.2	0.18	0.44	1.4	0.59
HB2	16.3	0.17	0.46	1.73	0.82
HB3	20	0.14	0.34	2.29	1.25
HB4	18.9	0.13	0.14	0.68	0.27
HB5	18.7	0.12	0.09	0.86	0.39
HB6	16.1	0.12	0.29	2.04	1.15
HB7	13.7	0.11	0.13	1.31	0.73
HB8	6.3	0.09	2.41	1.22	0.69
HB9	14.2	0.12	0.95	1.9	1.08
HB10	18.4	0.13	0.32	2.27	1.27
HB11	12.6	0.11	0.4	2.64	1.51
HB12	21	0.14	0.16	0.76	0.3
HB13	14	0.17	1.54	3.53	2.18
HB14	15.3	0.14	0.09	0.89	0.4
HB15	15	0.14	0.13	1	0.45
HB16	17.5	0.14	0.25	1.33	0.6
HB17	13.4	0.14	0.31	1.92	1

Report'Date:'3/20/2013

Analyte Symbol	Li	Na	Mg	Al	K
Unit Symbol	ppm	%	%	%	%
Detection Limit	0.5	0.01	0.01	0.01	0.01
Analysis Method	TD-MS	TD-MS	TD-MS	TD-MS	TD-MS
HB18	20.8	0.14	0.15	0.76	0.3
HB19	15.8	0.14	0.1	0.93	0.41
HB20	11.5	0.15	0.21	1.94	1.06
HB21	5.1	0.23	7.93	2.06	1.22
HB22	13.5	0.14	0.17	1.16	0.5
HB23	3.6	0.13	8.91	1.11	0.63
HB24	13.1	0.22	0.53	2.19	1.15

Report'Date:'3/20/2013

Analyte Symbol	Ca	Cd	V	Cr	Mn
Unit Symbol	%	ppm	ppm	ppm	ppm
Detection Limit	0.01	0.1	1	0.5	1
Analysis Method	TD-MS	TD-MS	TD-MS	TD-MS	TD-MS
JM1	1.25	< 0.1	159	83.7	448
JM2	1.12	< 0.1	77	84.2	376
JM3	0.83	0.1	142	69.1	320
JM4	0.9	0.1	141	80.4	306
JM5	0.87	0.2	110	66.2	230
JM6	0.55	< 0.1	159	72.4	235
JM7	1.62	0.1	130	68.5	439
JM8	1.83	0.1	128	56.5	494
JM9	1.3	0.1	123	62.9	371
JM10	0.63	0.2	162	72.1	264
JM11	0.41	0.1	158	88	248
JM12	0.55	0.2	149	84	303
JM13	0.72	< 0.1	131	76.2	357
JM14	0.76	< 0.1	140	59.4	390
JM15	0.56	0.2	148	65.6	311
JM16	0.62	0.4	155	67.3	243
JM17	0.64	0.2	169	79.6	286
JM18	0.75	0.2	131	70.2	305
JM19	0.77	0.2	167	70.8	263
JM20	0.99	0.2	163	62.2	282
JM21	0.97	0.7	114	49.8	217
JM22	1.02	0.5	93	49.6	208
JM23	0.37	0.2	131	60.7	188
JM24	0.65	0.2	116	62.3	258
JM25	0.3	0.2	144	75.5	172
JM26	0.36	0.2	145	77.2	199
JM27	0.48	0.1	141	75.2	207
JM28	0.5	0.1	139	60	193
JM29	0.48	0.1	134	57.7	188
CO1	5.97	4.3	677	43.5	75
CO2	0.47	9.6	921	17.7	17
CO3	0.1	13.4	> 1000	24.9	38
CO4	0.05	24.2	> 1000	30.2	36
CO5	0.13	3.8	529	37.2	68
CO6	0.71	2.5	487	48.9	66
CO7	1.32	2	337	46.7	152
CO8	0.48	2.5	233	42.1	67
CO9	0.63	1.7	238	48.8	63
CO10	0.52	9.6	> 1000	21	23

Report'Date:'3/20/2013

Analyte Symbol	Ca	Cd	V	Cr	Mn
Unit Symbol	%	ppm	ppm	ppm	ppm
Detection Limit	0.01	0.1	1	0.5	1
Analysis Method	TD-MS	TD-MS	TD-MS	TD-MS	TD-MS
CO11	0.61	2.2	231	50.7	51
CO12	0.81	2.2	226	60.5	73
CO13	1.36	3	226	66.3	100
CO14	0.72	2.5	503	53.9	57
CO15	0.51	2.5	233	31.3	74
CO16	0.59	10.2	> 1000	21.2	33
RU1	2.62	0.4	60	36.6	112
RU2	1.71	0.3	26	13.8	76
RU3	4.09	0.3	49	37.8	161
RU4	0.75	0.8	165	322	129
RU5	9.44	0.5	82	245	325
RU6	0.24	6.7	> 1000	76.6	98
RU7	0.07	14.3	659	94.4	99
RU8	0.12	0.4	202	65.7	131
RU9	5.02	0.3	94	37.5	185
RU10	0.18	1.8	420	72.5	89
RU11	0.35	2.7	430	99.1	95
RU12	2.39	0.5	55	35.7	95
RU13	0.24	6.1	> 1000	65.8	100
RU14	0.15	1.9	408	73.7	108
RU15	0.25	2	411	22.1	56
RU16	0.09	17.7	825	73.3	168
RU17	2.48	1.4	58	48.8	100
HB1	0.53	0.6	248	96.5	132
HB2	7.24	1.4	280	66.7	92
HB3	2.87	32.3	> 1000	143	71
HB4	0.21	0.7	77	24.6	30
HB5	0.03	61.9	> 1000	33.9	16
HB6	0.08	120	> 1000	74.2	44
HB7	10.9	13.1	592	67.7	26
HB8	21.9	2.7	644	76.6	299
HB9	5.8	1.4	363	88.2	105
HB10	0.09	129	> 1000	84.3	36
HB11	0.32	2.7	525	74.3	54
HB12	0.21	0.8	86	28.6	26
HB13	6.24	0.9	381	113	183
HB14	0.02	55.5	> 1000	36.9	45
HB15	0.09	5.1	813	26.1	35
HB16	0.19	6.3	988	27.9	29
HB17	0.19	8.8	> 1000	41.8	35

Report'Date:'3/20/2013

Analyte Symbol	Ca	Cd	V	Cr	Mn
Unit Symbol	%	ppm	ppm	ppm	ppm
Detection Limit	0.01	0.1	1	0.5	1
Analysis Method	TD-MS	TD-MS	TD-MS	TD-MS	TD-MS
HB18	0.2	0.7	83	33.9	35
HB19	0.03	52.9	> 1000	40	51
HB20	0.06	3.9	788	28.4	48
HB21	14	3.7	624	40.1	522
HB22	0.1	6.6	989	23.8	22
HB23	14.9	1.7	545	24.7	723
HB24	0.51	1.4	433	27.8	61

Report'Date:'3/20/2013

Analyte Symbol	Fe	Hf	Hg	Ni	Er
Unit Symbol	%	ppm	ppb	ppm	ppm
Detection Limit	0.01	0.1	10	0.5	0.1
Analysis Method	TD-MS	TD-MS	TD-MS	TD-MS	TD-MS
JM1	3.66	4.9	< 10	83.3	2.8
JM2	2.99	3	< 10	50.9	2.7
JM3	3.45	4.8	< 10	65.3	2.7
JM4	3.23	5	< 10	56.9	2.8
JM5	2.91	6.2	< 10	41.5	2.5
JM6	3.08	4.5	10	49.9	2.9
JM7	2.95	4.9	< 10	47.1	2.7
JM8	3.96	4.7	< 10	58.3	2.7
JM9	2.78	4.2	< 10	37.9	2.5
JM10	3.38	7.3	< 10	57.1	2.7
JM11	2.9	4.1	< 10	54.7	1.8
JM12	3.01	4.7	< 10	55.5	2.5
JM13	4.4	4.3	< 10	44.2	3
JM14	3.41	4.6	20	48.6	2.8
JM15	3.02	4.8	< 10	54.1	2.9
JM16	3.02	4.7	20	52.1	2.9
JM17	3.01	4.9	40	52.2	3
JM18	3.11	4.7	< 10	61.8	2.7
JM19	2.88	4.8	< 10	48.9	2.8
JM20	3.08	5	< 10	47.5	2.8
JM21	2.8	4.5	< 10	30.3	2.6
JM22	2.3	3.8	< 10	28	2.4
JM23	2.71	3.9	20	40.2	2.6
JM24	2.75	4.2	10	56.1	2.4
JM25	2.81	3.9	40	51.5	2.4
JM26	2.8	4.2	20	49	2.8
JM27	2.73	4.2	< 10	45.8	2.7
JM28	2.92	4.2	< 10	48.3	2.6
JM29	2.66	3.9	20	46.7	2.6
CO1	0.37	0.2	60	46.4	5.1
CO2	0.41	< 0.1	70	74.9	0.9
CO3	0.5	0.7	100	80.9	1.2
CO4	0.94	0.8	110	129	1.3
CO5	3.25	1.8	130	232	2.5
CO6	1.99	3.4	40	167	3.3
CO7	4.55	1.5	130	288	2.6
CO8	2.56	1.9	90	231	2.6
CO9	3.66	2	130	237	3.1
CO10	0.45	< 0.1	40	78.8	0.9

Report'Date:'3/20/2013

Analyte Symbol	Fe	Hf	Hg	Ni	Er
Unit Symbol	%	ppm	ppb	ppm	ppm
Detection Limit	0.01	0.1	10	0.5	0.1
Analysis Method	TD-MS	TD-MS	TD-MS	TD-MS	TD-MS
CO11	3.48	2	70	222	3
CO12	8.24	2.1	300	276	2.6
CO13	4.9	2.8	210	245	3.3
CO14	2.06	3.4	120	171	3.3
CO15	2.62	1.8	140	233	2.6
CO16	0.49	< 0.1	50	86.2	1
RU1	1.34	3	70	26.9	1.9
RU2	0.96	1.1	50	9.8	1
RU3	1.25	2.5	40	23.7	1.7
RU4	6.59	2.5	190	30.8	2.5
RU5	4.94	1.3	30	18.7	3.3
RU6	1.96	3	30	170	2.9
RU7	2.58	2.8	110	172	1.2
RU8	3.32	2.9	60	94.7	2
RU9	1.43	< 0.1	70	29.9	5
RU10	4.99	2.8	70	214	3.3
RU11	2.04	2.5	60	176	2.3
RU12	1.2	2.5	90	25	1.6
RU13	1.89	2.8	110	162	2.7
RU14	6.59	2.9	170	240	3.1
RU15	0.94	1	40	48	1
RU16	3.33	4.4	90	215	2.1
RU17	1.25	2.9	60	25.3	1.7
HB1	0.69	0.9	50	77.9	0.5
HB2	0.6	< 0.1	60	92.4	4.2
HB3	0.76	< 0.1	90	209	1.6
HB4	0.25	0.3	< 10	31.3	0.1
HB5	0.45	0.5	50	74.6	0.2
HB6	0.68	1	30	127	0.9
HB7	0.26	< 0.1	10	72.9	8.1
HB8	0.36	< 0.1	50	75.8	14.2
HB9	0.64	< 0.1	70	102	3.4
HB10	0.77	1.2	160	140	1
HB11	0.82	1.1	40	82.4	1.7
HB12	0.28	0.4	30	32.8	0.1
HB13	1.3	< 0.1	30	112	1.6
HB14	0.27	0.4	20	66.2	0.2
HB15	0.48	0.4	10	78.5	0.9
HB16	0.57	0.6	90	66.6	0.8
HB17	1.03	0.8	100	115	1.5

Report'Date:'3/20/2013

Analyte Symbol	Fe	Hf	Hg	Ni	Er
Unit Symbol	%	ppm	ppb	ppm	ppm
Detection Limit	0.01	0.1	10	0.5	0.1
Analysis Method	TD-MS	TD-MS	TD-MS	TD-MS	TD-MS
HB18	0.28	0.4	20	30.7	0.1
HB19	0.29	0.4	60	62.5	0.2
HB20	0.93	0.8	260	158	1.5
HB21	1.16	1	40	150	1.7
HB22	0.55	0.5	80	72.2	0.8
HB23	1	0.5	10	85.4	2.4
HB24	1.42	1	40	112	1.4

Report'Date:'3/20/2013

Analyte Symbol	Be	Ho	Ag	Cs	Co
Unit Symbol	ppm	ppm	ppm	ppm	ppm
Detection Limit	0.1	0.1	0.05	0.05	0.1
Analysis Method	TD-MS	TD-MS	TD-MS	TD-MS	TD-MS
JM1	2.9	0.9	0.31	10.3	30.6
JM2	3	0.9	0.06	9.9	17.4
JM3	2.7	0.9	0.32	10.2	19.5
JM4	2.2	0.9	0.3	10.3	16.1
JM5	1.6	0.8	0.35	8.8	17.5
JM6	2.8	1	0.35	11.9	16.5
JM7	2.3	0.9	0.34	9.61	15.9
JM8	1.6	0.9	0.33	9.11	20.3
JM9	2	0.8	0.31	9.37	13.2
JM10	2	0.8	0.4	11	18.7
JM11	1.6	0.6	0.3	8.1	15.5
JM12	2.2	0.8	0.32	9.92	17
JM13	1	1	0.31	10.7	16.8
JM14	1.6	0.9	0.35	10.7	17.8
JM15	2.8	1	0.36	11.3	16.7
JM16	2.4	0.9	0.38	11.7	17.4
JM17	3.2	1	0.37	12.7	16.4
JM18	3.1	0.9	0.36	10.8	18.3
JM19	2.5	0.9	0.44	11.8	16.2
JM20	3.1	0.9	0.34	11.6	16.4
JM21	2.4	0.8	0.43	10.8	11.1
JM22	2.3	0.8	2.74	9.21	10.7
JM23	2.5	0.8	0.61	11.7	13.9
JM24	2.6	0.8	0.54	9.7	16.2
JM25	2.4	0.8	0.46	11.3	15.9
JM26	3.4	0.9	0.36	11.9	16.1
JM27	2.4	0.9	0.37	11	15
JM28	2.3	0.9	0.37	11.1	15.7
JM29	2.7	0.8	0.31	10.6	14.9
CO1	0.8	1.8	1.49	1.27	2
CO2	0.4	0.3	0.51	1.31	2.5
CO3	0.9	0.4	0.64	2.45	3.2
CO4	1.8	0.4	1.58	3	7
CO5	3.2	0.8	0.85	5.95	30.9
CO6	5	1.1	0.7	9.93	23.7
CO7	2.5	0.9	0.6	4.18	44.3
CO8	3	0.9	0.48	3.76	39.5
CO9	3.6	1	0.52	4.87	49.6
CO10	< 0.1	0.3	0.43	1.29	2.6

Report'Date:'3/20/2013

Analyte Symbol	Be	Ho	Ag	Cs	Co
Unit Symbol	ppm	ppm	ppm	ppm	ppm
Detection Limit	0.1	0.1	0.05	0.05	0.1
Analysis Method	TD-MS	TD-MS	TD-MS	TD-MS	TD-MS
CO11	3.8	1	0.5	4.34	55
CO12	3.7	0.9	0.5	5.3	59.1
CO13	4.4	1.2	0.58	6.85	53.9
CO14	4.8	1.1	0.54	9.67	24.8
CO15	2.4	0.9	0.41	3.77	40.1
CO16	0.6	0.3	0.4	1.41	2.9
RU1	1.3	0.6	0.62	2.18	4.8
RU2	0.3	0.4	0.31	0.91	1.8
RU3	0.4	0.6	0.42	2.03	4.2
RU4	4	0.9	0.44	6.34	6.4
RU5	3.4	1.1	0.3	4.37	3.2
RU6	3.3	0.9	0.85	11.9	13.9
RU7	2.3	0.3	1.74	8.48	31.1
RU8	2.8	0.6	0.68	10.7	13.3
RU9	1.9	1.9	0.3	6.18	13.8
RU10	3.6	1.1	0.61	10.2	46.4
RU11	2.3	0.8	0.98	10	11.5
RU12	0.2	0.5	0.67	1.94	4.4
RU13	3.4	0.9	0.89	10.7	13.3
RU14	3.5	1.1	0.66	10.2	60.7
RU15	1.1	0.3	0.46	3.23	4
RU16	1.9	0.6	2.31	11.3	39.2
RU17	0.4	0.6	0.8	2.05	4.5
HB1	0.9	0.1	1.82	1.7	3.2
HB2	1.2	1.3	1.12	2.14	4
HB3	2.2	0.6	3.96	3.65	4.7
HB4	< 0.1	< 0.1	1.43	0.65	1.5
HB5	< 0.1	< 0.1	3.6	1.12	2.2
HB6	0.7	0.3	4.95	3.15	4.6
HB7	1.3	2.5	2.02	1.42	2.9
HB8	1.7	4.4	1.34	1.81	2.9
HB9	0.8	1.1	2.01	2.57	9
HB10	0.7	0.3	5.36	3.36	5.2
HB11	0.4	0.6	3.47	2.61	5
HB12	< 0.1	< 0.1	1.53	0.67	1.7
HB13	1.8	0.5	3.17	4.01	7.2
HB14	< 0.1	< 0.1	2.87	1.2	2
HB15	0.2	0.3	0.96	1.14	3.6
HB16	< 0.1	0.3	0.74	1.64	3.1
HB17	0.7	0.5	0.66	2.26	5.3

Report'Date:'3/20/2013

Analyte Symbol	Be	Ho	Ag	Cs	Co
Unit Symbol	ppm	ppm	ppm	ppm	ppm
Detection Limit	0.1	0.1	0.05	0.05	0.1
Analysis Method	TD-MS	TD-MS	TD-MS	TD-MS	TD-MS
HB18	< 0.1	< 0.1	0.89	0.64	1.6
HB19	< 0.1	< 0.1	2.28	1.15	2
HB20	0.3	0.5	0.73	2.06	10.4
HB21	1.7	0.6	0.63	1.67	9.1
HB22	< 0.1	0.3	0.62	1.33	4.1
HB23	1	0.8	0.62	0.96	8.8
HB24	0.8	0.5	0.59	2.39	13.9

Report'Date:'3/20/2013

Analyte Symbol	Eu	Bi	Se	Zn	Ga
Unit Symbol	ppm	ppm	ppm	ppm	ppm
Detection Limit	0.05	0.02	0.1	0.2	0.1
Analysis Method	TD-MS	TD-MS	TD-MS	TD-MS	TD-MS
JM1	1.22	0.41	0.3	76.6	20.6
JM2	1.06	0.37	< 0.1	72.9	19.6
JM3	1.11	0.39	0.3	68.4	20.2
JM4	1.24	0.36	0.7	61.2	19.7
JM5	1.09	0.32	0.3	67.8	17.4
JM6	1.32	0.36	0.8	62	21.7
JM7	1.27	0.36	0.5	52.2	17
JM8	1.26	0.34	0.4	67.8	17.3
JM9	1.15	0.33	0.1	56.9	17.3
JM10	1.13	0.4	0.6	81.8	20.8
JM11	0.6	0.41	< 0.1	56.1	19.9
JM12	0.95	0.4	< 0.1	78	19.8
JM13	1.31	0.41	0.7	47.2	18.8
JM14	1.33	0.41	0.5	52	19.1
JM15	1.33	0.44	0.9	65.9	19.3
JM16	1.32	0.4	1.2	130	19
JM17	1.38	0.4	2.1	57	20.5
JM18	1.17	0.42	1.2	67.8	18.8
JM19	1.15	0.48	1.2	57.7	19.7
JM20	1.16	0.42	0.6	49.5	18.8
JM21	1	0.34	0.6	184	18.3
JM22	1.01	0.35	0.4	108	17.4
JM23	1.11	0.38	1	54.5	19.9
JM24	1.02	0.36	1.7	57.9	17.2
JM25	1.05	0.43	1.3	58.2	19.3
JM26	1.24	0.39	1	57.5	19.8
JM27	1.25	0.34	0.9	53.4	19.7
JM28	1.21	0.37	0.5	55.9	19.7
JM29	1.16	0.34	0.3	59.1	18.9
CO1	1.69	0.1	22.2	195	2.9
CO2	0.48	0.09	8	873	3.5
CO3	0.41	0.12	11.5	1080	4.5
CO4	0.39	0.16	18.1	1560	5
CO5	0.99	0.35	13.2	316	12.4
CO6	1.38	0.33	4.9	206	18.7
CO7	1.03	0.32	9.6	349	9.3
CO8	1.04	0.31	5.5	243	11.5
CO9	1.24	0.37	7.3	187	14.2
CO10	0.48	0.09	9.2	923	3.2

Report'Date:'3/20/2013

Analyte Symbol	Eu	Bi	Se	Zn	Ga
Unit Symbol	ppm	ppm	ppm	ppm	ppm
Detection Limit	0.05	0.02	0.1	0.2	0.1
Analysis Method	TD-MS	TD-MS	TD-MS	TD-MS	TD-MS
CO11	1.15	0.34	6.4	235	13.2
CO12	1.17	0.33	15.8	235	13.1
CO13	1.53	0.41	8.3	228	15.8
CO14	1.39	0.31	5.9	217	19.6
CO15	1.03	0.32	5	253	11.6
CO16	0.53	0.1	9.7	1010	3.4
RU1	0.82	0.13	2.9	45.6	6.7
RU2	0.46	0.05	1.3	29.5	2.8
RU3	0.71	0.1	1.8	48.8	5.8
RU4	1.45	0.13	4.1	102	13.9
RU5	1.22	0.07	4.1	42.5	9.5
RU6	1.03	0.31	7.5	291	17
RU7	0.32	0.22	10.4	1260	17.3
RU8	0.57	0.26	8	207	19
RU9	2.47	0.24	4.4	43.5	11.7
RU10	1.39	0.35	8.2	326	15.9
RU11	0.73	0.27	13.4	664	17.2
RU12	0.74	0.11	3	47.1	6.2
RU13	0.96	0.29	8.1	277	16.1
RU14	1.31	0.4	10.4	354	17.2
RU15	0.32	0.11	2.9	128	4.9
RU16	0.61	0.29	12	1530	21.7
RU17	0.76	0.12	2.9	53	6.1
HB1	0.14	0.18	16.5	287	4
HB2	1.1	0.16	22.9	321	4.7
HB3	0.66	0.31	47.4	1220	8
HB4	< 0.05	0.08	6.9	127	2.3
HB5	0.1	0.12	61.6	2800	4.1
HB6	0.32	0.19	58.3	5480	6.5
HB7	1.81	0.14	21	513	3.4
HB8	3.29	0.12	23.9	339	2.2
HB9	0.96	0.21	32.5	324	5.7
HB10	0.35	0.24	67.1	5970	7.3
HB11	0.58	0.19	32.3	294	7.1
HB12	< 0.05	0.08	7.9	137	2.5
HB13	0.51	0.27	42.5	341	10.1
HB14	0.05	0.11	16	3160	4.2
HB15	0.28	0.08	9.8	456	2.7
HB16	0.26	0.1	7.5	595	3.4
HB17	0.5	0.14	13	918	4.8

Report'Date:'3/20/2013

Analyte Symbol	Eu	Bi	Se	Zn	Ga
Unit Symbol	ppm	ppm	ppm	ppm	ppm
Detection Limit	0.05	0.02	0.1	0.2	0.1
Analysis Method	TD-MS	TD-MS	TD-MS	TD-MS	TD-MS
HB18	< 0.05	0.07	7	132	2.3
HB19	0.06	0.12	17.4	3010	3.7
HB20	0.52	0.17	6.3	290	5.2
HB21	0.52	0.17	8	324	4.8
HB22	0.26	0.09	6.2	471	3
HB23	0.54	0.14	7.3	110	1.8
HB24	0.52	0.18	6.8	141	5.7

Report'Date:'3/20/2013

Analyte Symbol	As	Rb	Y	Sr	Zr
Unit Symbol	ppm	ppm	ppm	ppm	ppm
Detection Limit	0.1	0.2	0.1	0.2	1
Analysis Method	TD-MS	TD-MS	TD-MS	TD-MS	TD-MS
JM1	11.8	169	22.2	55.1	160
JM2	6.5	154	20.9	54.1	92
JM3	14.2	169	21	53.1	153
JM4	11.8	172	22.7	54.6	167
JM5	12.7	152	20.2	50.2	216
JM6	7.5	191	23	54.1	151
JM7	11.9	157	21.5	57.8	162
JM8	26.8	153	21.6	57.6	157
JM9	10.7	154	20.1	54.5	141
JM10	17	161	19.6	54.5	247
JM11	10.1	42.8	8.7	39.6	135
JM12	9.7	91.4	15	46.6	154
JM13	18.1	158	22.6	48.4	140
JM14	14.2	170	22.8	50.8	153
JM15	9.8	174	22.7	51.4	159
JM16	15.8	177	22.6	53.7	153
JM17	7.7	190	23.5	56.5	164
JM18	14.7	173	21.1	54.5	157
JM19	8.3	182	20.9	54.4	156
JM20	9.5	176	21.2	54.6	158
JM21	13.1	172	19.3	50.9	147
JM22	9.3	115	18.8	48.2	125
JM23	8	177	19.7	51	131
JM24	14.1	155	18.9	49	143
JM25	9.3	156	18.6	46.5	128
JM26	8.5	151	20.6	49.6	135
JM27	8	122	21.3	49	140
JM28	7.4	166	20.6	47.4	138
JM29	7.8	99.7	19.8	46.8	129
CO1	14.5	24	63.2	986	19
CO2	13.6	17.7	10.3	333	6
CO3	16.3	34	13.7	30.4	27
CO4	29	42.1	14.3	26.8	31
CO5	49.9	94.6	28.1	51.7	67
CO6	21.5	149	33.1	231	119
CO7	83.8	79	27.1	135	55
CO8	38.7	75.1	27.4	53	70
CO9	61.4	95.1	33.2	150	74
CO10	15	18	10.4	346	3

Report'Date:'3/20/2013

Analyte Symbol	As	Rb	Y	Sr	Zr
Unit Symbol	ppm	ppm	ppm	ppm	ppm
Detection Limit	0.1	0.2	0.1	0.2	1
Analysis Method	TD-MS	TD-MS	TD-MS	TD-MS	TD-MS
CO11	54.1	89.4	30.6	105	71
CO12	118	90.6	27.6	159	73
CO13	66.7	117	36.5	137	102
CO14	22.3	146	32.2	220	119
CO15	36.4	76.1	27.6	57.9	65
CO16	15.8	19.4	11.3	377	1
RU1	3.4	50.1	19.5	67.5	104
RU2	1.7	20.5	11.2	108	41
RU3	2.8	45.2	17	84.6	83
RU4	8.9	115	30	56.5	94
RU5	6.9	83.6	39.7	150	48
RU6	9.4	166	28.2	51.1	107
RU7	18.5	99.5	7.9	34.4	104
RU8	14	175	14.9	50.9	102
RU9	17.1	108	57.6	259	2
RU10	59.2	137	30.3	44.6	99
RU11	19.5	151	22.2	59.1	91
RU12	3	46.7	17.4	62.5	92
RU13	9.2	135	27	47.8	98
RU14	77.2	145	29.9	45.6	102
RU15	5.8	49	10.1	28.4	35
RU16	21.7	177	15.9	51.7	178
RU17	3.2	48.1	18.4	65.3	102
HB1	7.9	24.9	3.9	45.5	36
HB2	7.8	33.3	55.6	414	1
HB3	13.5	54.1	18.4	206	< 1
HB4	3.5	10.5	1.2	22.1	14
HB5	27.1	17.9	2.3	20.6	19
HB6	28.9	49.8	7.9	45.3	37
HB7	10.4	27.2	115	559	< 1
HB8	11.2	27.8	227	> 1000	12
HB9	19.7	41.1	43.2	316	< 1
HB10	33.6	54.7	8.7	49.9	44
HB11	18.6	52.9	18.2	367	42
HB12	6.1	11	1.1	21.7	16
HB13	21.9	74.8	19.2	354	5
HB14	11.7	17.9	1.4	14.3	14
HB15	12.6	18.5	11.6	37.5	18
HB16	10.9	25.8	9.7	68.2	24
HB17	16.3	39.7	18	121	31

Report'Date:'3/20/2013

Analyte Symbol	As	Rb	Y	Sr	Zr
Unit Symbol	ppm	ppm	ppm	ppm	ppm
Detection Limit	0.1	0.2	0.1	0.2	1
Analysis Method	TD-MS	TD-MS	TD-MS	TD-MS	TD-MS
HB18	5.4	10.2	1	19.8	15
HB19	11.6	17.6	1.5	14.2	14
HB20	17.1	38.1	18.7	90.9	34
HB21	17	40	21.9	519	37
HB22	9.5	22	9.2	31.1	21
HB23	14.7	22.9	30	603	23
HB24	23.2	44.2	15.8	88.5	39

Report'Date:'3/20/2013

Analyte Symbol	Nb	Mo	In	Sn	Sb
Unit Symbol	ppm	ppm	ppm	ppm	ppm
Detection Limit	0.1	0.1	0.1	1	0.1
Analysis Method	TD-MS	TD-MS	TD-MS	TD-MS	TD-MS
JM1	15.6	9.1	< 0.1	3	1.1
JM2	1.7	0.5	< 0.1	2	< 0.1
JM3	15.9	4.7	< 0.1	3	1.1
JM4	16.9	5.7	< 0.1	3	1
JM5	15.9	2.4	< 0.1	3	0.7
JM6	17	6.4	< 0.1	3	1.2
JM7	16.5	7.8	< 0.1	4	1
JM8	15.6	11.5	< 0.1	3	2
JM9	15	3.9	< 0.1	3	0.9
JM10	18.7	5.7	< 0.1	4	1.6
JM11	15.4	8.3	< 0.1	3	1.5
JM12	16.1	14.4	< 0.1	3	1.3
JM13	14.6	18.2	< 0.1	3	1.7
JM14	15.7	25.6	< 0.1	3	2.1
JM15	16.6	14.8	< 0.1	4	1.6
JM16	16.9	9.3	< 0.1	3	1.7
JM17	18.5	10.4	< 0.1	4	1.3
JM18	16.8	4.7	< 0.1	3	1.1
JM19	17.4	10.4	< 0.1	4	1.4
JM20	16.8	8.4	< 0.1	3	1.1
JM21	15.2	1.5	< 0.1	3	0.7
JM22	8.8	1.5	< 0.1	3	0.6
JM23	14.4	2.3	< 0.1	3	0.9
JM24	15	4.2	< 0.1	3	1.1
JM25	14.7	6	< 0.1	3	1.6
JM26	15.6	3.8	< 0.1	3	1.3
JM27	15.7	6	< 0.1	3	1.1
JM28	15.3	9.2	< 0.1	3	1.5
JM29	13.2	5.6	< 0.1	3	0.7
CO1	0.2	9.7	< 0.1	< 1	2.9
CO2	1.1	48.8	< 0.1	< 1	13.8
CO3	2.5	51.1	< 0.1	< 1	10.6
CO4	3.4	90.5	< 0.1	< 1	11.7
CO5	7.9	153	< 0.1	2	6
CO6	14.5	84.1	< 0.1	3	7.5
CO7	6.9	176	< 0.1	2	8.2
CO8	7.9	243	< 0.1	2	9.6
CO9	9.3	169	< 0.1	2	9.1
CO10	1.2	49.1	< 0.1	< 1	13.1

Report'Date:'3/20/2013

Analyte Symbol	Nb	Mo	In	Sn	Sb
Unit Symbol	ppm	ppm	ppm	ppm	ppm
Detection Limit	0.1	0.1	0.1	1	0.1
Analysis Method	TD-MS	TD-MS	TD-MS	TD-MS	TD-MS
CO11	9.2	127	< 0.1	2	6.9
CO12	9.2	119	< 0.1	2	9.3
CO13	11.5	194	< 0.1	2	8.6
CO14	14.9	84.6	< 0.1	3	6.7
CO15	8.1	239	< 0.1	2	10.2
CO16	1.2	52.4	< 0.1	< 1	14.2
RU1	7.9	1.4	< 0.1	1	0.8
RU2	2.6	0.5	< 0.1	< 1	0.5
RU3	6.6	0.9	< 0.1	1	0.6
RU4	5.4	0.9	< 0.1	1	3.1
RU5	3.5	1	< 0.1	1	1.5
RU6	11.8	118	< 0.1	3	8.4
RU7	11.1	63	< 0.1	4	6.2
RU8	12.1	9.8	< 0.1	3	2.5
RU9	< 0.1	2.7	< 0.1	< 1	0.6
RU10	10.9	193	< 0.1	2	9.3
RU11	9.8	29.1	< 0.1	2	5.7
RU12	7.1	1.2	< 0.1	1	0.8
RU13	11	110	< 0.1	2	7.5
RU14	11	205	< 0.1	2	8.5
RU15	3.6	29.4	< 0.1	< 1	3.5
RU16	13.9	77.8	< 0.1	4	7.3
RU17	7.5	1.4	< 0.1	1	0.7
HB1	3.3	5.2	< 0.1	< 1	2
HB2	0.3	11.3	< 0.1	< 1	0.9
HB3	0.6	52.8	< 0.1	< 1	5.4
HB4	1.2	4	< 0.1	< 1	1.8
HB5	1.3	40	< 0.1	< 1	23.4
HB6	3.3	112	< 0.1	1	55
HB7	0.1	14.6	< 0.1	< 1	2.4
HB8	0.9	11.4	< 0.1	< 1	4.3
HB9	< 0.1	12.9	< 0.1	< 1	1.6
HB10	3.6	120	< 0.1	1	45.6
HB11	4.8	13.6	< 0.1	< 1	11.2
HB12	1.3	3.9	< 0.1	< 1	1.9
HB13	0.7	20.7	< 0.1	< 1	9.6
HB14	1.1	43.8	< 0.1	< 1	23.4
HB15	1.4	56.1	< 0.1	< 1	10.1
HB16	2.1	39.4	< 0.1	< 1	10.7
HB17	2.8	71.2	< 0.1	< 1	11.7

Report'Date:'3/20/2013

Analyte Symbol	Nb	Mo	In	Sn	Sb
Unit Symbol	ppm	ppm	ppm	ppm	ppm
Detection Limit	0.1	0.1	0.1	1	0.1
Analysis Method	TD-MS	TD-MS	TD-MS	TD-MS	TD-MS
HB18	1.2	3.5	< 0.1	< 1	1.7
HB19	1	41.5	< 0.1	< 1	26.7
HB20	3	116	< 0.1	< 1	6.8
HB21	3.7	124	< 0.1	< 1	11.4
HB22	1.8	41.7	< 0.1	< 1	6.6
HB23	2.2	58.7	< 0.1	< 1	14.8
HB24	3.8	68.9	< 0.1	1	5.8

Report'Date:'3/20/2013

Analyte Symbol	Te	Ba	La	Ce	Pr
Unit Symbol	ppm	ppm	ppm	ppm	ppm
Detection Limit	0.1	1	0.1	0.1	0.1
Analysis Method	TD-MS	TD-MS	TD-MS	TD-MS	TD-MS
JM1	0.1	422	41.2	84.1	9.8
JM2	< 0.1	423	39.1	80	9.1
JM3	0.2	380	40.2	81.7	9.3
JM4	0.2	413	41.6	86.1	9.7
JM5	0.3	382	37.8	78.4	8.7
JM6	0.1	458	42.6	86.3	9.9
JM7	0.3	405	41	83.8	9.5
JM8	0.1	124	38.5	81.2	9.3
JM9	< 0.1	383	38	78.3	8.9
JM10	0.2	388	35	74.4	8.6
JM11	0.1	316	7.1	20.3	2.7
JM12	0.3	395	18	43.9	5.6
JM13	< 0.1	203	38	78.3	9
JM14	0.2	268	40.3	83.4	9.6
JM15	0.7	431	42.2	85.3	9.7
JM16	0.5	437	42.6	86.8	9.9
JM17	0.7	467	45.2	91.2	10.4
JM18	0.4	422	42.8	86.5	9.8
JM19	0.3	447	43.1	86.4	9.6
JM20	1	437	42.9	84.3	9.3
JM21	0.4	436	40.9	81.4	8.8
JM22	0.4	391	37.1	73.3	8.2
JM23	0.4	443	40.9	82.5	9.4
JM24	0.3	391	38.9	78.8	8.8
JM25	0.8	407	32.3	68.4	7.9
JM26	0.3	438	40.5	82.5	9.5
JM27	0.5	431	40.4	81.7	9.3
JM28	0.4	395	39.5	79.9	9.1
JM29	0.3	394	38.2	77.6	8.8
CO1	0.5	281	20.2	26	5.8
CO2	0.3	165	6.7	9.4	1.5
CO3	0.7	85	8.9	14.8	2.2
CO4	0.6	48	10.6	15.5	2.6
CO5	0.5	26	20.3	42.4	5.8
CO6	0.6	97	34.1	66.7	8.7
CO7	0.6	39	15.2	36.7	5.4
CO8	0.5	25	18.4	41.4	5.5
CO9	0.6	27	22.3	49	6.5
CO10	0.4	187	6.6	9.4	1.5

Report'Date:'3/20/2013

Analyte Symbol	Te	Ba	La	Ce	Pr
Unit Symbol	ppm	ppm	ppm	ppm	ppm
Detection Limit	0.1	1	0.1	0.1	0.1
Analysis Method	TD-MS	TD-MS	TD-MS	TD-MS	TD-MS
CO11	0.8	427	23.9	51.5	6.8
CO12	0.8	298	23.5	51.4	6.7
CO13	0.7	326	32.2	64.2	8.7
CO14	0.8	228	33.4	65.4	8.5
CO15	0.8	538	20.8	42.1	5.6
CO16	0.2	136	7.1	10.2	1.6
RU1	0.8	161	25.8	39.4	5.8
RU2	0.5	169	10.7	16.2	2.6
RU3	0.6	185	23.3	35.5	5.1
RU4	0.7	42	34.5	47.4	9.3
RU5	0.5	111	29.3	29.2	6.9
RU6	0.8	235	29.1	47.8	6.7
RU7	0.6	119	11	21.2	2.5
RU8	0.6	233	27.5	45.8	5.2
RU9	0.6	256	55.9	84.6	15.4
RU10	0.5	22	29.5	56.3	7.8
RU11	0.4	191	25.3	42	5.7
RU12	0.8	146	23.2	35.1	5.1
RU13	0.9	227	26.7	44.4	6.2
RU14	0.5	18	30	57.7	7.9
RU15	0.4	112	9.6	15.3	2
RU16	0.4	165	25.3	47.6	5.4
RU17	0.7	154	23.6	35.6	5.4
HB1	0.5	165	6.7	8.8	1.2
HB2	0.7	273	27.6	31.5	5.6
HB3	0.8	84	11.5	18.3	3.4
HB4	0.2	229	1.7	2.9	0.4
HB5	0.3	205	3.7	5.2	0.8
HB6	< 0.1	87	8.8	14.9	2.2
HB7	0.3	608	51	42.1	9.1
HB8	0.5	368	102	79.6	17.1
HB9	< 0.1	93	22.9	23.8	5.1
HB10	< 0.1	69	9.3	16	2.3
HB11	0.1	166	15.4	24.6	3.9
HB12	< 0.1	211	1.7	2.9	0.4
HB13	< 0.1	77	16.7	24.7	3.4
HB14	< 0.1	188	2.3	4.2	0.5
HB15	< 0.1	100	6.1	9.4	1.5
HB16	< 0.1	97	6.4	10.8	1.6
HB17	0.2	49	10.5	17.6	2.8

Report'Date:'3/20/2013

Analyte Symbol	Te	Ba	La	Ce	Pr
Unit Symbol	ppm	ppm	ppm	ppm	ppm
Detection Limit	0.1	1	0.1	0.1	0.1
Analysis Method	TD-MS	TD-MS	TD-MS	TD-MS	TD-MS
HB18	< 0.1	225	1.6	2.8	0.3
HB19	0.2	186	2.7	4.9	0.6
HB20	0.3	47	11	18.6	2.7
HB21	0.2	185	13.9	19.7	3
HB22	0.3	88	5	7.9	1.3
HB23	0.1	134	11.9	14	2.3
HB24	0.4	56	11.1	20.1	2.8

Report'Date:'3/20/2013

Analyte Symbol	Nd	Sm	Gd	Tb	Dy
Unit Symbol	ppm	ppm	ppm	ppm	ppm
Detection Limit	0.1	0.1	0.1	0.1	0.1
Analysis Method	TD-MS	TD-MS	TD-MS	TD-MS	TD-MS
JM1	35.6	6.3	5	0.7	4.5
JM2	32.8	5.6	4.4	0.7	4.4
JM3	33.5	5.8	4.5	0.7	4.2
JM4	36.1	6.5	5.1	0.7	4.6
JM5	31.7	5.5	4.4	0.7	4
JM6	36.6	6.6	5.2	0.8	4.7
JM7	35.2	6.4	5.2	0.8	4.5
JM8	34.6	6.6	5.3	0.8	4.5
JM9	32.9	6	4.8	0.7	4.3
JM10	31.9	5.6	4.6	0.7	4.2
JM11	11.8	2.8	2.5	0.4	2.7
JM12	22	4.7	3.9	0.6	3.8
JM13	33.7	6.3	5.3	0.8	4.8
JM14	35.5	6.6	5.4	0.8	4.7
JM15	36.1	6.6	5.4	0.8	4.7
JM16	36.2	6.5	5.3	0.8	4.7
JM17	37.4	6.6	5.3	0.8	4.9
JM18	35.7	6	4.7	0.7	4.3
JM19	33.9	5.8	4.6	0.7	4.4
JM20	32.6	5.6	4.5	0.7	4.3
JM21	31	5.2	4.1	0.6	4.1
JM22	29.2	5	4.2	0.6	3.8
JM23	34.2	5.7	4.4	0.7	4.1
JM24	31.8	5.5	4.3	0.6	3.9
JM25	29.2	5.4	4.1	0.6	3.8
JM26	34.9	6.2	5	0.7	4.5
JM27	34.3	6.4	5	0.7	4.4
JM28	33.5	6.2	4.9	0.7	4.3
JM29	31.5	5.9	4.7	0.7	4.2
CO1	25.8	6.4	8.2	1.3	8.4
CO2	6	1.4	1.5	0.2	1.4
CO3	8.6	1.8	1.9	0.3	1.8
CO4	10	1.9	1.9	0.3	2
CO5	23.6	4.6	4.3	0.6	4.1
CO6	33.2	6.5	6.1	0.9	5.5
CO7	22.2	4.5	4.5	0.7	4.2
CO8	22	4.6	4.9	0.8	4.5
CO9	26.1	5.2	5.3	0.8	5
CO10	5.9	1.3	1.5	0.2	1.4

Report'Date:'3/20/2013

Analyte Symbol	Nd	Sm	Gd	Tb	Dy
Unit Symbol	ppm	ppm	ppm	ppm	ppm
Detection Limit	0.1	0.1	0.1	0.1	0.1
Analysis Method	TD-MS	TD-MS	TD-MS	TD-MS	TD-MS
CO11	27	5.3	5	0.7	4.7
CO12	26.3	5.2	5	0.7	4.4
CO13	35.5	7.1	6.7	1	5.8
CO14	32.6	6.3	5.8	0.9	5.4
CO15	21.9	4.6	4.9	0.7	4.5
CO16	6.5	1.5	1.6	0.2	1.5
RU1	22.1	4	3.5	0.5	3.1
RU2	10.6	2.1	2	0.3	1.8
RU3	18.9	3.6	3.1	0.4	2.7
RU4	36.8	7.2	6.3	0.9	5
RU5	27.3	5.6	5.5	0.9	5.5
RU6	26.1	5	4.5	0.7	4.5
RU7	9.1	1.7	1.3	0.2	1.6
RU8	18	3	2.2	0.4	2.5
RU9	63.3	12.2	11.4	1.6	9.8
RU10	30.7	6.2	5.9	0.9	5.4
RU11	21.5	4	3.6	0.5	3.6
RU12	20	3.7	3.1	0.4	2.7
RU13	23.8	4.7	4.2	0.6	4.2
RU14	30.4	6.1	5.6	0.9	5.5
RU15	7.6	1.4	1.5	0.2	1.5
RU16	18.8	3.3	2.6	0.4	2.9
RU17	20.3	3.8	3.2	0.5	2.9
HB1	4.2	0.7	0.5	< 0.1	0.6
HB2	22.4	4.6	5.5	0.9	6.1
HB3	13.7	3	2.9	0.4	2.8
HB4	1.3	0.2	0.2	< 0.1	0.2
HB5	3.1	0.5	0.4	< 0.1	0.4
HB6	8.2	1.6	1.3	0.2	1.4
HB7	36.9	7.4	9.4	1.5	10.6
HB8	68.2	13.2	17.4	2.7	19.1
HB9	20.5	4.2	4.6	0.7	5
HB10	8.7	1.6	1.5	0.2	1.6
HB11	14.6	2.7	2.6	0.4	2.8
HB12	1.2	0.2	0.1	< 0.1	0.2
HB13	12.8	2.3	2.3	0.3	2.4
HB14	1.7	0.3	0.2	< 0.1	0.2
HB15	5.8	1.2	1.3	0.2	1.5
HB16	6.4	1.2	1.1	0.2	1.2
HB17	11.2	2.3	2.3	0.4	2.3

Report'Date:'3/20/2013

Analyte Symbol	Nd	Sm	Gd	Tb	Dy
Unit Symbol	ppm	ppm	ppm	ppm	ppm
Detection Limit	0.1	0.1	0.1	0.1	0.1
Analysis Method	TD-MS	TD-MS	TD-MS	TD-MS	TD-MS
HB18	1.2	0.2	0.1	< 0.1	0.2
HB19	1.9	0.3	0.2	< 0.1	0.3
HB20	10.9	2.2	2.3	0.4	2.5
HB21	12.1	2.3	2.4	0.4	2.4
HB22	5.2	1.1	1.2	0.2	1.3
HB23	9.4	2.1	2.9	0.5	3.6
HB24	11.1	2.2	2.3	0.4	2.3

Report'Date:'3/20/2013

Analyte Symbol	Cu	Ge	Tm	Yb	Lu
Unit Symbol	ppm	ppm	ppm	ppm	ppm
Detection Limit	0.2	0.1	0.1	0.1	0.1
Analysis Method	TD-MS	TD-MS	TD-MS	TD-MS	TD-MS
JM1	43.1	0.8	0.4	2.8	0.4
JM2	34.2	0.4	0.4	2.6	0.4
JM3	45.5	0.3	0.4	2.7	0.4
JM4	32.8	0.4	0.4	2.8	0.4
JM5	34.7	0.4	0.4	2.5	0.4
JM6	36.7	0.5	0.4	2.8	0.4
JM7	27.2	0.4	0.4	2.7	0.4
JM8	40.3	0.3	0.4	2.7	0.4
JM9	44.9	0.5	0.4	2.5	0.4
JM10	35.1	0.3	0.4	2.7	0.4
JM11	38.7	0.5	0.3	2	0.3
JM12	66	0.8	0.4	2.5	0.4
JM13	42.9	0.2	0.4	2.8	0.4
JM14	52.6	0.3	0.4	2.8	0.4
JM15	44.5	0.5	0.4	2.9	0.4
JM16	39.2	0.5	0.4	2.8	0.4
JM17	28.3	0.8	0.5	3.1	0.4
JM18	37.3	0.5	0.4	2.7	0.4
JM19	49.3	0.5	0.4	2.8	0.4
JM20	47.6	0.6	0.4	2.9	0.4
JM21	25.3	0.7	0.4	2.7	0.4
JM22	16.6	0.5	0.4	2.4	0.4
JM23	32.7	0.7	0.4	2.6	0.4
JM24	30.6	0.4	0.4	2.4	0.4
JM25	54.4	0.5	0.4	2.4	0.4
JM26	30.7	0.6	0.4	2.7	0.4
JM27	32.6	0.6	0.4	2.7	0.4
JM28	33.8	0.4	0.4	2.6	0.4
JM29	37.4	0.5	0.4	2.5	0.4
CO1	46.2	0.3	0.7	3.9	0.6
CO2	38.6	0.2	0.1	0.7	0.1
CO3	63.5	0.2	0.2	1	0.2
CO4	76.6	0.2	0.2	1.2	0.2
CO5	130	0.3	0.4	2.2	0.3
CO6	95.4	0.4	0.5	2.9	0.4
CO7	96.5	0.6	0.4	2.3	0.3
CO8	129	0.2	0.4	2.1	0.3
CO9	141	0.3	0.4	2.7	0.4
CO10	41.2	0.3	0.1	0.7	0.1

Report'Date:'3/20/2013

Analyte Symbol	Cu	Ge	Tm	Yb	Lu
Unit Symbol	ppm	ppm	ppm	ppm	ppm
Detection Limit	0.2	0.1	0.1	0.1	0.1
Analysis Method	TD-MS	TD-MS	TD-MS	TD-MS	TD-MS
CO11	133	0.3	0.4	2.4	0.4
CO12	163	1.3	0.4	2.2	0.3
CO13	166	0.3	0.5	3	0.4
CO14	93.3	0.4	0.5	2.9	0.4
CO15	135	0.3	0.4	2.1	0.3
CO16	44	0.2	0.1	0.8	0.1
RU1	21.5	0.2	0.3	1.7	0.3
RU2	7.3	0.2	0.1	0.8	0.1
RU3	16	0.2	0.2	1.5	0.2
RU4	13.4	0.8	0.3	1.8	0.3
RU5	8.8	0.3	0.5	2.6	0.4
RU6	99.8	0.3	0.4	2.5	0.4
RU7	68.5	0.3	0.2	1.4	0.2
RU8	68	0.3	0.3	2.2	0.3
RU9	16.7	0.5	0.6	3.6	0.5
RU10	113	0.3	0.5	3	0.4
RU11	168	0.3	0.4	2.2	0.3
RU12	19.8	0.2	0.2	1.5	0.2
RU13	90.7	0.3	0.4	2.5	0.4
RU14	115	0.3	0.5	2.9	0.4
RU15	30.7	0.1	0.2	1	0.1
RU16	81.7	0.4	0.3	2.2	0.4
RU17	19.7	0.1	0.3	1.6	0.2
HB1	73.4	0.1	< 0.1	0.6	0.1
HB2	92.1	0.2	0.6	3.5	0.6
HB3	160	0.5	0.2	1.4	0.2
HB4	27.3	0.2	< 0.1	0.2	< 0.1
HB5	69.2	1.1	< 0.1	0.3	< 0.1
HB6	115	1.5	0.1	0.9	0.1
HB7	68.4	0.6	1.2	7.7	1.2
HB8	72.8	0.6	2	12.5	2
HB9	89.7	0.3	0.5	3.2	0.5
HB10	127	0.7	0.1	0.9	0.1
HB11	112	0.2	0.3	1.5	0.2
HB12	28.3	0.1	< 0.1	0.2	< 0.1
HB13	139	0.3	0.3	1.6	0.2
HB14	68.5	0.6	< 0.1	0.2	< 0.1
HB15	41.7	0.1	0.1	0.8	0.1
HB16	48.7	0.1	0.1	0.8	0.1
HB17	73.3	0.2	0.2	1.3	0.2

Report'Date:'3/20/2013

Analyte Symbol	Cu	Ge	Tm	Yb	Lu
Unit Symbol	ppm	ppm	ppm	ppm	ppm
Detection Limit	0.2	0.1	0.1	0.1	0.1
Analysis Method	TD-MS	TD-MS	TD-MS	TD-MS	TD-MS
HB18	26	< 0.1	< 0.1	0.1	< 0.1
HB19	68.9	0.2	< 0.1	0.2	< 0.1
HB20	80	0.1	0.2	1.4	0.2
HB21	75.5	0.1	0.3	1.5	0.2
HB22	40.6	0.2	0.1	0.7	0.1
HB23	39.3	0.1	0.3	2.1	0.3
HB24	64.6	0.2	0.2	1.3	0.2

Report'Date:'3/20/2013

Analyte Symbol	Ta	W	Re	Tl	Pb
Unit Symbol	ppm	ppm	ppm	ppm	ppm
Detection Limit	0.1	0.1	0.001	0.05	0.5
Analysis Method	TD-MS	TD-MS	TD-MS	TD-MS	TD-MS
JM1	1.1	2.3	0.024	1.93	29
JM2	< 0.1	0.1	0.008	1.11	16.2
JM3	1.3	2.5	0.016	1.59	34.3
JM4	1.2	2.5	0.029	1.67	32.5
JM5	1.1	2.3	0.012	1.04	23.2
JM6	1.2	2.6	0.009	1.7	25.1
JM7	1.2	2.4	0.025	1.7	30.9
JM8	1.1	2.2	0.019	1.91	59.9
JM9	1.1	2.2	0.014	1.26	21.6
JM10	1.3	2.7	0.011	1.67	41.6
JM11	1.1	2.4	0.017	2.09	33.9
JM12	1.1	2.2	0.023	2.49	30.9
JM13	1.1	2.3	0.018	2.2	50.9
JM14	1	2.4	0.028	2.7	40.7
JM15	1.3	2.8	0.025	2.54	31.8
JM16	1.2	2.5	0.025	2.25	30.7
JM17	1.3	2.7	0.031	2.23	24.5
JM18	1.2	2.5	0.027	1.71	35.2
JM19	1.3	2.6	0.062	2.15	22.9
JM20	1.1	2.3	0.024	2.3	22.9
JM21	0.8	1.9	0.009	1	11.7
JM22	0.2	0.8	0.012	0.78	12.6
JM23	0.9	1.9	0.019	1.15	24.2
JM24	1.1	2.1	0.028	1.49	31.8
JM25	1.1	2.3	0.02	2.17	37.5
JM26	1.1	2.5	0.016	1.78	26.7
JM27	1.3	2.3	0.015	1.65	23.8
JM28	1.1	2.3	0.014	2.04	32.2
JM29	0.7	1.5	0.016	1.77	21.1
CO1	1.1	0.1	0.062	0.91	8.1
CO2	< 0.1	0.4	0.089	1.27	5.5
CO3	0.2	0.5	0.107	1.62	7.9
CO4	0.1	0.6	0.259	2.56	10.4
CO5	0.3	1.3	0.226	11.3	22.6
CO6	1.1	2.2	0.326	6.68	27.1
CO7	0.4	1.2	0.3	22	21.2
CO8	0.3	1.9	0.27	11.3	28.8
CO9	0.4	1.5	0.245	13.4	31.5
CO10	< 0.1	0.4	0.087	1.46	5.5

Report'Date:'3/20/2013

Analyte Symbol	Ta	W	Re	Tl	Pb
Unit Symbol	ppm	ppm	ppm	ppm	ppm
Detection Limit	0.1	0.1	0.001	0.05	0.5
Analysis Method	TD-MS	TD-MS	TD-MS	TD-MS	TD-MS
CO11	0.5	1.5	0.229	15	32.4
CO12	0.6	1.3	0.222	17	37.3
CO13	0.7	1.6	0.316	13.2	34.3
CO14	1	2	0.328	6.72	26.5
CO15	0.5	1.5	0.25	11.2	30.5
CO16	< 0.1	0.5	0.087	1.7	6
RU1	1.3	1.1	0.028	0.53	6.1
RU2	0.2	0.4	0.025	0.18	2.4
RU3	0.4	0.9	0.035	0.37	4.8
RU4	0.3	0.6	0.044	0.53	8.2
RU5	0.2	0.6	0.042	0.3	3.9
RU6	0.8	1.9	0.256	3.27	17.9
RU7	0.7	1.7	0.447	4.47	27.7
RU8	0.8	2.2	0.018	1.21	14.2
RU9	< 0.1	0.3	0.012	0.64	14.2
RU10	0.7	1.4	0.232	17.2	24.1
RU11	0.7	1.7	0.217	1.65	10.3
RU12	0.7	0.9	0.03	0.44	5.6
RU13	0.8	1.8	0.241	3.15	17.2
RU14	0.8	1.5	0.267	23	27
RU15	0.2	0.6	0.078	1.03	5.8
RU16	0.9	2.4	0.536	5.79	35.6
RU17	0.4	1	0.022	0.52	5.4
HB1	0.2	1.1	0.053	0.35	6.1
HB2	< 0.1	0.8	0.063	0.44	6.1
HB3	< 0.1	0.7	0.289	0.67	10.9
HB4	< 0.1	0.5	0.028	0.18	2.5
HB5	< 0.1	0.4	0.119	1.13	10.3
HB6	< 0.1	0.8	0.191	2.6	11.8
HB7	< 0.1	0.6	0.092	0.56	7.8
HB8	< 0.1	0.9	0.072	0.42	7.9
HB9	< 0.1	0.3	0.062	1.2	7.3
HB10	< 0.1	0.9	0.208	2.76	13.3
HB11	0.2	0.9	0.054	0.86	8.5
HB12	< 0.1	0.5	0.028	0.19	2.6
HB13	< 0.1	1.1	0.087	0.99	11.7
HB14	< 0.1	0.2	0.086	0.66	7.1
HB15	< 0.1	0.6	0.125	1.28	6
HB16	< 0.1	0.4	0.081	1.23	5.9
HB17	< 0.1	0.5	0.14	1.86	9.2

Report'Date:'3/20/2013

Analyte Symbol	Ta	W	Re	Tl	Pb
Unit Symbol	ppm	ppm	ppm	ppm	ppm
Detection Limit	0.1	0.1	0.001	0.05	0.5
Analysis Method	TD-MS	TD-MS	TD-MS	TD-MS	TD-MS
HB18	< 0.1	0.5	0.026	0.23	2.7
HB19	< 0.1	0.3	0.072	0.64	13.7
HB20	0.1	0.8	0.254	3.25	10.3
HB21	0.3	0.8	0.177	3.09	8.3
HB22	< 0.1	0.3	0.126	1.48	5.2
HB23	0.4	0.7	0.152	3.37	6
HB24	0.1	0.7	0.118	4.59	9.3

Report'Date:'3/20/2013

Analyte Symbol	Sc	Th	U	Ti	P
Unit Symbol	ppm	ppm	ppm	%	%
Detection Limit	1	0.1	0.1	0.0005	0.001
Analysis Method	TD-ICP	TD-MS	TD-MS	TD-ICP	TD-ICP
JM1	19	12.9	7.1	0.544	0.021
JM2	18	12.8	11.6	0.335	0.014
JM3	20	13.2	10.5	0.605	0.018
JM4	19	13.8	6.3	0.625	0.02
JM5	18	12.6	4.9	0.621	0.019
JM6	21	13.7	6.4	0.627	0.024
JM7	17	13.4	5.9	0.588	0.022
JM8	17	12.8	5.6	0.552	0.024
JM9	17	12.2	4.9	0.545	0.021
JM10	19	12.3	5.9	0.658	0.025
JM11	15	3.3	6.5	0.543	0.023
JM12	17	7.2	8.7	0.581	0.021
JM13	19	11.8	8.8	0.541	0.023
JM14	20	13	10.8	0.586	0.024
JM15	21	14	9.8	0.631	0.022
JM16	21	14	7.9	0.619	0.022
JM17	21	15.4	8.7	0.636	0.021
JM18	20	14.1	6.2	0.588	0.019
JM19	21	14.5	7.3	0.627	0.018
JM20	20	14.5	6.2	0.61	0.015
JM21	20	13.8	4.2	0.578	0.014
JM22	18	12.2	4	0.496	0.015
JM23	20	12.7	4.9	0.55	0.017
JM24	18	12.4	5.5	0.55	0.017
JM25	19	11.3	5.1	0.547	0.02
JM26	20	13.1	5.9	0.556	0.02
JM27	20	13.1	6.1	0.563	0.023
JM28	20	13	6.4	0.567	0.023
JM29	19	12.5	5.7	0.552	0.021
CO1	22	4.2	74.9	0.0147	2.73
CO2	3	1.1	14.4	0.0562	0.231
CO3	5	2	17.2	0.108	0.018
CO4	6	2.2	22	0.143	0.01
CO5	9	3.9	41.7	0.304	0.012
CO6	14	9.9	56.8	0.474	0.081
CO7	9	2.6	77.6	0.226	0.016
CO8	9	4	50.8	0.278	0.013
CO9	10	3.9	48.3	0.297	0.063
CO10	3	1.1	14.1	0.0589	0.23

Report'Date:'3/20/2013

Analyte Symbol	Sc	Th	U	Ti	P
Unit Symbol	ppm	ppm	ppm	%	%
Detection Limit	1	0.1	0.1	0.0005	0.001
Analysis Method	TD-ICP	TD-MS	TD-MS	TD-ICP	TD-ICP
CO11	10	5.1	39.7	0.316	0.04
CO12	10	6.2	56.4	0.299	0.065
CO13	12	7.7	80.8	0.359	0.068
CO14	14	9.7	56.2	0.479	0.075
CO15	9	5.6	52.4	0.273	0.013
CO16	3	1.2	15.7	0.0596	0.235
RU1	7	5.6	3.8	0.295	0.04
RU2	3	1.9	1.3	0.0953	0.024
RU3	6	4.9	3.3	0.252	0.031
RU4	11	5.6	5.9	0.181	0.299
RU5	7	3.2	2.9	0.107	0.056
RU6	15	9.6	33	0.387	0.04
RU7	14	5.9	6.9	0.424	0.021
RU8	18	9.4	8.4	0.44	0.035
RU9	11	9.4	11.5	0.0421	1.36
RU10	15	7.7	67.1	0.407	0.042
RU11	15	8.8	15.8	0.343	0.14
RU12	7	4.7	3.3	0.287	0.039
RU13	15	9.2	31.7	0.377	0.038
RU14	15	8	66.4	0.4	0.038
RU15	5	2.7	11.7	0.143	0.024
RU16	18	10.9	10.1	0.495	0.026
RU17	7	4.9	3.5	0.285	0.039
HB1	5	2.2	3.2	0.0947	0.013
HB2	14	2.7	20.7	0.0225	2.88
HB3	9	3.5	17.7	0.105	1.23
HB4	2	0.9	1.8	0.0484	0.027
HB5	3	1.1	7.9	0.0591	0.007
HB6	6	2.7	15.9	0.154	0.033
HB7	5	0.8	45.8	0.0224	4.01
HB8	17	1.6	39.5	0.0359	6.37
HB9	9	2.5	19	0.028	1.87
HB10	7	2.8	16.9	0.164	0.037
HB11	9	3.2	7.3	0.232	0.075
HB12	2	0.8	1.6	0.0496	0.019
HB13	7	4.3	8.4	0.114	1.53
HB14	2	1.2	4.3	0.0526	0.006
HB15	3	1.2	15.4	0.0612	0.022
HB16	4	1.4	11.1	0.0816	0.051
HB17	6	1.9	17.2	0.121	0.054

Report'Date:'3/20/2013

Analyte Symbol	Sc	Th	U	Ti	P
Unit Symbol	ppm	ppm	ppm	%	%
Detection Limit	1	0.1	0.1	0.0005	0.001
Analysis Method	TD-ICP	TD-MS	TD-MS	TD-ICP	TD-ICP
HB18	2	0.9	1.5	0.0444	0.017
HB19	2	1.1	4.1	0.0509	0.005
HB20	5	1.9	31.3	0.126	0.025
HB21	5	2.9	19.6	0.111	0.037
HB22	3	1.2	14.4	0.068	0.015
HB23	4	1.7	26.6	0.0682	0.017
HB24	6	2.3	25.5	0.131	0.016

Report'Date:'3/20/2013

Analyte Symbol	S
Unit Symbol	%
Detection Limit	0.01
Analysis Method	TD-ICP
JM1	0.77
JM2	0.44
JM3	0.96
JM4	0.78
JM5	0.76
JM6	0.68
JM7	0.72
JM8	1.72
JM9	0.6
JM10	0.96
JM11	0.73
JM12	0.71
JM13	2.25
JM14	1.21
JM15	0.75
JM16	0.77
JM17	0.67
JM18	0.88
JM19	0.75
JM20	0.71
JM21	0.76
JM22	0.53
JM23	0.55
JM24	0.88
JM25	0.85
JM26	0.65
JM27	0.65
JM28	0.84
JM29	0.7
CO1	0.52
CO2	0.64
CO3	0.65
CO4	1.25
CO5	3.35
CO6	1.57
CO7	4.47
CO8	2.61
CO9	3.26
CO10	0.64

Report'Date:'3/20/2013

Analyte Symbol	S
Unit Symbol	%
Detection Limit	0.01
Analysis Method	TD-ICP
CO11	3.27
CO12	7.32
CO13	4.29
CO14	1.59
CO15	2.59
CO16	0.64
RU1	0.74
RU2	0.52
RU3	0.64
RU4	4.58
RU5	1.79
RU6	1.14
RU7	1.8
RU8	2.21
RU9	1.01
RU10	4.73
RU11	1.33
RU12	0.72
RU13	1.14
RU14	6.11
RU15	0.86
RU16	2.1
RU17	0.71
HB1	0.71
HB2	0.84
HB3	1.31
HB4	0.41
HB5	0.74
HB6	1.13
HB7	0.54
HB8	0.61
HB9	0.84
HB10	1.24
HB11	1.17
HB12	0.41
HB13	1.43
HB14	0.54
HB15	0.61
HB16	0.67
HB17	1.18

Report'Date:'3/20/2013

Analyte Symbol	S
Unit Symbol	%
Detection Limit	0.01
Analysis Method	TD-ICP
HB18	0.37
HB19	0.51
HB20	1.19
HB21	1.36
HB22	0.67
HB23	1.12
HB24	1.47

VITA

Keith Thomas Rivera

Candidate for the Degree of

Master of Science

Thesis: GEOLOGIC CONTROLS ON NITROGEN ISOTOPES IN MARINE BLACK SHALE: A CASE STUDY OF THE WOODFORD SHALE, ANADARKO BASIN, OKLAHOMA

Major Field: Geology

Biographical:

Education:

Completed the requirements for the Master of Science/Arts in your major at Oklahoma State University, Stillwater, Oklahoma in December, 2013.

Completed the requirements for the Bachelor of Science/Arts in your major at California State University San Bernardino, San Bernardino, California in 2011.

Experience:

Chesapeake Energy, Oklahoma City, OK, Geoscience Intern from May 2012 to August 2012.

Imperial Barrel Award, Oklahoma State University, OK, Team member for the Spring 2012 program.

California Regional Water Quality Control Board, Lahontan Region, Victorville, CA, Student Intern from May 2010 – August 2011.

Professional Memberships:

American Association of Petroleum Geologists
Geological Society of America
Society of Exploration Geophysicists
Society for Sedimentary Geology